By sensing with poly resistors or diodes, the sensor can be located close to the center of the power device near the source bond pads where the current density is the highest and, consequently, the highest die temperature occurs. The thermal conductivity of the oxide that separates the polysilicon diodes from the power device is two orders of magnitude less than that of silicon. However, because the layer is thin, the polysilicon element offers an accurate indication of the actual peak junction temperature.

A very low on-resistance power FET that incorporates a temperature sensing diode is shown in Fig. 5.12. The power device achieves an on-resistance of 5 milliohms (including packaging resistance) at 25 °C utilizing a production power FET process. The power FET process was chosen instead of a power IC process because a large die size was required to meet the power dissipation requirements of a very cost sensitive application. A minor modification (the addition of a single masking layer) to a production power FET process allows both sensing and protection features to be integrated. Devices that are produced using the SMARTDISCRETE technology, as this approach is called by Motorola, are one way to provide more cost-effective, smart power semiconductors, especially for high-current or low on-resistance power applications.

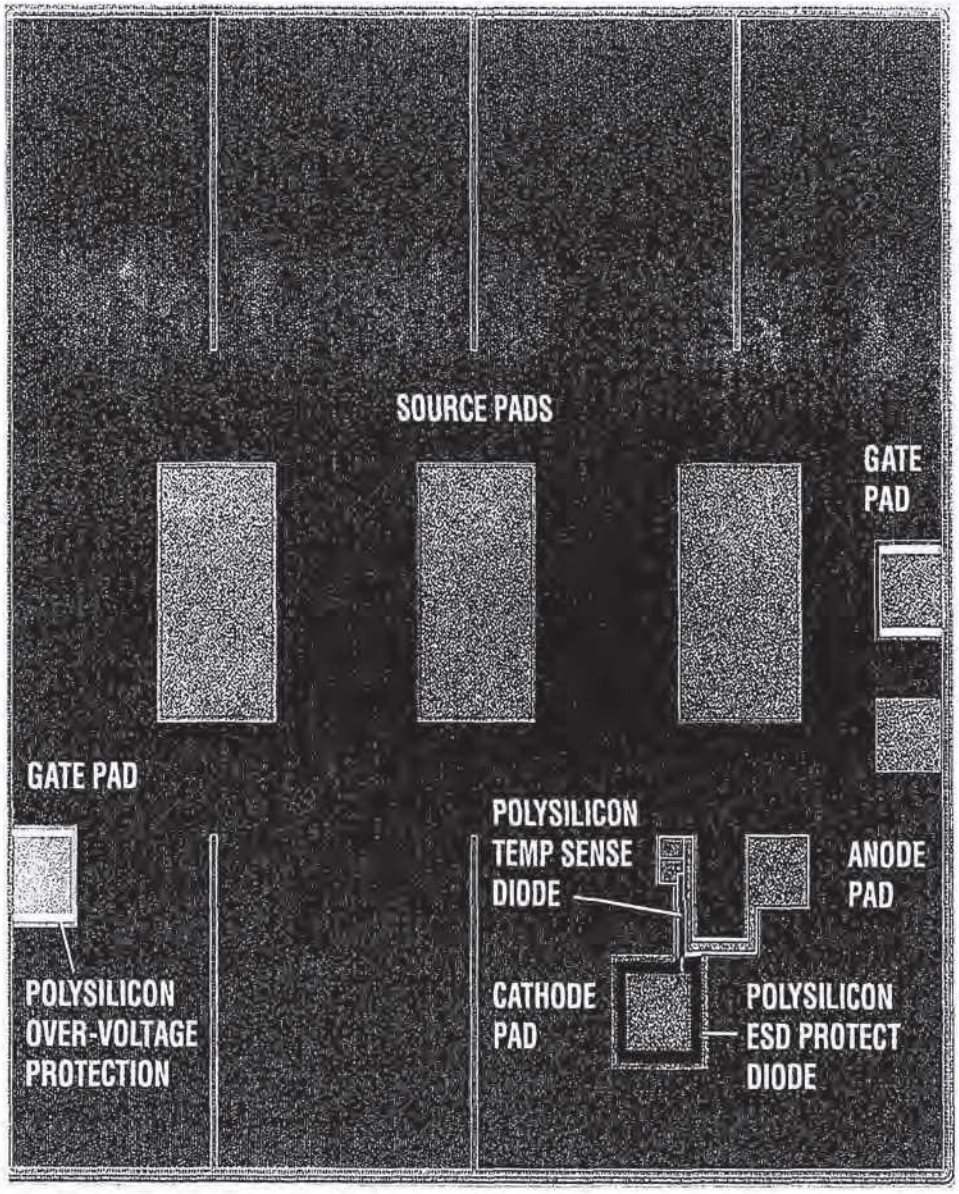


FIGURE 5.12 Temperature sensor integrated in power MOSFET. *(Die photomicrograph Courtesy Motorola Inc.)*

IPR2023-01234
Petitioner - Ex. 1017 - Page 101

An accurate indication of the maximum die temperature is obtained by monitoring the output voltage when a constant current is passed through the integrated polysilicon diode(s). A number of diodes are actually provided in the design. A single diode has a temperature coefficient of 1.90 mV/°C. Two or more diodes can be placed in series if a larger output is desired. For greater accuracy, the diodes can be trimmed during wafer-level testing by blowing fusible links made from polysilicon. The response time of the diodes is less than 100 μs which has allowed the device to withstand a direct short across an automobile battery with external circuitry providing shutdown prior to device failure. The sensing capability also allows the output device to provide an indication (with additional external circuitry) if the heatsinking is not proper when the unit is installed in a module or if a change occurs in the application which would ultimately cause a failure.

A smart power IC, like Motorola's SMARTMOS™ process, can have multiple power drivers integrated on a single monolithic piece of silicon. Each of these drivers can have a temperature sensor integrated to determine the proper operating status and shut off only a specific driver if a fault occurs. The temperature sensor is basically a band gap reference. In this case, two diodes' junctions are biased with different current densities. Circuitry in the smart power IC process establishes a voltage reference and a trip point.

5.4.7 Thermostat (Mechanical Temperature Sensing)

The earliest method of temperature regulation used in vehicles is still in use today—the thermostat. The expansion element usually activates a valve which redirects the flow of coolant into a radiator bypass line when a specific temperature is reached.

5.4.8 Fiber Optic Temperature Sensors

High-temperature sensors capable of operating up to 1800 °C have been developed using optical fibers. The response time of the sensor is on the order of 500 ms and the accuracy is within ±0.5 percent. The noncontact sensor uses a single optical fiber that has an outside diameter of 0.5 to 1.0 mm. The probe structure is critical to the sensor's sensitivity and the distance coefficient that relates the detection surface area to the distance at which the probe will be placed for measurement.

A sapphire fiber optic sensor has been developed to measure high temperatures such as those found near the tip of a spark plug during combustion. The sensor can withstand temperatures up to 4000 °C and has an accuracy of 0.2 percent at 1000 °C. The sensor has been used to identify knock and to characterize flame front propagation.

5.4.9 Temperature Indicators

Temperature-indicating materials have been developed with melting points that can be calibrated to ±1 °C. When the temperature of the device is exceeded, a phase change occurs and the material changes color. The material is available in paint, patch, pellet, and applicator stick form. Temperature ranges from 38 to 1371 °C are available. This kind of indication is useful during the development phase of automotive components to verify that a critical design temperature has not been exceeded.

5.4.10 Infrared Temperature Sensing

Blackbody emittance is the basis for infrared (IR) thermometry. Objects at temperatures above –273 °C emit radiant energy in an amount proportional to the fourth power of their

IPR2023-01234
Petitioner - Ex. 1017 - Page 102

temperature. An IR sensor consists of collecting optics, lenses, and/or fiber optics, spectral filtering, and a detector as the front end. The primary characteristic of the optics is the field of view (FOV) which allows a specific target to be measured at a prescribed distance.

Infrared sensors have been used extensively for noncontact temperature measurements in process control. In automobiles, infrared sensors use temperature variations to produce a monochrome image in night vision systems. Board-level temperature testing also utilizes IR-sensing techniques to identify hot spots and potential failure points.

5.4.11 Thermal Actuators/Thermal Cooling

Chemical sensors like the oxygen sensor described in Sec. 5.2.6 require a minimum operating temperature to be effective. Semiconductor technology allows platinum and silicon heaters and temperature sensors to be produced on a thin diaphragm, or window, etched into a silicon substrate. Temperatures can be produced in the window which exceed 1200 °C, while the supporting rim of silicon remains essentially at room temperature. This ability may allow fast-response sensors to be developed for vehicle applications.

Other silicon development activity using micromachining techniques may allow heat pipes and silicon-level heatsinks to remove heat more effectively from rapidly switching semiconductor devices.

5.5 HUMIDITY SENSORS

Humidity sensors are used extensively during vehicle and component development, especially in determining the ability to withstand humidity and temperature cycling tests. Engine performance can be affected by humidity. A sensor that can pass rigorous automotive qualification tests and meet the desired specifications and cost criteria would provide additional input for the engine control system. In a less rugged application, HVAC systems may benefit from the input from humidity sensors. Humidity sensors are not used on production vehicles at the present time. However, some potential techniques that are used in development and nonautomotive applications are described in this section.

Techniques to measure humidity are listed in Table 5.6. Most of these are actually laboratory instruments. The most well known approach to humidity measurements is the use of wet bulb and dry bulb thermomometer readings interpreted through the use of a psychrometric chart which relates all basic humidity readings. The effect of humidity on polymers and the use of semiconductor-processing techniques has created actual sensors that do not require the constant calibration, have less drift, improved reliability, and potentially can achieve automotive cost objectives. Three sensing techniques that have potential for future vehicle use are capacitive, resistive, and oxidized porous silicon.

5.5.1 Capacitive Humidity Sensors

A thin-film polymer capacitive-type relative humidity sensor can be produced by using semiconductor technology. The dielectric constant of the polymer thin film changes linearly with changes in atmospheric relative humidity. A desirable feature, in addition to long-term stability and operation to 180 °C, is fast wet-up/dry-down performance.

A temperature sensor can easily be added to the RH sensor, which increases the operating range and the functionality.

IPR2023-01234
Petitioner - Ex. 1017 - Page 103

TABLE 5.6 Techniques for Measuring Humidity/Moisture

Principle	Type measurement
Gravimetric hygrometer	Instrument
Pressure-humidity generator	Instrument
Wet bulb/dry bulb (psychrometer)	Instrument
Hair element	Instrument
Electric conductivity	Instrument
Dew cell	Instrument
Chilled mirror	Instrument
Karl Fisher titration	Instrument
Electrolytic	Instrument
Lithium chloride	Instrument
Capacitance hygropolymer	Production sensor
Bulk polymer (resistance)	Production sensor
Thin-film polymer (capacitance)	Production sensor
Gold/aluminum oxide	Production sensor
Oxidized porous silicon (OPS)	Experimental sensor

5.5.2 Resistive Humidity Sensors

Both surface and bulk polymer resistance sensors have been developed for measuring relative humidity. In bulk polymer film units, mobile ions are released from the molecular structure with increased humidity levels resulting in orders-of-magitude change in resistance over the operating range. Diode temperature compensation is used to improve accuracy over the temperature range. With an ac excitation at 1 kHz, a change from 10 to 100 percent RH produces a corresponding resistance variation from $2 \cdot 10^7$ to $2 \cdot 10^3$ ohms.

5.5.3 Oxidized Porous Silicon

A capacitive-type sensor has been developed that uses oxidized porous silicon (OPS) as a moisture-absorbing dielectric between the electrodes of the capacitor. An electrolysis process is used to create a thin porous layer on the top of a silicon wafer. The silicon is converted to OPS by a high-temperature treatment in either oxygen or steam. Metal electrodes are deposited on the top and back of the OPS to complete the capacitive structure.

When water vapor contacts the sensor, it permeates through the porous structure between the electrodes. The response of a typical sensor increases 800 percent when exposed to an RH change from 1 to 40 percent. Since semiconductor techniques are used in the manufacturing process, the potential to integrate signal conditioning and other sensors may provide an attractive solution for future vehicle sensing requirements.

5.6 CONCLUSIONS

Several factors are influencing the temperature-sensing requirements for future vehicles. The ultra-efficient vehicle will operate at higher temperatures and utilize brake energy-recovery. Both of these aspects will increase the temperature environment for other vehicle components.

The requirements for sensors in future vehicle systems include improved performance (sensitivity) and reliability in spite of operating at higher temperatures, lower cost, space and weight reduction, greater functionality including diagnostics and self-test, and ease of inter-

IPR2023-01234
Petitioner - Ex. 1017 - Page 104

facing with an MCU for adaptive control and interchangeability. The capability of semiconductor technology to provide sensing information for failure detection provides a means for increased reliability in several vehicle subsystems.

All trademarks are the property of their respective owners.

GLOSSARY

Accuracy A comparison of the actual output signal of a device to the true value of the input. The various errors (such as linearity, hysteresis, repeatability, and temperature shift) attributing to the accuracy of a device are usually expressed as a percent of full-scale output (FSO).

Maximum operating temperature The maximum body temperature at which the thermistor will operate for an extended period of time with acceptable stability of its characteristics. This temperature is the result of the internal or external heating, or both, and should not exceed the maximum value specified.

Negative temperature coefficient (NTC) An NTC thermistor is one in which the zero-power resistance decreases with an increase in temperature.

Operating temperature range The range of temperature between minimum and maximum temperature at which the output will meet the specified operating characteristics.

Self-generating Providing an output signal without applied excitation, such as a thermoelectric transducer.

Self-heating Internal heating resulting from electric energy dissipated within the unit.

Storage temperature range The range of temperature between minimum and maximum which can be applied without causing the sensor (unit) to fail to meet the specified operating characteristics.

Temperature coefficient of full-scale span The percent change in the full-scale span per unit change in temperature relative to the full-scale span at a specified temperature.

Temperature hysteresis The difference in output at any temperature in the operating temperature range when the temperature is approached from the minimum operating temperature and when approached from the maximum operating temperature with zero input applied.

Thermal time constant The thermal time constant is the time required for a thermistor to change to 63.2 percent of the total difference between its initial and final body temperature when subjected to a step function change in temperature under zero-power conditions.

Transfer function A mathematical, graphical, or tabular statement of the influence which a system or element has on the output compared at the input and output terminals.

BIBLIOGRAPHY

Automotive Electronics Reliability Handbook, SAE, Warrendale, Pa., 1987.
Automotive Handbook, Robert Bosch GmbH, 1986.

IPR2023-01234
Petitioner - Ex. 1017 - Page 105

BR923/D Discrete and Special Technologies Group Reliability Audit Report 1Q90, Motorola Semiconductor Products Sector, Phoenix, Ariz.

Collings, N., W. Cai, T. Ma, and D. Ball, "A linear catalyst temperature sensor for exhaust gas ignition (EGI) and on board diagnostics of misfire and catalyst efficiency," SAE SP-957, *U.S. and European Automotive Technology Emissions Technology,* International Congress and Exposition, Detroit, March 1–5, 1993.

De Vera, D., T. Glennon, A. A. Kenny, M. A. H. Khan, and M. Mayer, "An automotive case study," *Quality Progress,* June 1988, pp. 35–38.

Dosher, J., "Smart and active sensors," *Proceedings of Sensors Expo West,* 1991, pp. 103C-1–6.

Hao, T., E. F. Malinowski, and C-C. Liu, "High temperature fiber optic sensor for industrial applications," *Proceedings of Sensors Expo West,* San Jose, Calif., March 2–4, 1993, pp. 227–228.

Norton, Harry N., "Section 10—Transducers and Sensors," in D. G. Fink and D. Christiansen (eds.), *Electronics Engineers' Handbook* (3d ed.), McGraw-Hill, New York, 1989.

Pressure Sensor Device Data, Motorola Semiconductor Products Sector, Phoenix, Ariz., 1993.

Recommended Environmental Practices for Electronic Equipment Design, SAE J1211, Warrendale, Pa., Nov. 1978.

Temming, J., "Measuring seat comfort," *Automotive Engineering,* July 1993, pp. 25–30.

IPR2023-01234
Petitioner - Ex. 1017 - Page 106

CHAPTER 6
EXHAUST GAS SENSORS

H.-M. Wiedenmann, G. Hötzel,
H. Neumann, J. Riegel, and H. Weyl
Robert Bosch GmbH
Lambda Oxygen Sensor Development

6.1 BASIC CONCEPTS

6.1.1 Combustion

The sole products of complete fuel combustion are the nontoxic substances carbon dioxide and water:

$$C_mH_n + \left(m + \frac{n}{4}\right) 0_2 \rightarrow m\, CO_2 + \frac{n}{2}\, H_2O \tag{6.1}$$

The theoretical air requirement for this process is 14.7 kg air for each kilogram of fuel; this corresponds to approximately 10 m^3 air per liter of fuel. The air/fuel ratio is defined as stoichiometric when the engine is supplied with the exact quantity of air required for complete combustion.

6.1.2 Definition of Normalized air/fuel Ratio Lambda

The mixture ratio is defined by the normalized air/fuel ratio lambda (λ):

$$\lambda = \frac{\text{current air-fuel ratio}}{\text{stoichiometric air-fuel ratio}} \tag{6.2}$$

Because the conditions within the engine do not correspond to the absolute ideal required for perfect combustion, a number of products of incomplete combustion occur, even if a stoichiometric air/fuel ratio ($\lambda = 1$) is maintained. Thus, the CO_2 and H_2O are joined by CO, H_2, and HC (hydrocarbons C_xH_y) along with corresponding amounts of not reacted (free) oxygen. The water-gas equilibrium defines the ratio of CO to H_2. At high combustion temperatures, the N_2 and O_2 in the air supply form nitrous oxides such as NO, NO_2, N_2O (generic designation: NO_x).

6.1.3 Composition of Untreated Exhaust Gas

The composition of the exhaust gases entering the catalytic converter (untreated or raw emissions) varies according to the quality of combustion and, even more importantly, as a function

IPR2023-01234
Petitioner - Ex. 1017 - Page 107

of the normalized air/fuel ratio lambda (λ) (Fig. 6.1). Rich mixtures (lambda < 1, excess fuel) produce high concentrations of CO, H_2, and HC, while lean mixtures (lambda > 1, excess oxygen) generate higher levels of NO_x and free oxygen. The lower combustion-chamber temperatures associated with mixture ratios of lambda > 1.2 result in reductions in NO_x concentrations accompanied by increased HC concentrations. Maximum emissions of CO_2 (greenhouse gas) occur at a slightly lean mixture (lambda ≈ 1.1).

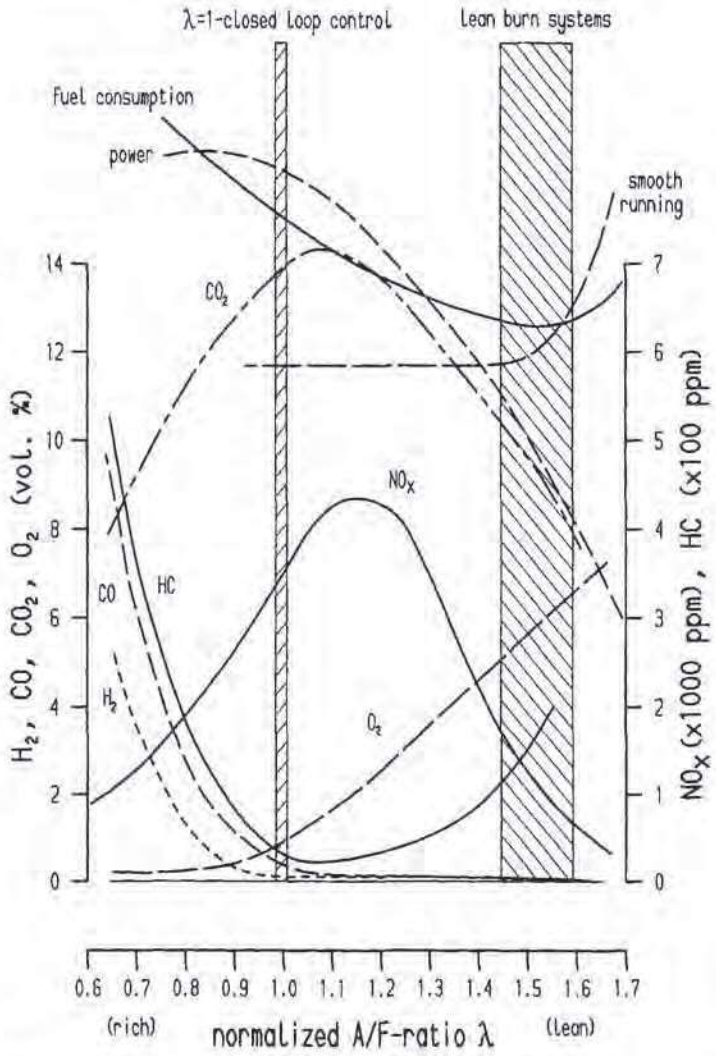


FIGURE 6.1 Typical curves for fuel consumption, power, smoothness, and composition of raw exhaust gases relative to lambda in a spark-ignition engine.

6.1.4 Lambda Closed-Loop Control: Design Concepts

Lambda Control Ranges. The main elements considered in defining the range of the lambda closed-loop control system (Table 6.1) are engine design, emission limits, fuel consumption, and the requirements for performance and smooth running.

Treatment of Exhaust Gases. Catalytic treatment of exhaust gases is essential for achieving compliance with the stringent current United States emission standards (Table 6.2). In the catalytic process, CO, H_2, and HC are oxidized to form CO_2 and H_2O, while the constituents of

IPR2023-01234
Petitioner - Ex. 1017 - Page 108

TABLE 6.1 Lambda Control Ranges

	Lambda = 1—spark ignition engine	Lean-burn concept	Lean-mix concept	Diesel engine
Lambda-control range	Lambda = 1 ± < 0.005	1.4–1.7	1.4–1.7 and lambda = 1	1.1–7
Target	Opt. catalytic aftertreatment	Fuel economy low CO, HC, (NO_x)*	Improved fuel economy within allowable emission	Reduced emissions particles and NO_x
Lambda sensors	Lambda = 1 sensor	Lean A-F sensor	Wide-range A-F sensor	Lean A-F sensor
Exhaust gas aftertreatment	Three-way-catalyst (TWC)	Oxi-cat NO_x-cat*	TWC NO_x-cat*	Particle filter* NO_x-cat*
Control concepts	Conventional or continuous	Continuous	Lean: continuous lambda = 1: conventional	Full-load and EGR-control
Series production	Discont. control	—	Yes	—

* Not available yet.
TWC: three-way-catalyst; Oxi-cat: oxidation-catalyst; NO_x-cat: NO_x-reduction-catalyst.

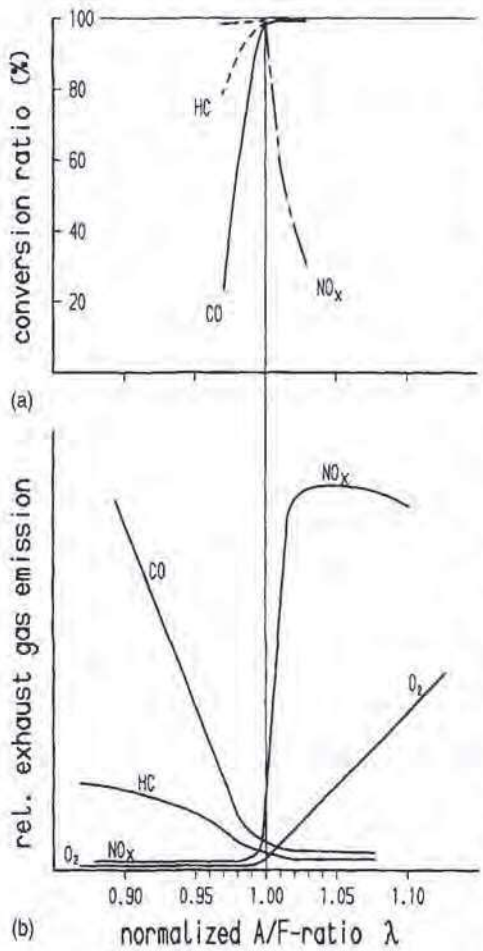


FIGURE 6.2 (*a*) Conversion rates for CO, NO_x, and HC in a new three-way catalytic converter; (*b*) typical curve for exhaust-gas composition downstream from a new three-way catalytic converter.

NO_x are reduced to N_2 and O_2. A three-way catalytic converter TWC (selective catalytic converter) and closed-loop control system featuring a lambda sensor are essential elements in achieving adequate reductions in all three pollutants (Fig. 6.2). The engine must be operated within a narrow range of $|\Delta\lambda| < 0.005$ at lambda = 1.

Oxidation catalysts are sometimes employed to reduce CO and HC emissions from lean-burn and diesel engines. Meanwhile, NO_x reduction catalysts and particle filters are being developed for future applications (Table 6.1).

Lambda Closed-Loop Control. Lambda closed-loop control is incorporated in the engine's electronic control system. The control system regulates lambda upstream from the catalytic converter with the aid of an oxygen sensor. System lag results in relatively long control-response delays, especially at low rpm. For this reason, the system must incorporate a pilot-control function capable of adjusting the mixture to the desired lambda with the highest possible degree of precision. This arrangement makes it possible to avoid excessive control deviations and harmful emission peaks of the kind that lead to high emission levels and reduced vehicle performance.

Conventional Closed-Loop Lambda Control. The closed-loop control concept pre-

IPR2023-01234
Petitioner - Ex. 1017 - Page 109

TABLE 6.2 Summary of Emission Levels for Spark-Ignition Engines
(Status: July 1992)

		Exhaust emission limits						
	Start of sale	HC	CO	NO_x	HC + NO_x	Unit	Remarks	
California	MY 1993	0.25	3.4	0.4	—	g/mile		
	MY 1994	0.125	3.4	0.2	—	g/mile	TLEV 10 %	% of fleet,
	MY 1997	0.075	3.4	0.2	—	g/mile	LEV 25 %	stepwise
	MY 1997	0.04	1.7	0.2	—	g/mile	ULEV 2 %	increase
	MY 1998	0.0	0.0	0.0	—	g/mile	ZEV 2 %	
USA (Fed.)	MY 1983	0.41	3.4	1.0	—	g/mile		
	MY 1994	0.25	3.4	0.4	—	g/mile		
	MY 2003	0.125	1.7	0.2	—	g/mile	on need	
Japan	4/1981	0.25	2.1	0.25	—	g/km	10-mode	
EG	1992	—	2.72	—	0.97	g/km	MVEG I	
	10/1996	0.15	2.1	0.3	—	g/km	MVEG II	proposal parliament
		—	2.2	—	0.5	g/km		proposal commission
	1996	—	1.5	—	0.2	g/km	MVEG III	proposal Germany

TLEV: Transitional Low-Emission Vehicles
ULEV: Ultra Low-Emission Vehicles
LEV: Low-Emission Vehicles
ZEV: Zero-Emission Vehicles
MVEG: Motor Vehicle Emission Group

sently in use in spark-ignition engines is based on 2-point lambda = 1 control (Fig. 6.3) with the mixture composition oscillating around the optimum lambda. When the exhaust mixture shifts from rich to lean, the voltage from a lambda = 1 probe drops from approximately 800 mV (lambda < 1) to approximately 100 mV (lambda > 1), with a steep signal change (lambda jump) occurring at lambda = 1 (Sec. 6.2.1). Once the signal from the sensor crosses beyond the specified threshold value (e.g., 450 mV), the system responds by progressively leaning out the mixture until the probe signal drops below this border again. Once this process is completed, the system reverts to graduated mixture enrichment. Depending upon the system lag, the subsequent control-oscillation rate will lie in the 0.5 . . . 5 Hz range, with an amplitude of $\Delta\lambda = \pm 0.01 \ldots 0.05$ relative to the median lambda. During the lean-operation period, the catalytic converter stores oxygen for release during the rich-mixture phases. This arrangement ensures high conversion rates despite the control oscillations. Preferably an algorithm with proportional plus integral characteristics (PI controller) is used. Variations in system lag and integrator pitch affect the amplitude and the frequency of the oscillations. The proportional factors have to be adapted. Because load and rpm have a major effect on system lag, control parameters are defined and stored in a load/rpm control map.

Continuous Lambda = 1 Control. A continuous lambda = 1 control can be employed to achieve substantially smaller control deviations, providing attendant reductions in emissions, especially when used with aged catalytic converters. An oxygen sensor with a roughly linear or linearized lambda characteristic curve is required for this arrangement (Secs. 6.2.5 and 6.2.6).

6.1.5 On-Board Diagnosis (OBD II)

From the 1994 model year onward, on-board devices capable of monitoring the operation of all emission-relevant vehicle components will be required in the United States. Pollutant emission sensors (see Sec. 6.6) to measure levels of CO, NO_x, and HC emissions downstream from the catalytic converter represent an ideal means of monitoring the performance of both converter and oxygen sensor. Unfortunately, there are still no sensors of this type suitable for

IPR2023-01234
Petitioner - Ex. 1017 - Page 110

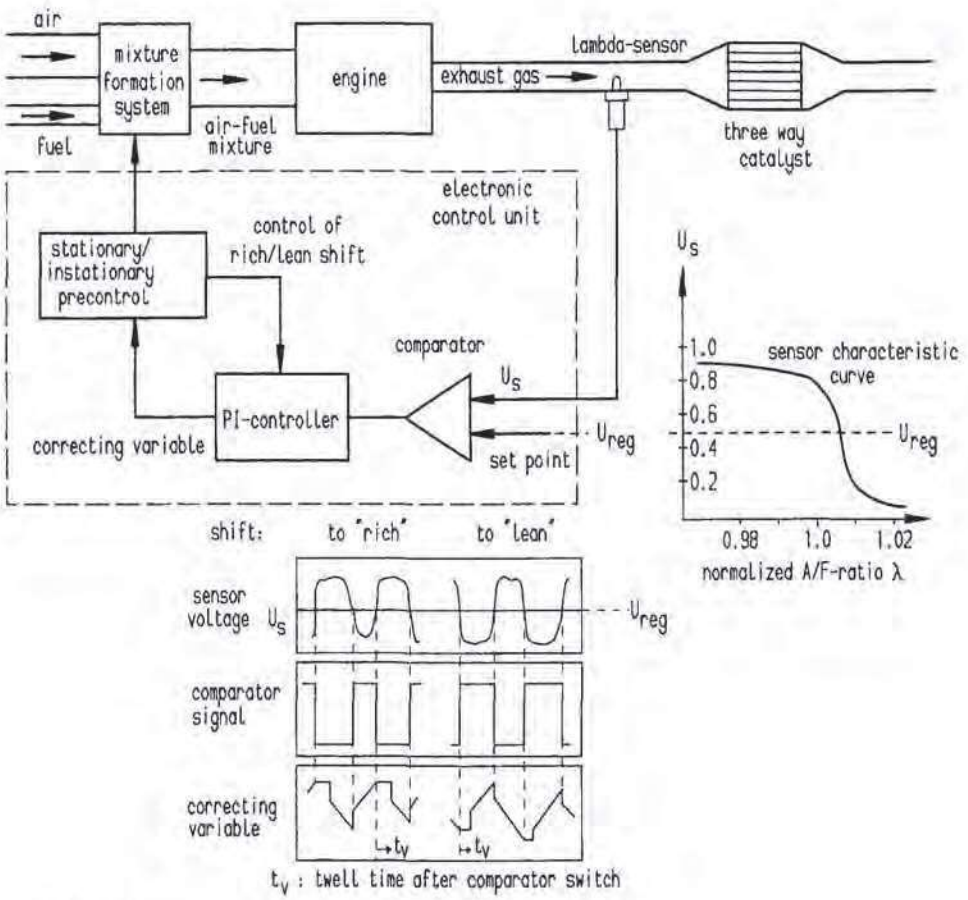


FIGURE 6.3 Operating diagram for lambda control.

use in the engine's exhaust stream. As an alternative, there exist concepts that employ a second oxygen sensor behind the catalytic converter to detect aging in the converter and/or the lambda sensor.

6.2 PRINCIPLES OF EXHAUST GAS SENSORS FOR LAMBDA CONTROL

6.2.1 Lambda = 1 Sensor: Nernst Type (ZrO_2)

Sensing Mechanism. In principle, the lambda sensor operates as a solid-electrolyte galvanic oxygen-concentration cell (Fig. 6.4). A ceramic element consisting of zirconium dioxide and yttrium oxide is employed as a gas-impermeable solid electrolyte. This mixed oxide is an almost perfect conductor of oxygen ions over a wide temperature range (Sec. 6.3). The solid electrolyte is designed to separate the exhaust gas from the reference atmosphere. Both sides feature catalytically active platinum electrodes. At the inner electrode (air; $pO_2'' - 0.21$ bar), the electron reaction

$$O_2 + 4e^- \rightarrow 2\,O^{2-} \tag{6.3}$$

incorporates oxygen ions in the electrolyte. These migrate to the outer electrode (exhaust gas; pO_2' variable < pO_2''), where the counterreaction occurs at the three-phase boundary (elec-

IPR2023-01234
Petitioner - Ex. 1017 - Page 111

trolyte-platinum-gas). A counteractive electrical field is created, and an electrical voltage U_s corresponding to the partial-pressure ratio is generated in accordance with the Nernst equation:

$$U_s = \frac{RT}{4F} \ln \frac{pO_2''}{pO_2'} \tag{6.4}$$

where R = general gas constant
F = Faraday's constant
T = absolute temperature
pO_2 = partial pressure of oxygen

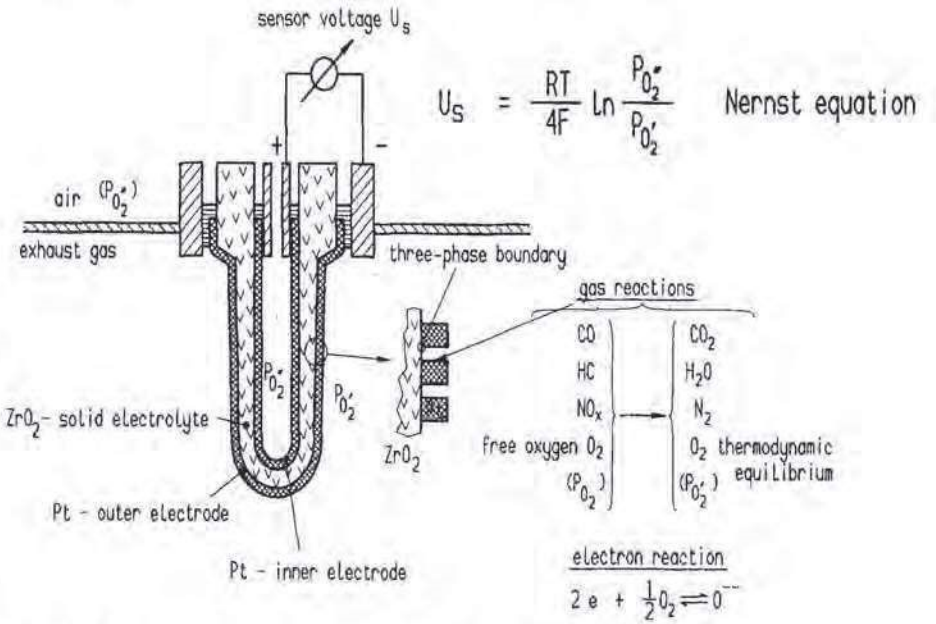


FIGURE 6.4 Diagram illustrating design and operation of a lambda = 1 sensor.

Catalytic Process. Measurements of oxygen content can only serve as the basis for unambiguous conclusions regarding the lambda of the exhaust gas when a state of thermodynamic gas equilibrium is established at the catalytically active electrodes on the oxygen sensor (residual oxygen). The absolute concentrations of the individual components in the engine's exhaust gases fluctuate across a wide range in accordance with the instantaneous operating conditions (warm-up, acceleration, steady-state operation, deceleration). The oxygen sensor must thus be capable of converting the gas mixture that it receives into a state of complete thermodynamic equilibrium. The resulting requirements are a high level of catalytic activity at the electrode and a protective layer capable of limiting the gas quantity. Should it prove impossible to achieve thermodynamic equilibrium at the electrode, the sensor's lambda signal will be erroneous.

Characteristic Curve. The concentration of residual oxygen fluctuates exponentially (by several orders of 10) in the vicinity of a stoichiometric air/fuel mixture (lambda = 1). In accordance with Eq. (6.4), this leads to massive variations in sensor voltage (lambda = 1 jump) with the characteristic lambda curve (Fig. 6.5).

Reference Atmosphere. Ambient air is the most commonly used O_2 reference. Alternatives include a metal-metal oxide mixture or a pumped reference medium. With this method, an O_2 reference pumping current is superimposed on the voltage measurement to generate an approximately constant O_2 partial pressure at the encapsulated reference electrode.

IPR2023-01234
Petitioner - Ex. 1017 - Page 112

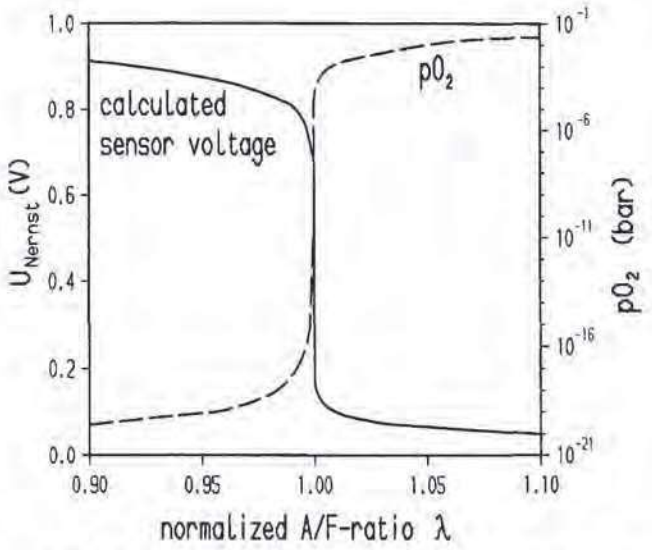


FIGURE 6.5 Equilibrium partial pressure of oxygen pO_2 and resulting curve for Nernst voltage at ≈ 700 °C relative to the normalized air-fuel ratio lambda.

6.2.2 Lambda = 1 Sensor: Semiconductor Type

Sensing Mechanism. Oxidic semiconductors such as TiO_2 and $SrTiO_3$ rapidly achieve equilibrium with the oxygen partial pressure in the surrounding gas phase at relatively low temperatures. Changes in the partial pressure of the adjacent oxygen produce variations in the oxygen vacancy concentration of the material (TiO_{2-x} respectively $SrTiO_{3-x}$), thereby modifying its volume conductivity.

$$R_T = A\ pO_2^{n} \exp\left(\frac{E}{kT}\right) \tag{6.5}$$

where R_T = semiconductor resistance
A = constant
E = activation energy
k = Boltzmann constant
T = absolute temperature
$n \approx 1/4$.

This effect, which is exploited to determine lambda, is also superposed by the conductivity's temperature dependence. Electrical resistance and sensor response times are both inversely proportional to temperature, as equilibrium is achieved more rapidly through diffusion in the oxygen vacancies.

Design. The ability to dispense with an O_2 reference allows an extremely simple design featuring an integrated heater. The porous semiconductor thick-film layer is generally positioned and sintered onto a planar Al_2O_3 substrate between two electrodes. Thin-film layers are also being developed as an alternative.

Characteristic Curve. At lambda = 1, the sensor layer displays an extreme change in conductivity due to the large pO_2 variation (see Sec. 6.2.1 and Fig. 6.5). When new, TiO_2 sensors provide essentially the same response as ZrO_2-based lambda = 1 probes. Variations in the rates of increase for lean and rich resistance and for response time occur over its lifetime, with the emission-control system undergoing a significant shift toward lean.

IPR2023-01234
Petitioner - Ex. 1017 - Page 113

Principles of Operation. A voltage is applied to the TiO_2 resistor R_T and a serial reference resistor. The voltage drop at the serial resistor depends on R_T, respectively on lambda. In a three-pole version, the applied voltage is taken from the heater voltage; for the four-pole version (insulated ground) a separate supply is employed. Temperature compensation may be required, depending upon the specific application.

6.2.3 Lean A/F Sensor: Nernst Type

Sensing Mechanism. It is always possible to employ a potentiometric lambda = 1 sensor (Sec. 6.2.1) as a lean A/F sensor by using the flat part of the Nernst voltage curve (Sec. 6.4 and Fig. 6.5) to derive the values at lambda > 1. The diminutive characteristic sensor voltages in this lambda range ($U_S < 65$ mV at lambda > 1.05) mean that stringent requirements for consistency must be met. Minute voltage deviations of just a few mV are sufficient to produce substantial errors in lambda.

Design. For this reason, special sensors must be employed in applications in which quantitative determination of lambda > 1.05 is required. To this end, special electrode manufacturing techniques are used to enhance catalytic activity, while a power heater (18 W) is used in conjunction with a protection tube featuring a lower gas-flow rate to provide a more constant ceramic temperature.

Principles of Operation. A high-output input amplifier is required for measurement of the low voltage levels associated with lean exhaust gases. In vehicle testing, lambda control has proven effective when used together with a classical mixture regulator. Even alternating operation (lambda = 1 and lean) with a sensor in the same vehicle is possible. Depending upon accuracy requirements, lean operation is possible in a range extending to lambda ≈ 1.5.

Nonautomotive Applications. Lambda-controlled operation can be employed to maintain narrow tolerances and to limit drift in oil- and gas-fired units; the benefits include low fuel consumption, enhanced safety, and lower emissions. The use of sensors in stationary power plants—for instance, in central heating plants—is particularly interesting as a potential means of dealing with fluctuations in the calorific content of the fuel.

6.2.4 Lean A/F Sensor: Limiting-Current Type

Sensing Mechanism. An external electrical voltage is applied to two electrodes on a heated ZrO_2 electrolyte to pump O_2 ions from the cathode to the anode (electrochemical O_2 pumping cell) (Fig. 6.6*a*). When a diffusion barrier impedes the flow of O_2 molecules from the exhaust gas to the cathode, the result is current saturation beyond a certain pumping voltage threshold (limiting current condition). Because the resulting limiting current I_1 is roughly proportional to the exhaust gas' oxygen concentration c_{O2}

$$I_1 = 4FD \frac{Q}{L} c_{O2} \tag{6.6}$$

where F = Faraday's constant
D = diffusion coefficient
Q = effective diffusion cross section
L = effective diffusion length

Design. Figure 6.6*b* provides a schematic illustration of this sensor type featuring planar technology and an integrated electric heater element.

IPR2023-01234
Petitioner - Ex. 1017 - Page 114

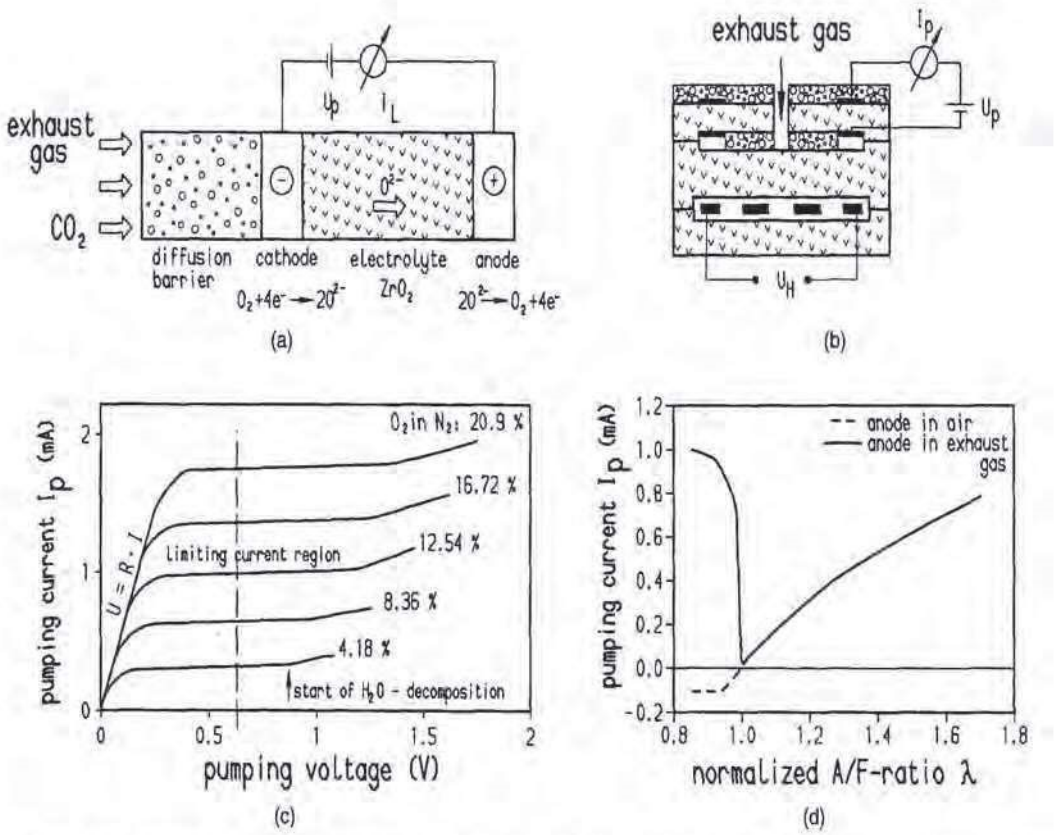


FIGURE 6.6 Limiting current sensor: (*a*) principle of operation; (*b*) schematic diagram; (*c*) current/voltage characteristics; (*d*) response curve as function of lambda.

Characteristic Curve. Figure 6.6*c* shows the current-voltage pattern for a limiting current sensor at various O_2 concentrations. If, at a constant pumping voltage, the pumping current is entered above lambda instead of c_{O2}, the resulting curve will correspond to Fig. 6.6*d*. In lean exhaust gas, the signal drops in response to reductions in lambda as indicated in Eq. (6.7), but below lambda = 1 there is a radical surge. This response pattern is at variance with the basic theory, and can be explained as the result of decomposition effects at the cathode. As a result, this sensor is only suitable for use in lean gases. Depending upon the design of the diffusion barrier (pore radius to free path length for the gas molecules, according to the proportion of gas phases to Knudsen diffusion), various relationships are observed between pumping current (measurement signal) and exhaust pressure and sensor temperature.

Principles of Operation. Depending on the accuracy requirements, a stable operating temperature in the range 600 to 800 °C is needed. Pumping voltages must always be selected to satisfy the conditions for limiting current. In addition, this limiting current has to be calibrated due to the manufacture scattering of the diffusion gap.

6.2.5 Wide-Range A/F Sensor: Single-Cell

Design and Operation. When the anode of a limiting current sensor of the type described in Sec. 6.2.4 is exposed to reference air instead of to the exhaust gas, the total voltage U_S at the probe will be the sum of the effective pumping voltage U_P and a superimposed Nernst voltage U_N.

$$U_S = U_P + U_N \tag{6.7}$$

IPR2023-01234
Petitioner - Ex. 1017 - Page 115

In operation, holding U_S to, as an example, 500 mV will produce a positive pumping voltage in lean exhaust gases ($U_N < 500$ mV); the diffusion limits the rate at which O_2 is pumped from the cathode to the anode. At lambda = 1 ($U_N \approx 500$ mV), the pumping voltage and, with it, the pumping current drop toward zero. In rich exhaust gas ($U_N > 500$ mV), the effective pumping voltage U_P becomes negative, causing oxygen to be pumped from the reference air electrode to the exhaust gas electrode ($I_P < 0$), where it reacts with the rich gas components CO, H_2, and HC.

Characteristic Curve. The pumping current displays a uniform upward trend between mildly rich and extremely lean lambda values (Fig. 6.6*d*).

Applications. This type of sensor is in series production as a thimble-type design for lean-mix concepts. In this application, operation as a limiting current sensor is restricted to lean conditions; during operation at lambda = 1, the pumping voltage is switched off and the Nernst voltage serves as the control signal.

6.2.6 Wide-Range A/F Sensor: Dual-Cell

Design. Skillful combination of a limiting-current sensor with a Nernst concentration cell on a single substrate will produce a dual-cell wide-range A/F sensor. The pumping and concentration cells are made of ZrO_2. Each cell is coated with two porous platinum electrodes, and they

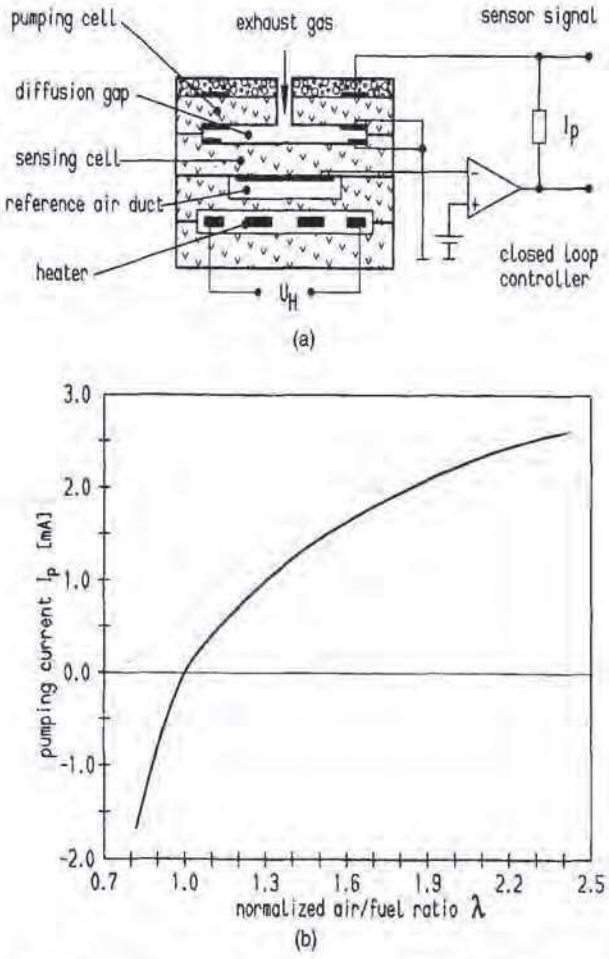


FIGURE 6.7 Dual-cell wide-range A-F sensor: (*a*) schematic diagram; (*b*) response curve as function of lambda ($T_{gas} \approx 400$ °C, $P_H \approx 12$ W).

IPR2023-01234
Petitioner - Ex. 1017 - Page 116

are arranged with a measurement gap of approximately 10 to 50 μm in height between them. A gas-intake opening in the solid electrolyte connects this measurement gap to the exhaust gas while the gap is serving as a diffusion barrier to control limiting current (Fig. 6.7).

Operation Mode. An electronic circuit regulates the current applied to the pumping cell to maintain a constant gas composition (for instance, lambda = 1) in the measurement gap. This corresponds to a Nernst-cell voltage of $U_N \approx 450$ mV. If the exhaust gas is lean, the pumping cell drives the oxygen outward from the measurement gap. If the exhaust gas is rich, the flow direction is reversed and oxygen from the surrounding exhaust gas (e.g., from decomposition of CO_2 and H_2O) is pumped into the measurement gap.

Characteristic Curve. The pumping current is proportional to the oxygen concentration (or oxygen requirement). With the attendant electronic control circuitry, an unambiguous, linear signal increase over a wide lambda range of 0.7 < lambda < infinite (air) can be obtained if the current is calibrated due to the manufacture scattering (Fig. 6.7). The integrated heating element provides an operating temperature in excess of 600 °C.

6.3 TECHNOLOGY OF CERAMIC EXHAUST GAS SENSORS

6.3.1 ZrO_2-based Sensors

The zirconium dioxide used to manufacture oxygen sensors is not pure; instead, the solid electrolyte consists of a mixed oxide, ZrO_2/Y_2O_3. The Y_2O_3 concentration used for actual applications lies in the 4 to 5 mol% range. This level is commensurate with optimum sensor operation in the important properties of ion conductivity, thermal stability, and mechanical strength.

Ion Conductivity. The substitution of trivalent yttrium ions for quadrivalent zirconium ions leads to the formation of oxygen vacancies through which the oxygen ions can move. Initially, the increases in ion conductivity are roughly proportional to the rise in Y_2O_3 content, as they are accompanied by a simultaneous rise in the number of oxygen vacancies. This pattern is observed with yttrium as well as with other bi- and trivalent alkaline earth metals, at least until a certain level of defect concentration is reached. Beyond this limit, the mutual influence of the vacancies reaches such levels that any further increases in defect concentration are accompanied by reductions in ion conductivity. The maximum is obtained at approximately 9 to 10 mol% Y_2O_3.

Phase Composition and Mechanical Stability. At room temperature, zirconium dioxide is monocline. It becomes tetragonal (metastable) above 1200 °C, and assumes a cubic form beyond 2370 °C. Yttrium doping can be employed to partially or completely stabilize the tetragonal and cubic modification, even at room temperature (PSZ—partially stabilized zirconium; FSZ—fully stabilized zirconium, above approximately 10 mol%, with certain manufacturing processes 7 to 8 mol% Y_2O_3). ZrO_2, with an essentially monocline structure, does not display sufficient resistance to temperature fluctuations for application in automotive exhaust systems—the changes in the geometry of the individual crystallites which accompany the phase transition lead to fatigue symptoms in the ceramic material. At the same time, the cubic phase does not possess the physical strength required to resist the physical shocks and thermal stresses. However, good mechanical characteristics can be obtained by using partially stabilized ceramic materials, with maximum strength being achieved within the range of 2 to 4 mol% Y_2O_3.

Manufacture of Partially Stabilized ZrO_2 Ceramics. The most common procedure consists of mixing and grinding the ZrO_2 and Y_2O_3 together (mixed oxide). The differences in the

IPR2023-01234
Petitioner - Ex. 1017 - Page 117

length of the diffusion paths—the two oxides are located adjacently as separate powder particles—do not generally produce a completely homogeneous distribution of yttrium in the ZrO_2. Thus, both fully stabilized cubic crystallites and tetragonal crystallites can be formed during the sintering process. During the phase transition to monocline ZrO_2 that takes place during cooling, the latter provoke internal tension, causing the ceramic material to harden. Certain combinations of yttrium concentration and manufacturing techniques can be employed to obtain exclusively tetragonal crystallites, which remain stable even after cooling (TSZ—tetragonal stabilized zirconia). Due to the absence of a phase transition within the temperature range associated with the intended application, stabilized tetragonal zirconium dioxide displays a virtually constant coefficient of thermal expansion. Both of the partially stabilized ZrO_2 ceramics described here are used in the manufacture of oxygen sensors.

6.3.2 Thimble-Type Sensors

Shaping. The ceramic base (Fig. 6.4) is shaped in the usual manner with dry pressing of granulated ZrO_2 and subsequent grinding of the compact material.

Electrodes. The application of the gas-permeable platinum electrodes is one of the most critical processes in the manufacture of oxygen sensors. A basic distinction is made between two different procedures:

Thin-Film Process. In this process, a thin microporous platinum layer (electrode thickness < 1 μm) is applied to the previously sintered base using one of three methods: thermal evaporation, sputtering, or chemical deposition with subsequent thermal treatment.

Thick-Film Process. In this process, a (for example) platinum-cermet layer (mixture of noble metal and ceramic phase) is printed onto the unsintered base (electrode thickness 5 to 10 μm).

As far as actual operation is concerned, the salient difference between the two processes resides in the fact that the three-phase boundary required for the conversion of oxygen (common border of platinum, zirconia, and gas phase) remains restricted to the surface of the base when thin-film electrodes are used. In contrast, the use of thick-film cermet electrodes with a ceramic phase of ZrO_2 results in a substantially larger border area along with enhanced high-temperature adhesion.

Protective Layer. As the outer electrode is exposed to the exhaust gases, a suitable protective layer, combining the requisite porosity with optimal adhesive properties, is essential to ensure the long-term stability of the oxygen sensor. In the conventional plasma or flame-spraying process, a porous layer 50 to 300 μm in thickness (e.g., magnesium spinel) is applied to the sintered and electrodes-equipped base. A cofiring technique with ZrO_2-based protective layers or a combination of both processes is being employed in the production of a new generation of oxygen sensors with enhanced long-term stability.

Well-defined porosity levels must be maintained to ensure satisfactory operation. With cofired protective layers, the required porosity level can be obtained by using organic pore-forming substances, which are burned out during sintering, or by adding a second, sinter-inactive ceramic phase, such as Al_2O_3. Porous protective layers also provide a diffusion barrier for the exhaust-gas molecules before they reach the electrodes. These layers thus exercise a determining influence on the sensor's control characteristics because the components of the exhaust gas which exhibit various diffusion coefficients are not in a state of thermodynamic equilibrium (see Sec. 6.4). This effect can be partially neutralized through defined pigmentation in the protective layers, which not only display catalytic characteristics, but can also inhibit contamination.

6.3.3 Planar Oxygen Sensors

The planar oxygen sensor derives its designation from the fact that, as opposed to the thimble-type sensor, its design arranges all operating layers in plain, consecutive surfaces. The

IPR2023-01234
Petitioner - Ex. 1017 - Page 118

technology applied in their manufacture is quite similar to the multilayer technology employed to produce ceramic multilayer capacitors and high-density electronic circuit boards (e.g., MCM—multichip modules).

Manufacture of Ceramic Green Sheet. First, an organic binder phase is added to the ZrO_2 powder in a tape-casting process to produce ceramic substrate layers.

Printing on the Ceramic Green Sheet. A screen-printing process (thick-film process) is employed to attach the individual function groups, e.g., galvanic cell, pumping cell, reference-air duct and heater (see also Sec. 6.2) to the green tape in the desired layer sequence. Several printed layers are generally required for each side of the tape; these layers can also consist of various inorganic materials.

Lamination. A number of screen-printed substrates can be stacked and laminated (bonded in a process combining temperature and pressure) to form composite structures representing virtually any desired level of complexity. A simplified version of a lambda = 1 sensor in planar technology is illustrated in Fig. 6.8.

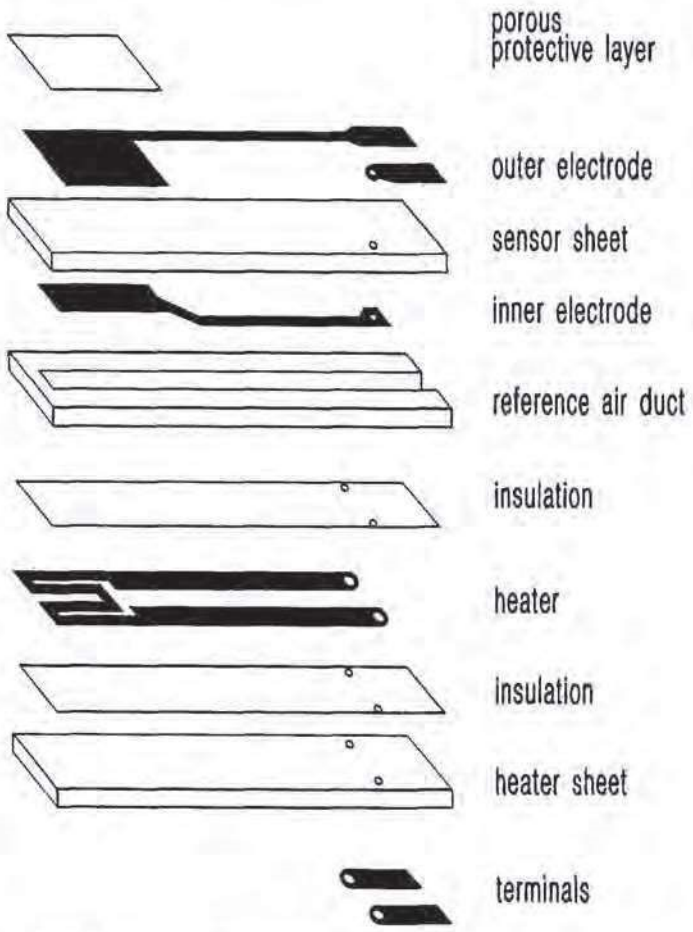


FIGURE 6.8 Layer structure of planar lambda = 1 sensor.

Advantages of Planar Technology. The application of surface-design technology also provides an additional advantage by making it possible to combine a number of individual elements on a single substrate for subsequent separation (multiple application) and sintering to form monolithic sensors with integrated heating elements. The coefficients of thermal expan-

IPR2023-01234
Petitioner - Ex. 1017 - Page 119

sion of the ZrO_2, cermet, and insulation layers must be precisely matched to ensure that the resulting ceramic elements display adequate thermal and mechanical stability.

Sensor elements manufactured with this new technology offer a number of advantages: the integration of heater and sensor provides a single unit with a lower total thermal mass, allowing substantial reductions in the continuous heating requirement (30 to 40 percent of that required with a thimble-type sensor), shorter delay between activation and readiness for active control, and smaller sensor dimensions. These characteristics make the unit ideal for meeting the demands of the modern motor vehicle (reductions in energy requirements, weight and space savings, and more stringent emission requirements). In addition, planar technology is an essential factor in obtaining complicated operating abilities such as those found in the dual-cell wide-range A/F sensor (see Sec. 6.2.6).

6.3.4 Al_2O_3-based Sensors

Sensors for oxygen and other exhaust gases which employ variations in the conductivity of the sensor material (TiO_2, SnO_2, etc.) to detect changes in the gas concentration are usually designed as planar sensors. The preferred substrate material is Al_2O_3. As the combinations of functions (e.g., heater, electrodes, etc.) are essentially those required with planar ZrO_2 sensors, the manufacturing techniques are also quite similar. Al_2O_3 provides advantages in the form of lower material costs and a simplified internal structure, made possible by the fact that Al_2O_3 maintains its good insulation properties at high temperatures. A disadvantage, particularly in terms of long-term stability, is the difficulty with sintering and sensor-material adhesion, as cofiring technology cannot be employed for this procedure.

6.3.5 Construction

Figure 6.9 shows completely assembled a heated thimble sensor and a planar lambda sensor. Although similar in external appearance—the planar sensor is somewhat shorter and narrower—the two units differ substantially in their respective internal structures. The differences are largely a result of the fact that heater and sensor in the heated thimble-type sensor are two separate components requiring assembly and electrical contact. Various ceramic support components are incorporated to enhance structural integrity and to ensure an impermeable seal between the reference air and the exhaust gases while also providing a degree of impact protection for the sensor unit. On the exhaust-gas side, the sensor elements receive both physical and thermal protection from a protection tube. Due to its basic design configuration, the planar sensor element does not share the rotational symmetry of its thimble-type counterpart. Thus, it must be installed in a specific position; the protection tube features a partial double wall to facilitate orientation. The offset inlet openings provide a uniform flow of exhaust gases past the measurement electrode, regardless of its position relative to the exhaust-gas stream. Thermal insulation from the exhaust gases is also improved.

Although unheated thimble-type sensors are still on the market, they are becoming less important due to the increasing demands for precision of emission control systems.

6.4 FACTORS AFFECTING THE CONTROL CHARACTERISTICS OF LAMBDA = 1 SENSORS

6.4.1 Factors Affecting the Static Curve

Due to the porous protective layer around the electrode, the steep voltage change in the sensor's characteristic curve does not occur at precisely lambda = 1; instead, it is displaced a small

IPR2023-01234
Petitioner - Ex. 1017 - Page 120

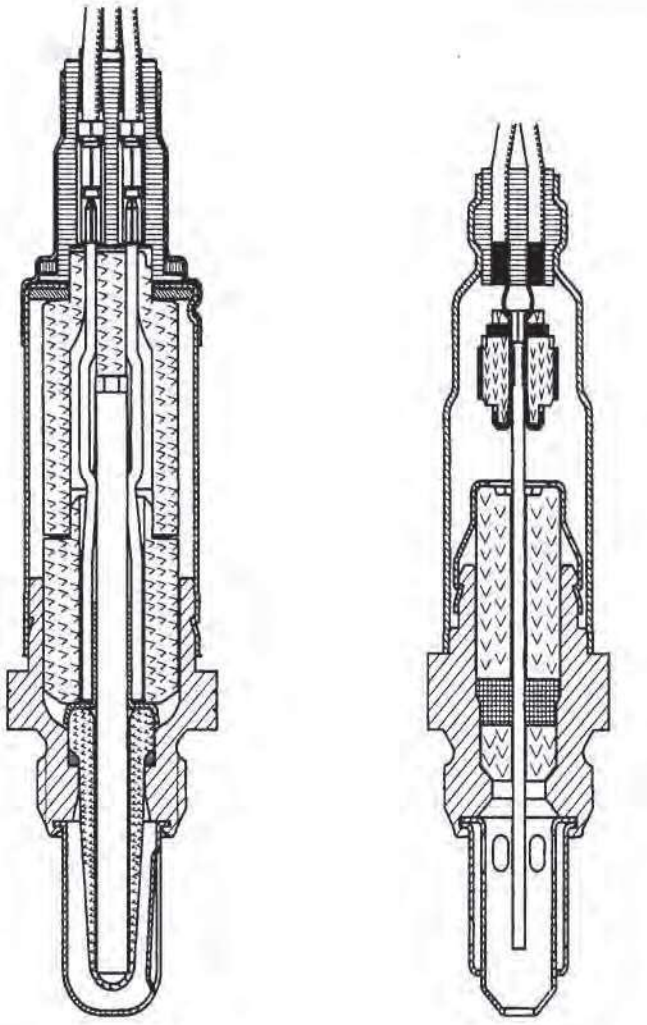


FIGURE 6.9 Construction of thimble-type and planar-type oxygen sensors.

amount into the lean range. The lower the porosity of the protective layer, the greater the diffusion of H_2 relative to O_2 toward the electrode. This phenomenon induces changes in the lambda value at the electrode relative to the lambda of the exhaust gas, the electrode detects richer exhaust gas and the lambda characteristic curve is displaced into the lean range.

Lean Shift. The lean shift is caused by exhaust-gas residue, such as oil ash and SiO_2, which partially plug the pores of the protective layer, and by reductions in sensor temperature.

Rich Shift. Fractures and flake-off of the protective layer lead to reductions in response times and shift the static characteristic curve toward rich. Electrode deactivation, especially due to lead contamination, will produce a flatter static response curve, as free, unconverted oxygen will also be detected. This effect also displaces the switchpoint threshold toward a lower lambda. A similar effect occurs when the reference atmosphere is contaminated (Chemical Shift Down, or CSD), for instance, with exhaust gases or water. Figure 6.10 shows typical characteristic curves for these conditions.

IPR2023-01234
Petitioner - Ex. 1017 - Page 121

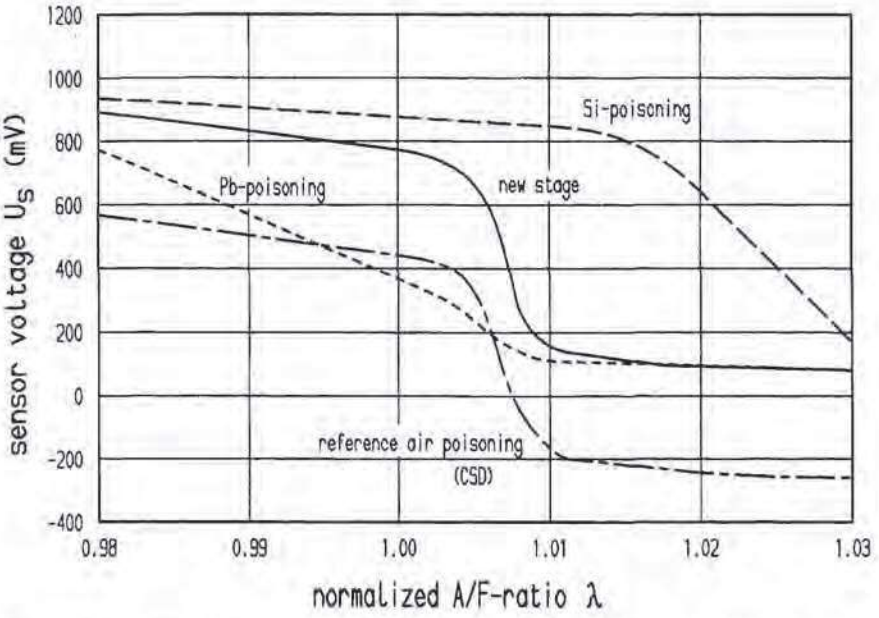


FIGURE 6.10 Effects of contamination on the static response curve of a lambda = 1 sensor as measured at laboratory test stand at $T_{gas} \approx 350$ °C.

6.4.2 Factors Affecting Sensor Dynamics and Control State

Factors. The control state (adjusted lambda) depends upon a number of factors. These include static sensor characteristics, sensor dynamics and asymmetry in sensor response times (switching times), t_{rs} (rich to switchpoint) during the surge from rich to lean, and t_{ls} (lean to switchpoint) during the jump from lean to rich. The sensor switching times t_{rs} and t_{ls} are strongly influenced by the configuration of the protection tube, the protective layer, and the sensor's temperature. Without the protection tube, switching times of less than 10 ms have been measured for ZrO_2 sensors with $T_{ceramic} \approx 900$ °C. However, such rapid response times are neither necessary nor desirable with many of the systems presently in use.

Response Times. An increase in response time that is not accompanied by a variation in the differential between t_{rs} and t_{ls} results in worse emissions with a constant control state due to the fact that the control amplitude increases while the conversion rate of the catalytic converter is reduced (see sec. 6.1.4 and Fig. 6.2).

Asymmetry. An asymmetrical increase in the response times t_{rs} and t_{ls} will also affect the control state due to the lambda shift.

Lean Shift. A pronounced increase in t_{rs} leads to a displacement toward lean. This can occur for any of several reasons. The dwell time in the rich exhaust gas is determined by control frequency and amplitude, and affects t_{rs} through the adsorption of CO and HC. Should the protective layer be obstructed (for instance, by oil ash), or should the sensor temperature drop, t_{rs} will generally rise more than t_{ls}.

Rich Shift. In contrast, a more pronounced rise in t_{ls} will lead to a displacement toward the rich range. The conversion rate of the electrode and the protective layer exercise a major influence on t_{ls}. Lead deposits diminish catalytic activity, causing t_{ls} to rise without exercising any substantive effect on t_{rs}.

Temperature. As a general rule, the susceptibility to sensor contamination is inversely proportional to electrode temperature. The factors determining the temperature of the ceramic material are the heater, the gas temperature, the gas flow rate (rpm, load), and the protection

IPR2023-01234
Petitioner - Ex. 1017 - Page 122

tube. Depending upon the installation location, the ceramic temperature generally lies between 350 and 1000 °C for exhaust temperatures ranging between 150 and 900 °C. The flow velocity of the gas varies between 2 m/s at idle, 40 m/s at moderate rpm and load, and up to 80 m/s under full load. The influence exercised by gas temperature and the protection tube can be seen in Fig. 6.11. The ceramic temperature has a major effect on the controlled lambda. A protection tube providing a lower gas flow (see Fig. 6.11: 1 hole/4 flaps) and a higher heater

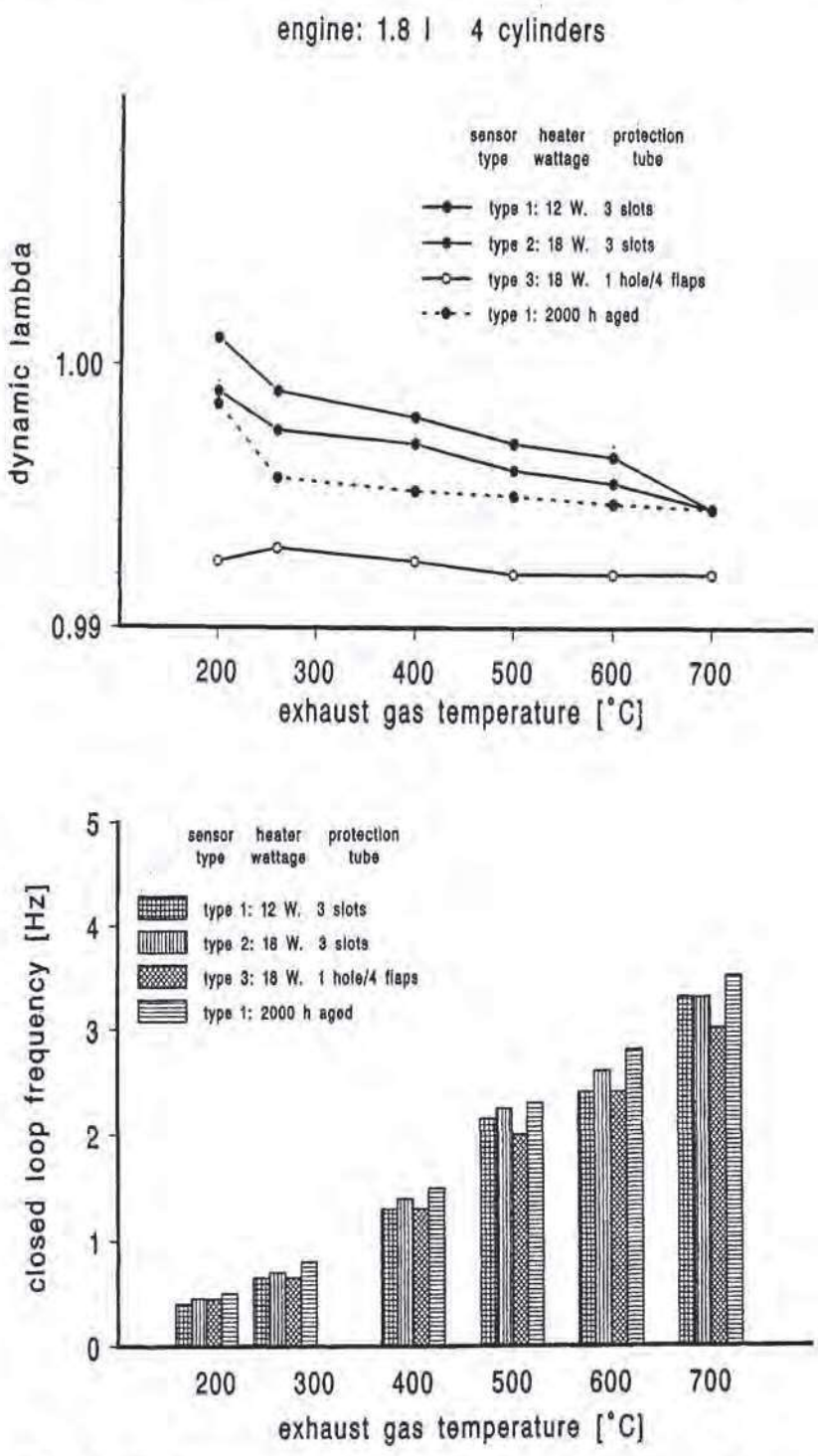


FIGURE 6.11 Effects of exhaust-gas temperature (rpm) on dynamic lambda and control frequency.

IPR2023-01234
Petitioner - Ex. 1017 - Page 123

power (18 W) will lead to higher ceramic temperatures with enhanced temperature consistency relative to exhaust temperature. This measure is employed to obtain a more stable controlled lambda. The lambda value displays a moderate rich shift compared to that obtained with a more open tube (see Fig. 6.11: 3 slots) and 12 W heater power.

System Lag. System lag is dependent on the sensor's installation position (0.2 to 2 m downstream from the exhaust manifold, with approx. 1 meter downstream from the exhaust valve being typical) and the gas velocity as determined by load, rpm, and the exhaust pipe diameter. It can be up to 500 ms at idle, and drops down to delays as low as 20 ms at full load. The sensor (protection tube, heater power) is of secondary significance (Fig. 6.11). The influence of sensor response times (t_{rs}, t_{ls}) on the control state increases as a function of their share of the total system lag.

tv Shift. The cumulative effect of all extraneous influences is a slight lean control state of the lambda = 1 sensor. Electronic compensation for the lean shift is available in the form of an asymmetrical control-oscillation pattern (see Sec. 6.1.4). This is provided either by means of a switching delay after the sensor surge (tv shift, Fig. 6.3), through variations in the controller's surge amplitude, and/or via asymmetrical ramp slope. Those parameters for the electronic lambda displacement which vary according to load and rpm can be stored as a program map in the electronic control unit (ECU). This method can be employed for lambda corrections up to $|\Delta\lambda| \leq 0.015$.

6.5 APPLICATIONS

6.5.1 Operating Conditions

Environmental Factors. Table 6.3 provides a summary of the types and magnitudes of the major stress factors affecting the sensor. Beyond the actual function of the sensor itself, optimal selection and precise mixture of all applied materials (ceramics, metals, synthetics) are essential factors in obtaining the thermal, mechanical, and chemical characteristics needed to achieve the obligatory extended service life of over 100,000 miles.

Sensor Installation Location. Because it is of determining significance for both external influences and control function, correct sensor location is a critical factor in calibrating the performance of the total lambda-control system. The sensor must be far enough from the exhaust valves to ensure that it monitors representative exhaust gases for all cylinders, but near enough to hold system lag to acceptable levels. Both factors affect emissions.

Thermal Stress. Thermal stresses at the sensor stem from the high-potential exhaust-gas temperatures as well as from the temperature gradients that occur. Exhaust temperature is essentially a function of engine speed, and can reach a maximum of 1000 °C at the sensor on high-performance engines. The most extreme temperature gradients at the sensor occur during hard driving directly in the wake of a warm start at which the exhaust system and the sensor have already cooled off. These conditions can produce exhaust-gas temperature gradients of up to 500 K/s.

Thermal Shock. In the warm-up phase following a cold start, condensation on the pipe walls can cause the ceramic material to crack once the electric heater warms it beyond the critical temperature of approximately 300 °C. Accumulations of condensation can be largely avoided by locating the sensor as close as possible to the engine to provide rapid heating of the upstream exhaust pipe. Depending upon the specific vehicle, a time delay for switching on the sensor heater may be required.

IPR2023-01234
Petitioner - Ex. 1017 - Page 124

TABLE 6.3 Overview of Stress Factors for Exhaust Gas Sensors

Mechanical stress	Stress caused by environmental conditions	Thermal stress	Stress caused by exposition to exhaust gas
Vibrational stress (<1300 m/s²) by engine vibration (<5 kHz) by pulsation of the exhaust gas (< ±300 mbar) by ambient wind (cable, <10 Hz)	Splash water, gush of water (in case containing NaCl, $CaCl_2$, $MgCl_2$)	Exhaust gas temperature (150 °C ... 1000 °C)	Exhaust gas composition ch between lambda = 0.85 (fuel load enrichment) and lambda infinite (overrun fuel)
Stone impact (<1.5 Nm)	Dust (organic, inorganic origin)	Exhaust gas temperature gradients at cold start (<500 K/s) at overrun fuel cutoff (<200 K/s)	Catalyst poisoning from fuel additives: permissible lead content: <0.013 g/l sulfur content: <0.1 % Br-, Cl-compounds
Installation/removal (torque about 50 Nm when assembled)	Oil, dirt undercarriage protection	Temperature increase after engine stalling (<300 °C at cable outlet)	Oil ash (Ca-, P-, S-, Zn-compounds up to 1 kg within ~60000)
Wire pull test (>70 N)	Fluctuation of the electrical supply system (9 ... 15 V)	Radiant heat (may require corresponding protective measures)	Miscellaneous corrosion products (e.g., Fe-oxides)
Handling (shock load up to 1000 g)	EMC (<200 V/m)		Condensation water
	Variation of climatic conditions (−40 °C ... +50 °C, 10 ... 100% rel. humidity)		

Mechanical Stresses. The main sources of mechanical stress on the sensor are vibration, exhaust-gas pulsation, stone impact, and cable tension (Table 6.3).

Sealing. The cable outlet of the sensor must be sealed to prevent water splash from penetrating to its interior and distorting the reference air (see Sec. 6.4.1 and Fig. 6.10). At the same time, the sealing element must be flexible enough to absorb the accelerative forces associated with vibration as well as any tensile forces transmitted through the cable.

6.5.2 Emission Certification

It would be impossible for a vehicle equipped only with an unregulated catalytic converter and lacking an oxygen sensor to achieve compliance with the American emission standards. When a regulated catalytic converter is used together with an oxygen sensor, emissions remain well below the limits. Even after vehicle mileage corresponding to more than 100,000 miles, the sensor limits emission increases to a minimum (Fig. 6.12). The introduction of a new system must be accompanied by precise calibration of the engine-control system to match the production tolerances and aging characteristics which affect the sensor's control response. The considerable effects that temperature and aging exercise on the catalytic converter must also be considered.

Durability Tests

Life Cycle. To determine aging behavior, the sensors undergo a standard durability test in the exhaust-gas stream of a test engine. The test cycle is designed to simulate combined urban and rural operation, and has been adopted by many automobile manufacturers as a standard program. The mean average speed is approximately 100 km/h for a midrange car. All newly developed products must withstand 2000 h (more than 100,000 miles) operation in this program without failure.

Hot Durability Testing. In a substantially more demanding test, essentially consisting of simulated full-load operation, the sensors must survive at least 1000 h (roughly 100,000 miles). The main stress factors for the sensors in these tests are thermal exposure (exhaust-gas temperatures reaching 950 °C, housing temperatures up to 650 °C), exhaust gas loads, and vibration.

IPR2023-01234
Petitioner - Ex. 1017 - Page 125

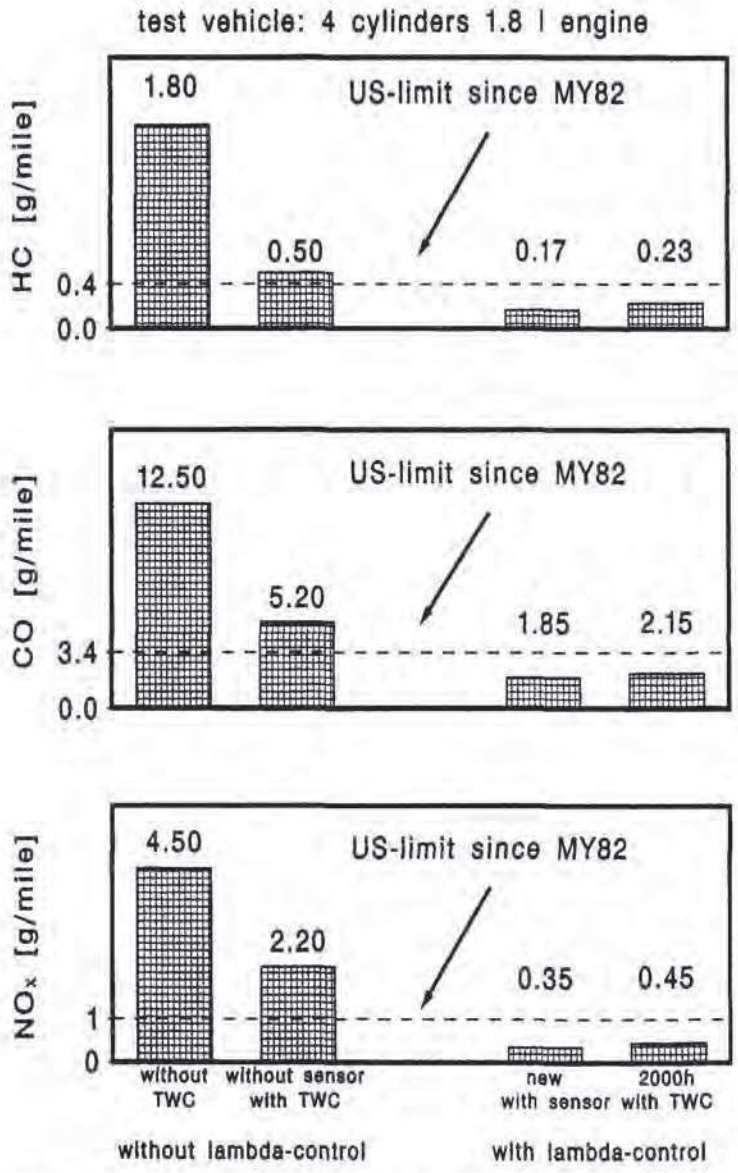


FIGURE 6.12 Comparison of emissions levels without catalytic converter, with unregulated converter, with controlled converter (new and old sensors, converter approx. 10,000 km).

Durability Testing of Contamination Resistance. Short durability tests featuring higher levels of Pb, Si, and oil are employed to determine the sensor's resistance to contamination damage.

6.6 SENSOR PRINCIPLES FOR OTHER EXHAUST GAS COMPONENTS

Sensors capable of monitoring the levels of the regulated toxic exhaust substances—CO, NO_x, and HC—would be desirable as elements of the On-Board Diagnosis systems (OBD I and OBD II) specified by the California Air Resources Board. Due to the extreme operating con-

IPR2023-01234
Petitioner - Ex. 1017 - Page 126

ditions, only a few of the many tested configurations have a chance to be used in engine-exhaust gas.

6.6.1 Mixed-Potential Sensors

Sensing Mechanism. If reduced catalytic activity prevents gas equilibrium from being achieved at the electrode of a galvanic ZrO_2 cell, competing reactions can occur. These, in turn, prevent a state of reduction/oxidation equilibrium in the oxygen, and lead to the formation of a mixed potential. This potential is determined by electrode activity, temperature, and gas composition. It is difficult to design manufacturing techniques that can consistently produce electrodes capable of maintaining specific, defined rates of catalytic activity over extended periods of time. Every change in electrode activity (for instance, due to aging) leads to a variation in mixed potential. Pt electrodes give rise to a mixed potential at very low temperatures, with extended response delays relative to lambda sensors. Other electrode materials with lower rates of catalytic activity continue to provide a mixed potential at higher temperatures, making it possible to achieve response times < 1 s.

Selectivity. Careful selection of electrode materials, operating temperature, and selective precatalyzation layers offers opportunities for improving selectivity.

Operation Mode. Because the effect is temperature-sensitive, a constant sensor temperature must be regulated in the range of 300 to 600 °C, depending upon the individual application.

6.6.2 Semiconductor Gas Sensors

Sensing Mechanism

Ceramic and Thick-Film Layers. On the surface of nonstoichiometric metal oxides such as SnO_2, TiO_2, In_2O_3, and Fe_2O_3 (*n*-type semiconductors), oxygen is absorbed and dissociated in air at high temperatures and is bonded to the crystal lattice. This leads to the formation of a thin depletion layer at the crystallite surface with a resultant arch in the potential curve. This phenomenon produces reductions in surface conductivity and higher intercrystalline resistance at the boundaries between two crystallites; this is the major factor determining the total resistance of the polycrystalline metal oxide. Oxidation gases such as CO, H_2, and C_xH_y, which react with surface oxygen, increase the density of charge carriers in the boundary layer and reduce the potential barrier. Reduction gases, such as NO_x and SO_x raise the potential barrier and, with it, the surface/intercrystalline resistance.

Thin-Film Layers. Compared to porous polycrystalline materials, thin-film layers display only limited numbers of crystalline boundaries at the layer surface for reaction with the exhaust gases. The depletion-layer barrier makes up a substantial proportion of the layer thickness on thin-film devices, meaning that changes in charge-carrier density within the barrier layer due to adsorbed gases will also result in substantial variations in the total resistance.

Selectivity. Selected doping materials and temperatures can be employed to achieve selectivity for CO, HC, or NO_x. The resistance of metal-oxide semiconductors is always a function of the partial pressure of the O_2.

Specific Influences of Exhaust Gas. Engine exhaust gas with minimal, highly variable O_2 partial pressures is characterized by a high level of O_2 cross-axis sensitivity. Within the lambda = 1 to lambda < 1 operating range, an irreversible long-term change in sensor resistance leading to disintegration of the metal oxide is also possible. High operating temperatures are conducive to the diffusion of oxygen vacancies and doping materials. When amplified by sintering effects, these lead to resistance drift and attenuated sensor response.

IPR2023-01234
Petitioner - Ex. 1017 - Page 127

Standard operating temperatures for metal-oxide gas sensors range from 100 to 500 °C, with up to 600 °C being seen in some restricted applications. With SnO_2, a high level of selectivity for, for example, CO can be achieved at temperatures as low as the 100 to 200 °C range. However, the response times can be measured in minutes. At higher temperatures, in the 300 to 550 °C range, response times of less than 1 s can be obtained, but with reduced selectivity.

6.6.3 Catalytic Gas Sensors

Sensing Mechanism. The catalytic gas sensor is essentially a temperature sensor featuring a catalytically active surface. An exothermic reaction (basically an oxidation reaction in air) at the catalytically active surface causes the temperature of the sensor to rise. The increase in temperature is proportional to the concentration of an oxidation gas in an excess-oxygen atmosphere. A temperature sensor of the same basic design—but without the catalytic response—is employed to enhance sensitivity and to provide temperature compensation by means of differential-signal evaluation. Materials employed for the temperature sensor include coiled Pt wire, Pt thin-film and thick-film layers, transistors, and NTC and PTC thermistors.

Operating Conditions. Catalytic gas sensors are relatively insensitive and can be employed in a range >1000 ppm. Excess oxygen is required to monitor concentrations. Due to the sensitivity to flow rate, these units are generally operated in flowheads with diffusion limiters. Measurement and reference sensors must be exposed to the same flow conditions, with no mutual thermal influences. Symmetrical configurations in pellet form are thus preferred over planar shapes. Operating temperatures for commercial sensors are in the 500 to 600 °C range, but extension to higher temperatures is possible. The requirement for long-term stability in the catalytic converter is the limiting factor governing the operating temperature. Catalytic gas sensors are not selective, instead providing a summing signal for all combustion gases. Thus catalytic sensors for application in exhaust gases are restricted to monitoring the state of the catalytic converter.

BIBLIOGRAPHY

Arndt, J., "Ceramics and Oxides," in W. Göpel, J. Hesse, and J. N. Zemel (eds.), *Sensors—Fundamentals and General Aspects,* vol. 1, S.252 ff, VCH Verlagsgesellschaft, Weinheim, 1989.

Barnes, G. J., R. L. Klimisch, and B. B. Krieger, "Equilibrium Considerations in Catalytic Emission Control," SAE Paper 730200, *SAE National Automobile Engineering Meeting,* Detroit, Jan. 1973.

Bosch, *Automotive Electric/Electronic Systems,* VDI, Düsseldorf, May 1987.

Bosch, *Automotive Handbook,* VDI-Verlag, Düsseldorf, 1986.

Duecker, H., K.-H. Friese, and W.-D. Haecker, "Ceramic Aspects of the Bosch Lambda-Sensor," SAE Paper 750223, *SAE National Automobile Engineering Meeting,* Detroit, 1975.

Gruber, H. U., and H. M. Wiedenmann, "Three Years Field Experience with the Lambda-Sensor in Automotive Control Systems," SAE Paper 800017, *SAE National Automobile Engineering Meeting,* Detroit, Feb. 1980.

Moseley, P. T., and B. C. Tofield (eds.), *Solid State Gas Sensors,* Adam Hilger, Bristol and Philadelphia, 1987.

Saji, K., "Characteristics of Limiting Current-Type Oxygen Sensor," *J. Electrochem. Soc.: Electrochem. Science and Technology,* vol. 134, no. 10, 1987, pp. 534–542.

Saji, K., H. Kondo, T. Takeuchi, and I. Igarashi, "EMF Characteristics of Zirconia Oxygen Sensor in Non-equilibrium Gas Mixtures Containing Combustible Gas and Oxygen," *Proc. 1st Sensor Symposium,* Tsukuba, Japan, June 1981, pp. 103–107.

Soejima, S., and S. Mase, "Multi-Layered Zirconia Oxygen Sensor for Lean Burn Engine Application," SAE Paper 850378, *SAE National Automobile Engineering Meeting,* Detroit, 1985.

IPR2023-01234
Petitioner - Ex. 1017 - Page 128

Takami, A., "Development of Titania Heated Exhaust-Gas Oxygen Sensor," *Ceramic Bulletin*, vol. 67, no. 12, 1988, pp. 1956–1960.

Wiedenmann, H. M., "Characteristics of Oxygen Sensors for Lean Exhaust Gas," *VDI Berichte* 578, S.129–151, VDI-Verlag, Düsseldorf, 1985.

ABOUT THE AUTHORS

HANS-MARTIN WIEDENMANN studied physics and meterology in Tübingen and Munich, where he received his Ph.D. in Physics in 1969. He joined Bosch in 1970 and is now senior manager for the development of lambda oxygen sensors.

GERHARD HÖTZEL studied chemistry in Konstanz and received his Ph.D. in 1986 at the University of Stuttgart. At Bosch, he is responsible for physical bases and measurement techniques for lambda oxygen sensors.

HARALD NEUMANN studied solid-state electronics in Aachen where he received a Ph.D. in 1988. Since that time, at Bosch he has been responsible for the technology of planar-type ceramic sensors.

JOHANN RIEGEL studied electrical engineering in Karlsruhe and received a Ph.D. in 1989. At Bosch he is responsible for the investigation of planar-type ceramic sensors.

HELMUT WEYL studied mechanical engineering in Darmstadt and was graduated from there in 1966. He has been with Bosch since 1968 and is now responsible for proving lambda oxygen sensors.

IPR2023-01234
Petitioner - Ex. 1017 - Page 129

CHAPTER 7
SPEED AND ACCELERATION SENSORS

William C. Dunn
Motorola Inc.
Semiconductor Products Sector

7.1 INTRODUCTION

In the automotive arena, speed and acceleration sensors are used in a wide variety of applications, from improving engine performance through safety to helping to provide creature comforts.

Speed sensing can be divided into rotational and linear applications. Rotational speed sensing has two major application areas: engine speed monitoring to enhance engine control, and performance and antilock breaking and traction control systems for improved road handling and safety. Linear sensing can be used for ground-speed monitoring for vehicle control, obstacle detection, and crash avoidance. Acceleration sensors are used in air bag deployment, ride control, antilock brake, traction, and inertial navigation systems.

In most cases, there are a number of different sensor types available for a specific monitoring function. However, the choice of sensor for a specific application can be difficult to make. The selection may be determined by the familiarity of the system's designer with the sensor. On the other hand, the output from one sensor can be used for several applications, and the individual requirements of each application may eventually determine the sensor to be used.

Electronics and electronic sensors are making rapid inroads into the automotive market. In order to analyze the large amounts of sensor data needed for low emissions and efficient engine control, it is necessary to process the information using microcontrollers (MCUs), which can operate at high speeds and in real time. Sensors that can convert information directly into a digital format for MCU compatibility have a distinct advantage over an analog output format. Digital signals are also supply-line voltage-insensitive, virtually unaffected by noise, and have better resolution than can be obtained with analog signals. If the addition of an analog-to-digital converter (on or off the MCU) is required for compatibility, the system cost is increased. The accuracy of the control system is only as good as the integrity of the sensor data supplied to the MCU. Hence, the importance of the performance of the sensor.

This chapter concentrates on speed and acceleration, and therefore does not go into all the other different types of applications for which many of these sensors can be used in the automobile.

IPR2023-01234
Petitioner - Ex. 1017 - Page 131

7.2 SPEED-SENSING DEVICES

In automotive applications, the environment must be taken into consideration. The sensing must be accurate, the devices must be rugged and reliable, and they must function in the presence of oil, grease, dirt, and inclement weather conditions. These requirements have severely limited the use of a number of otherwise practical alternatives, such as optical sensors and contact sensing.

In the area of rotational speed monitoring, the most practical devices use magnetic field sensing. These sensors are Hall effect devices, variable reluctance (VR), and magnetoresistive or magnetic resistance element (MRE) devices. Both the Hall effect and VR devices have been widely used and have a proven track record. The MRE device has only recently come into its own with improved technology and provides a viable alternative to the Hall effect device. The MRE device has a higher sensitivity and a wider operating temperature range than the Hall effect device.

For the measurement of ground speed and object detection, optical, radar, laser, infrared, and ultrasonics have been explored. Linear sensing devices typically use the Doppler effect for speed sensing and pulse modulation for distance measuring. These devices are used for object detection in blind spots when reversing or changing lanes, and in such applications as collision avoidance systems.

7.2.1 Variable Reluctance Devices

Variable reluctance devices are in effect small ac generators with an output voltage proportional to speed, but they are limited in applications where zero speed sensing is required. The operating frequency range of the VR device is from about 10 Hz to 50 kHz. It is insensitive to mechanical stress and has a wide temperature operating range from –40 to 190 °C. The supply voltage and offset drift will depend upon the control electronics. The VR device, originally designed around existing automotive electromechanical systems, was adapted for electronic control. The ferrous metal in the VR system is designed for maximum output voltage at low rpm (revolutions per minute), to get as close as possible to zero speed sensing without generating excessive voltages at maximum rpm (up to 150 V). This device gives a linear output voltage with frequency. Most systems use MCUs for data processing, so the VR device needs an analog-to-digital (A/D) converter to generate a digital signal for compatibility with the MCU. Although the VR device itself is inexpensive, the extra costs for data conversion may eventually lead to its demise in many automotive applications.

7.2.2 Hall Effect Devices

The Hall effect exists when a current flowing in a carrier experiencing a magnetic field perpendicular to the direction of current flow results in the current being deflected perpendicular to the field and to the direction of the current. The Hall effect is shown in Fig. 7.1. A current I_c flowing through the device between terminals 1 and 2 will produce a potential VH between terminals 3 and 4, when a magnetic field **B** is applied perpendicular to the device. The potential VH is determined by the strength of the magnetic field and the current flowing. Hall effect devices can be manufactured with indium, gallium arsenide, or silicon. A comparison of their properties is given in Table 7.1.

As can be seen, silicon is the most sensitive material. It is compatible with ICs and has a wide operating temperature range. The Hall effect device is well known both in industry and in the automotive arena for rotational and position-sensing applications. However, recent developments in Hall sensing devices, such as differential sensing and integration, have given improved sensor characteristics, which may result in greater potential in automotive applications.

IPR2023-01234
Petitioner - Ex. 1017 - Page 132

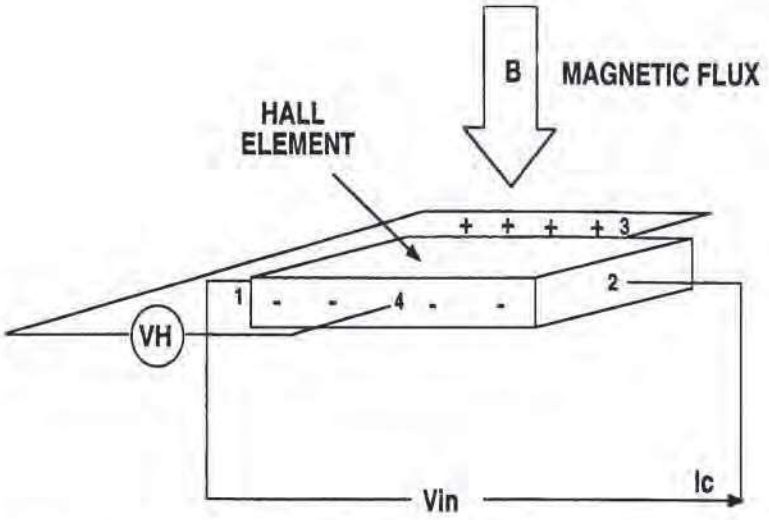


FIGURE 7.1 Hall effect.

The Hall effect device is very versatile, flexible in use, easy to package, and can be used for zero speed sensing (it can give an output when there is no rotation). Hall devices give a frequency output that is proportional to speed, making them compatible with MCUs. The Hall device is normally configured as a bridge to minimize temperature effects and to increase the sensitivity of the sensor.

A typical Hall effect sensor configuration with waveforms is shown in Fig. 7.2. The teeth of the ferrous wheel concentrate the magnetic flux when the teeth come into close proximity to the Hall sensor and magnet. The output from the sensor is a sinusoidal waveform, whose frequency is the rpm of the ferrous wheel multiplied by the number of teeth on the wheel. The resolution of the system depends on the number of teeth in the wheel (typically 20).

7.2.3 Magnetoresistive Devices

The magnetoresistive effect is the property of a current-carrying ferromagnetic material to change its resistivity in the presence of an external magnetic field. For example, a ferromagnetic (permalloy) element (an alloy containing 20 percent iron and 80 percent nickel) will change its resistivity by 2 to 3 percent when it experiences a 90° rotation in a magnetic field.[1] The resistivity value rises to a maximum when the direction of current and magnetic field are coincident, and is a minimum when the fields are perpendicular to each other. This relationship is shown in Fig. 7.3. This attribute is known as the Anisotropic Magneto Resistive Effect. The resistance R of an element is related to the angle q between the current and the magnetic field directions by the expression:

$$R = R_{\parallel} \cos^2 q + R_{l} \sin^2 q \tag{7.1}$$

TABLE 7.1 Comparison of Properties of Hall Effect Materials

Material	Operating temp. °C	Supply voltage	Sensitivity @ 1 kA/m	Frequency range
Indium	–40 to 100	1V	7 mV	0 to 1 MHz
GaAs	–40 to 150	5 V	1.2 mV	0 to 1 MHz
Si (with conditioning)	–40 to 150	12 V	94 mV	0 to 100 kHz

IPR2023-01234
Petitioner - Ex. 1017 - Page 133

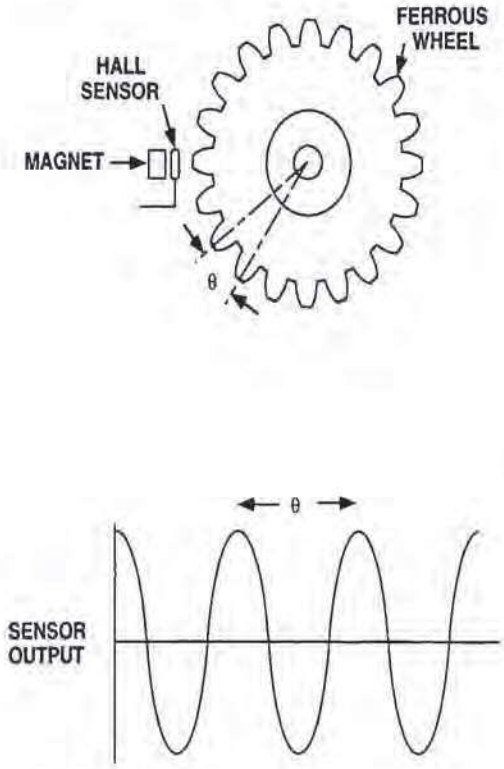


FIGURE 7.2 Hall sensor and output waveforms.

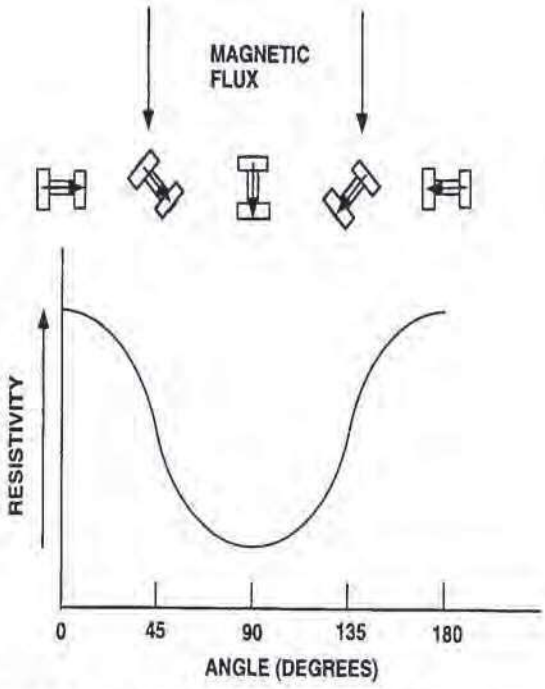


FIGURE 7.3 Relationship between magnetic field and resistivity change in MRE devices.

where $R_{\parallel}$ is the resistance when the current and the magnetic field directions are parallel and $R_{\perp}$ is the resistance when the current and the magnetic field directions are perpendicular.

MRE devices give an output when stationary, which make them suitable for zero speed sensing. MRE devices also give an output frequency that is proportional to speed, making for ease of interfacing with an MCU. For good sensitivity and to minimize temperature effects, a bridge configuration is normally used. In an MRE sensor, aluminum strips can be put across the permalloy element to linearize the device. This configuration is shown in Fig. 7.4 together with a typical MRE characteristic. The low-resistance aluminum stripes cause the current to flow at 45° in the permalloy element, which biases the element into a linear operating region.

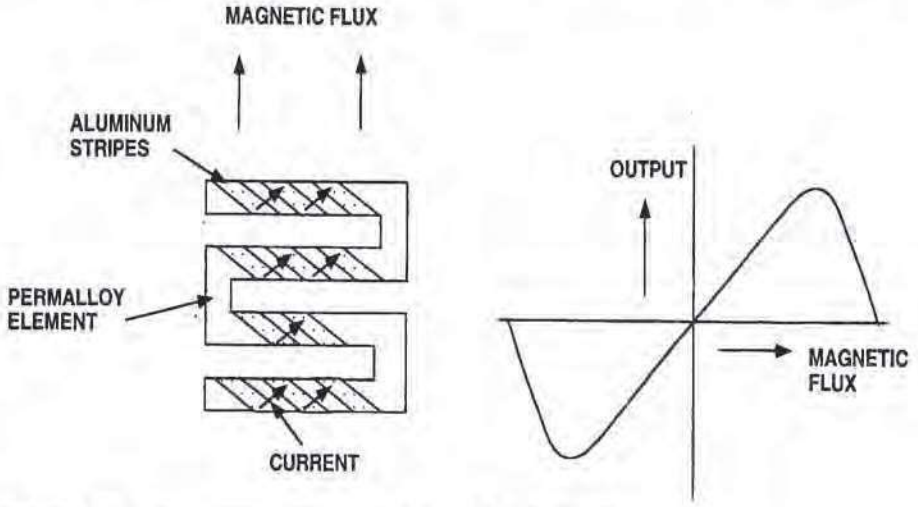


FIGURE 7.4 Use of permalloy strip for linearization in MRE devices.

Integrated MRE devices can typically operate from –40 to 150 °C, over a supply voltage range of 8 to 16 V, and at frequencies from 0 to 1 MHz. In comparing the MRE sensor to a Hall effect device, the MRE has a higher sensitivity, is less prone to mechanical stress, has a wider operating frequency range, has the potential of being more cost effective, gives better linearity, and is more reproducible. However, it is more sensitive to external magnetic fields. Table 7.2 shows a comparison of rotational sensing devices.

TABLE 7.2 Comparison of Sensing Devices

Sensor type	Operating temperature (°C)	Sensitivity 1 kA/m (mV)	Frequency range	Mechanical stress
Hall effect	–40 to 150	90	0 to 100 kHz	High
MRE	–40 to 150	140	0 to 1 MHz	Low
VR	–40 to 190		1 to 50 kHz	None
Magnetic transistor	–40 to 150	250	0 to 500 kHz	Low

It should be noted that Hall effect and MRE devices have many applications in the automobile outside of rotational speed sensing, such as position sensing, fuel-level sensing, and active suspension. The magnetic transistor is showing potential in rotational speed sensing and position-sensing applications, and may eventually be another viable contender to the Hall effect device in the automotive market.

7.2.4 Ultrasonic Devices

Ultrasonic devices can be used to measure distance, ground speed, and as a proximity detector. To give direction and beam shape, the signals are transmitted and received via specially configured horns and orifices. The transmitter and receiver horns are similar in shape, but are normally separate to accommodate different characteristics. The ultrasonic devices are made from PZT crystal-oriented piezoelectric material ($PbZrO_3$—$PbTiO_3$).

For the measurement of distance or object detection, a pulse of ultrasonic energy is transmitted and the time is measured for the reflected pulse to return to the receiver. The frequency of the transmitted ultrasonic waves are typically about 40 kHz and travel with a velocity of 340 m/s at 15 °C. This velocity changes with temperature and pressure. However, these parameters can be measured and corrections made if high accuracy is required. The repetition frequency and power requirements depend on the distance to be measured. To measure speed, the distance variation with time can be measured and the velocity calculated. A more common method is to use the Doppler effect, which is a change in the transmitted frequency as detected by the receiver due to motion of the target (or, in this case, the motion of the transmitter and receiver).

7.2.5 Optical and Radio Frequency Devices

Optical devices are still being used for rotational speed sensing. They are normally light-emitting diodes (LEDs) with optical sensors. Figure 7.5 shows a typical optical sensor system. An optical sensor detects light from an LED through a series of slits cut into the rotating disc, so that the output from the sensor is a pulse train whose frequency is equal to the rpm of the disc multiplied by the number of slits. The higher the number of slits in the disc, the smaller the angle of rotation that can be measured. The optical sensor can be a single photodiode or a photodiode array as shown. This array gives a more accurate determination of the position of the slit, resulting in higher resolution of the position of the disc.

IPR2023-01234
Petitioner - Ex. 1017 - Page 135

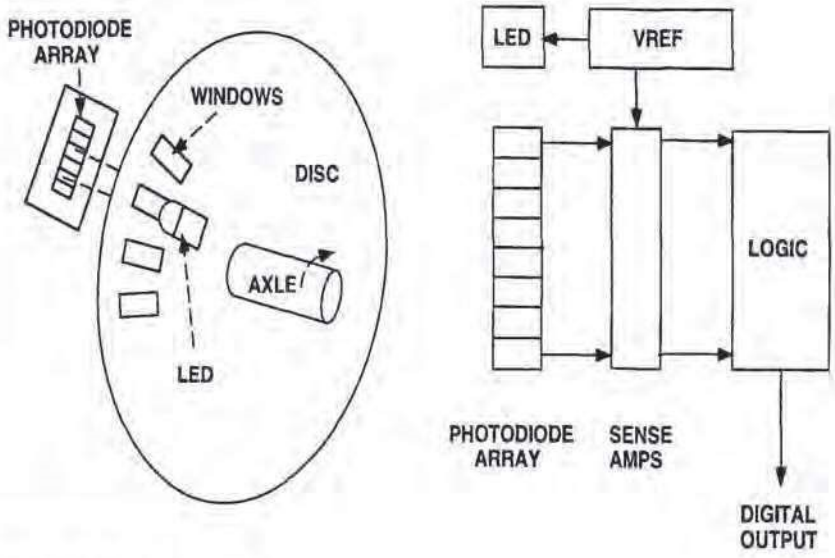


FIGURE 7.5 Optical sensor.

Optical and radio frequency (RF) devices are used for object detection, linear approach speed, and distance measurements in crash avoidance systems where distances greater than about 10 m are involved. These devices use the same principles as the ultrasonic devices. Optical devices normally use lasers or infrared devices for the transmitting source and optical sensors for the receivers. RF devices use gallium arsenide or Gunn devices to obtain the power and high frequency (about 100 GHz) required in the transmitter. The high operating frequency is set to a large extent by the need for a small antenna. These applications are under development and are discussed in Sec. 7.7.2.

7.3 AUTOMOTIVE APPLICATIONS FOR SPEED SENSING

There are several applications for rotational speed sensing. First it is necessary to monitor engine speed. This information is used for transmission control, engine control, cruise control, and possibly for a tachometer. Electronics and electronic sensing in the automobile were brought about by the need for higher-efficiency engines, better fuel economy, increased power and performance, and lower emissions. Second, wheel speed sensing is required for use in transmissions, cruise control, speedometers, antilock brake systems (ABS), traction control (ASR), variable ratio power steering assist, four-wheel steering, and possibly in inertial navigation and air bag deployment applications.

Linear speed sensing can be used to measure the ground speed. This measurement also has the possibly of use in ABS, ASR, and inertial navigation. Similar types of sensors can be used in crash avoidance, proximity, and obstacle detection applications.

7.3.1 Rotational Applications

The high timing accuracy that can be obtained with fuel injection systems and replacement of points by sensors have made cost-effective engine control and low maintenance a reality. Adjustment of the stoichiometric ratio of air to fuel, accurate ignition timing, and oxygen sensors in the exhaust system, have vastly improved engine performance and greatly reduced emissions over widely varying operating conditions. The two important factors in engine con-

IPR2023-01234
Petitioner - Ex. 1017 - Page 136

trol are the engine speed in rpm and the crank angle. These signals are used by the engine control MCU for determination of fuel injection and ignition timing. The engine rpm measurement range is from 50 to (say) 8000 rpm. A resolution of about 10 rpm is required for an accuracy of about 0.2 percent. For injection and ignition control in a six-cylinder engine, the interval between combustion at maximum rpm is 2.5 ms, so that this time sets the injection period. In practice, a crank angle accuracy of between 1 and 2 degrees per revolution is required. Newer systems with sequential fuel injection, may also require information on TDC (top dead center) for each cylinder to determine the timing. With the low frequencies involved in this application, either Hall effect or MRE devices can be used for monitoring both the engine rpm and crank angle.

Vehicle speed measurements are in the range 0 to 180 km/h (120 mph) and digital displays must have an accuracy of 1 km/h. Some systems have a mechanical pickoff from the drive shaft, which can then use optical sensors for the measurement of road speed. However, newer systems have a pickoff located directly on the drive shaft, which makes optical devices less practical. It is preferred to eliminate the remote sensing via mechanical coupling to save the cost of the associated mechanical components, seals, maintenance, and so on. One method of pickoff is a ring magnet with between 4 and 20 magnetic poles (depending on the required resolution). Figure 7.6 shows such a system using an MRE sensing device. The magnetic flux changes are sensed by an MRE bridge sensor when the magnet disc is rotating. The bridge is supplied from a voltage reference circuit, and its output is amplified and shaped to give a frequency output that is proportional to shaft rotation speed. A ferrous toothed wheel pickoff with magnet and flux concentrator can also be used (see Fig. 7.2). Vehicle speed sensing can be performed with Hall effect, MRE, or VR devices. The number of pulses P per second from the detector are counted to measure speed S, from the following relationship:

$$P = N \times S \times K \tag{7.2}$$

where N = the number of magnetic poles on ring magnet or wheel teeth
K = a constant determined by axle ratio and wheel size

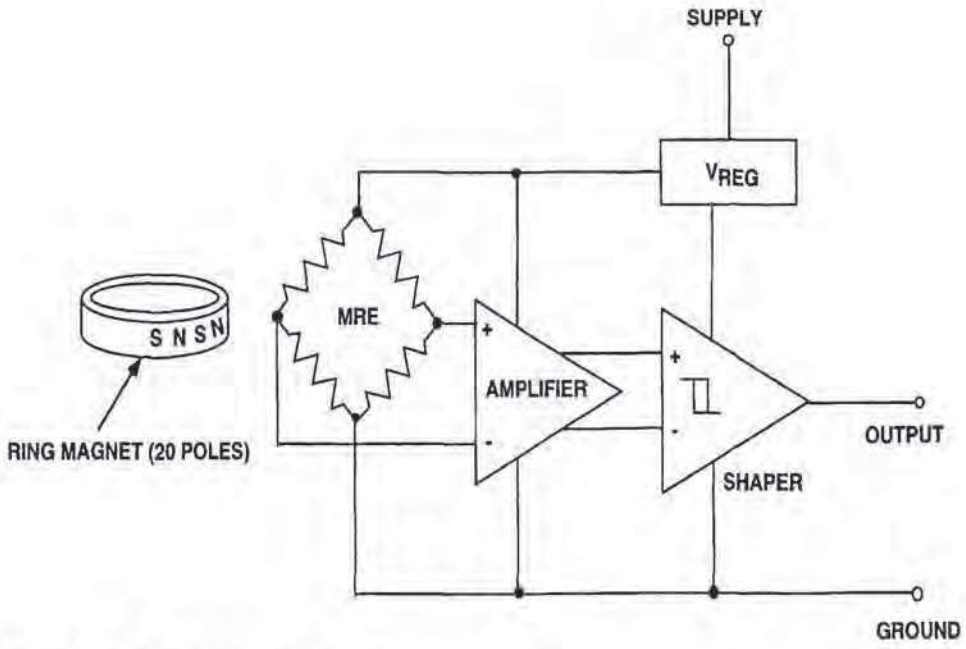


FIGURE 7.6 MRE speed-sensing module.

IPR2023-01234
Petitioner - Ex. 1017 - Page 137

The resolution in vehicle speed is then:

$$\frac{P}{S} = N \times K \tag{7.3}$$

The typical system requirements are an operating temperature of –40 to 120 °C, rotational speed detection of 5 to 3000 rpm (1000 p/s), and a duty cycle ratio of 50 ± 10%.

In applications such as ABS, ASR, and four-wheel steering, additional speed sensors are attached to all four wheels so that the slip differential between the wheels can be measured. VR devices have been used and are very cost effective in this application. But the cost of other devices is dropping and as they become cost effective, they are being designed into new systems. In electronic transmission applications, information from the road and engine speed sensors, as well as torque data and throttle position are required for the MCU to select the optimum gear ratio. Electronic control can ensure smooth transition between gear ratios. Transmissions using electronic control are also smaller than conventional automatic transmissions, thus enabling more gear ratios for better performance, higher torque, efficiency, and acceleration.

Cruise control systems require information from the road and engine speed sensors to control the throttle position, and possibly the optimum selection of transmission ratios. Variable ratio assisted power steering also requires information from the wheel speed sensors for adjustment of the steering ratios for ease of turning at low speeds and good road control at high speeds. If automatic tire pressure adjustment becomes a reality, this system may also require information from the wheel speed sensors.

Another application for rotational speed sensing is to control the speed of the radiator cooling fan. The speed of the fan is determined by the coolant temperature. Hall effect devices (MRE can also be used) have been used to monitor the position of the armature and speed of the cooling fan motor. The motor controller uses this information to modulate the power to the motor through a three-phase bridge driving circuit for the control of the fan motor speed.

7.3.2 Linear Applications

Under linear applications are the detection of obstacles close to the vehicle, crash avoidance, distance of the chassis relative to the ground for ride control, measurement of ground speed for ABS, ASR, and inertial navigation. Ultrasonic devices are normally used for short distance measurements (<10 m) and RF devices for long distance measurements (see Sec. 7.6.2). For the measurement of objects from 0.5 to 2 m using ultrasonics, a pulse repetition rate of about 15 Hz is used. The reflected pulses take from 3 to 12 ms to return. The return time T is given by

$$L = C \times \frac{T}{2} \text{ (m)} \tag{7.4}$$

where L = distance to target
C = the transmission speed [given by $C = 331 + 0.6\,t$ (m/sec)]
T = temperature (at 15 °C), the speed of ultrasonic waves is 340 m/s.

In the case of chassis-to-ground measurements for ride control and ground speed measurements, the distance to be measured is from 15 to 50 cm and a higher pulse repetition rate can be used (up to 50 Hz). In this case, the reflected pulse takes from 0.9 to 3 ms to return. For ride control applications, an accelerometer has an advantage over distance measurement, in that it is unaffected by varying distance measurements over rough terrain.

7.4 ACCELERATION SENSING DEVICES

Acceleration sensors vary widely in their construction and operation. In applications such as crash sensors for air bag deployment, mechanical devices (simple mechanical switches) have

IPR2023-01234
Petitioner - Ex. 1017 - Page 138

been developed and are in use. Mechanical switches are normally located at the point of impact in the crash zone. With the development of micromachined devices, solid state analog accelerometers have been designed for air bag applications. The analog accelerometers are centrally placed on the automotive frame. These devices can be very cost effective when compared to mechanical switches and are rapidly replacing the electromechanical devices. Silicon micromachined sensors provide a higher degree of functionality, can be programmed, have high reliability, have excellent device-to-device uniformity, and can be integrated with memory circuits to create a more accurate sensor. Additional features such as self-test and diagnostics are also available.

7.4.1 Mechanical Sensing Devices

Mechanical switches are simple make-break devices. Figure 7.7 shows the cross section of a Breed type of switch or sensor. The device contains a spring, a metal ball, and electric contacts in a tube. On impact, the inertia in the ball causes it to move against the retaining force of the spring and closes the electric contacts at the end of travel. An alternative to this device is the one shown in Fig. 7.8. It consists of a cylindrical mass wound in a flat spring. The seismic mass

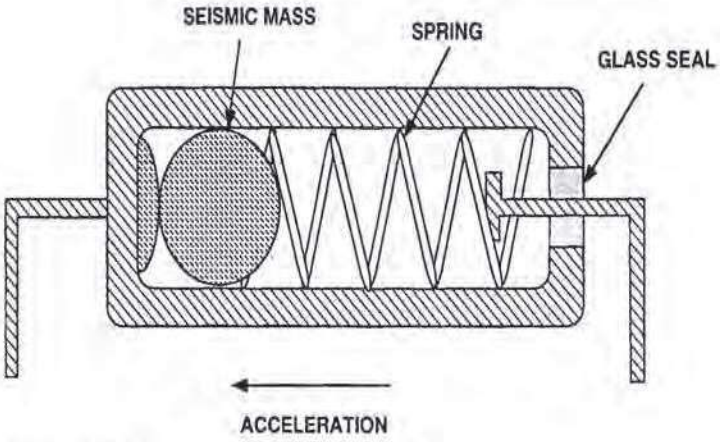


FIGURE 7.7 Cross section of mechanical sensor.

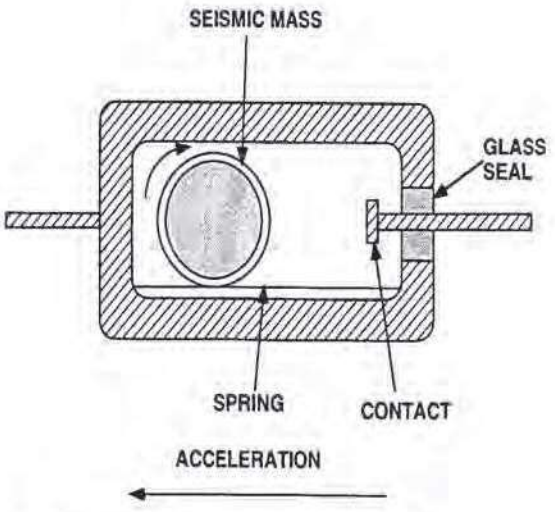


FIGURE 7.8 Cross section of mechanical switch.

IPR2023-01234
Petitioner - Ex. 1017 - Page 139

rolls on impact against the spring tension, and again makes electrical contact at the end of travel. The machining tolerances on these devices are high and give wide variations in the acceleration trigger point.

7.4.2 Piezoelectric Sensing Devices

Piezoelectric devices consist of a layer of piezoelectric material (such as quartz) sandwiched between a mounting plate and a seismic mass. Electric connections are made to both sides of the piezoelectric material. The cross section of such a device is shown in Fig. 7.9. Piezoelectric material has the unique property that when a force or pressure is applied to opposite faces of the material, an electrical charge is produced. This charge can be amplified to give an output voltage that is proportional to the applied force. Piezoelectric devices can be effective in some applications, but are not suitable for sensing zero- or low-frequency acceleration, that is <5 Hz due to offset and temperature problems (pyroelectric effect). Piezoelectric sensors have a high Q, low damping, and a very high output impedance. Self-test features are also difficult to implement. The main advantages of piezoelectric devices are their wide operating temperature range (up to 300 °C), and high operating frequency (100 kHz).

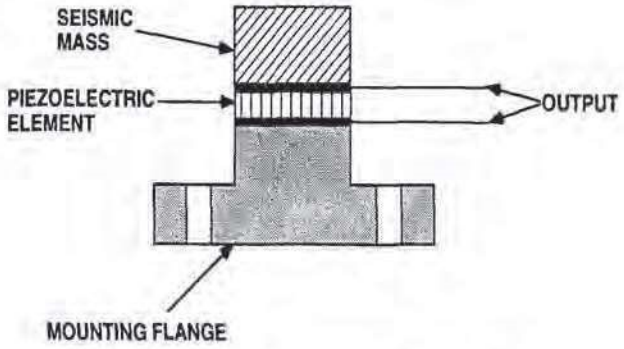


FIGURE 7.9 Cross section of a piezoelectric accelerometer.

Figure 7.10 shows a typical signal-conditioning circuit[2] and the trimming network used with piezoelectric sensors. The output from the sensor is fed to a charge amplifier, which converts the charge generated by the sensor into a voltage proportional to the charge. The circuit

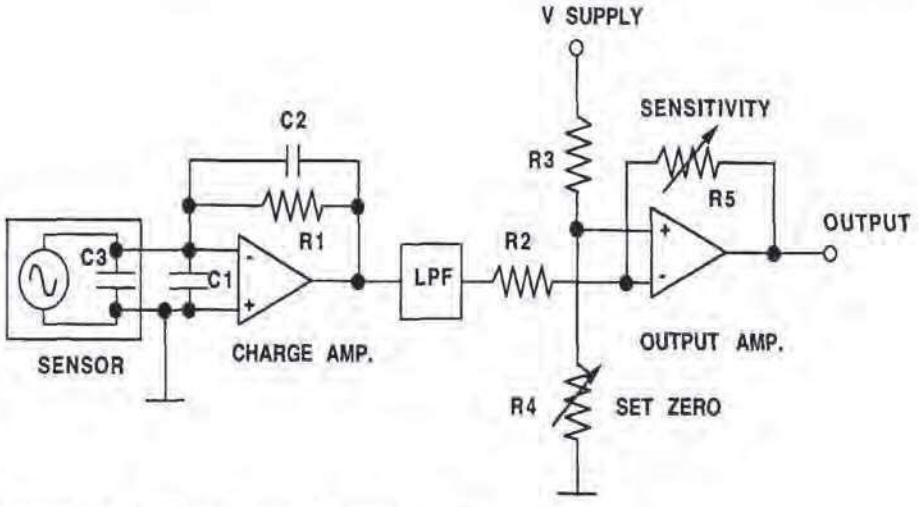


FIGURE 7.10 Piezoelectric signal-conditioning circuit.

IPR2023-01234
Petitioner - Ex. 1017 - Page 140

is a modified virtual ground voltage amplifier. Feedback via capacitor C2 and resistor R1 is used to maintain the input at a virtual ground potential. This type of circuit minimizes the effect of stray or ground capacitance C1. The output voltage from the amplifier is fed via a low-pass filter (LPF) to an output amplifier, where it is trimmed for offset by R4 and sensitivity by R5. In system development, the sensitivity is set by the piezoelectric material used. Higher-sensitivity materials however, exhibit higher sensitivity to temperature variations.

7.4.3 Piezoresistive Sensing Devices

The property of some materials to change their resistivity when exposed to stress is called the piezoresistive effect. In silicon, the sensing resistors can be either P or N type doped regions, which can be very sensitive to strain. The resistors are also sensitive to temperature, so that the strain gauge is normally designed as a bridge configuration to minimize temperature effects and to obtain higher sensitivities (see also Chap. 2). In order to maintain good linearity, the operating temperature of piezoresistive devices is limited to about 100 °C. The nonlinearity is caused by excessive junction leakage current at high temperatures. Higher operating temperatures have been obtained using oxide-isolated strain gages (up to 175 °C). An uncompensated strain gauge has a typical error of 3 percent over the operating temperature range −20 to 80 °C. This error can be reduced with a compensating resistor, and still further reduced to about 0.5 percent by the use of thermistors, over an improved operating temperature range of −40 to 110 °C.

Piezoresistive sensing can be used with bulk micromachined accelerometers. Such a device is shown in Fig. 7.11. The strain-sensing elements are diffused into the suspension arms. These elements can then detect strain in the arms caused by acceleration forces on the seismic mass.

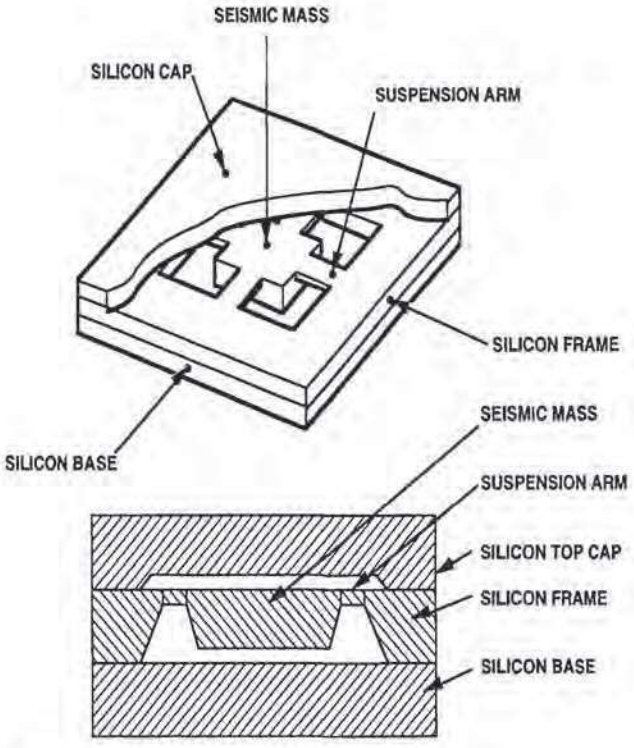


FIGURE 7.11 Bulk micromachined accelerometer.

IPR2023-01234
Petitioner - Ex. 1017 - Page 141

7.4.4 Capacitive Sensing Devices

When used with micromachined structures as shown in Figs. 7.11 and 7.12, differential capacitive sensing has a number of attractive features when compared to other methods of sensing: easily implemented self-test, temperature insensitivity, and smaller size. In addition, comparing capacitive sensing to piezoelectric sensing reveals that capacitive sensing has the advantages of dc and low-frequency operation and well-controlled damping. When compared to piezoresistive sensing; differential capacitive sensing has the advantage of a wider operating temperature range and requires less complex trimming. Capacitive sensing has one other major advantage over other sensing methods in that it can be used in closed-loop servo systems. In these systems, voltages can be applied to the capacitive plates to produce electrostatic forces, which will balance the forces on the seismic mass due to acceleration. The main advantage of closed-loop operation is to make the sensor to a large extent independent of process variations. Signal-conditioning circuits can be designed to detect changes in capacitance of <0.1 fF, so that plate capacitances in the range of 200 to 400 fF can be used. The small spacing between capacitor plates in micromachining technology (2 μ) enables practical acceleration sensors as small as 500 μ × 500 μ. When designing capacitive sensors, care must be taken to ensure that the sensing voltages are properly balanced to minimize offsets due to electrostatic forces. These forces can also be produced by internal noise sources. The attributes of capacitive sensing are a linear response, operation over wide temperature ranges (–40 to 150 °C), and a frequency response from dc to about 2 kHz.

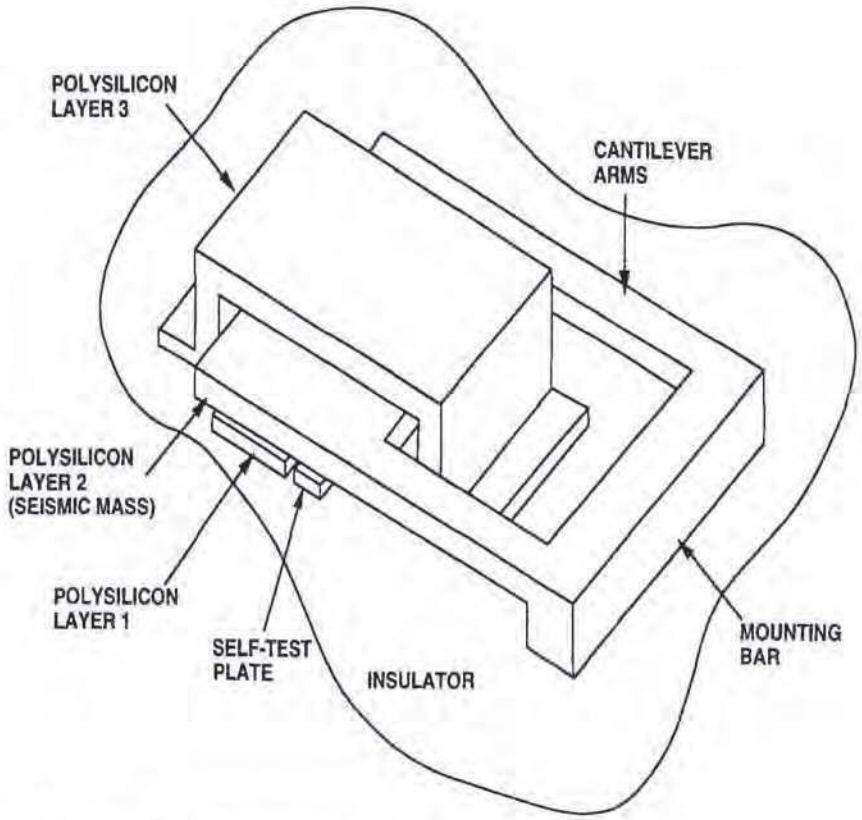


FIGURE 7.12 Surface micromachined accelerometer.

Micromachined Structures. There are a variety of types of micromachined structures that can be used in accelerometers. These structures fall into two technologies: bulk micromachined structures and surface micromachined structures. Bulk micromachined devices are structures

IPR2023-01234
Petitioner - Ex. 1017 - Page 142

etched out of silicon wafers. Figure 7.11 shows the cross section of a bulk micromachined device consisting of three layers of silicon bonded together. The center layer is shaped to form a seismic mass suspended by four arms[3] (a cantilever structure has also been designed with two suspension arms[4]). When acted upon by acceleration forces, the seismic mass moves between the top and bottom plates. In this case, the movement can be sensed using piezoresistive elements diffused into the suspension arms, or differential capacitive sensing can be used between the seismic mass and the upper and lower silicon plates. The top and bottom plates can also be made of glass with metalized areas to form the top and bottom capacitors. Such devices have been designed to operate from the high g range (>1000 g), down to sensors with resolution in the μg range. Closed-loop control techniques are normally used in these lower g ranges.

The surface micromachined device shown in Fig. 7.12 is built using layers of polysilicon and sacrificial glass, which are alternately deposited and shaped. In this case, three layers of polysilicon and two layers of sacrificial glass were used. After deposition of the third polysilicon layer, the sacrificial glass is etched away leaving the freestanding structure as shown. A number of etch holes are normally placed in the second and third layer of polysilicon to speed up the etch process. These etch holes are also used to control the squeeze film damping and bandwidth of the device. The seismic mass of the second-layer polysilicon in these devices is of the order of 5×10^{-10} kg. A second plate under the middle polysilicon can be used for self-test. This function is achieved by applying a voltage to the self-test plate, which in turn will produce an electrostatic force on the center polysilicon plate causing it to deflect. This deflection will simulate an external acceleration force. An alternative to the polysilicon and glass structure is nickel with sacrificial copper.[5]

Differential capacitive sensing is used with all of these structures. Both bulk and surface micromachined devices have a very rugged construction. These devices use squeeze film damping to control bandwidth and to ensure critical damping of the resonant frequency (about 2 kHz for bulk and 10 kHz for surface micromachined devices). Film damping also ensures high resistance to shock in the sensing direction. In the directions perpendicular to the sensitive axes, the devices are rugged by construction with low cross-axis sensitivity (<3 percent). An accelerometer designed to sense a few g will typically have a shock tolerance of well over 5000 g. As already noted, surface micromachined devices that have been developed for air bag deployment have analog outputs. These devices normally operate from a 5-V supply, have a bandwidth of about 1 kHz and a sensitivity of 40 mV per g, giving a full-scale output with ±50 g input. Both open- and closed-loop techniques have been used for sensing. In comparing bulk and surface micromachined devices, the bulk structure is larger, using crystal-oriented etching with end stops, which require extra diffusions; whereas, the surface micromachined device uses isotropic etching (masking) with different materials acting as end stops. Surface structures have the potential for easier integration and use a simpler less costly process, but do require annealing.

Open-Loop Sensing. Open-loop signal-conditioning circuits amplify and convert the capacitance changes into a voltage. Such a CMOS circuit using switched capacitor techniques is shown in Fig. 7.13. The circuit contains a virtual ground amplifier to minimize the effect of stray capacitance. The positive input of the amplifier is referenced to a voltage of $V_{REF}/2$, when switch $S2$ is closed the amplifier has unity gain, and the voltage on the middle plate of the sensor is set to $V_{REF}/2$. After $S2$ is opened, $S1$ is switched so that any differences between sensor capacitors C_1 and C_2 produces a charge at the negative input of the amplifier. This charge produces a voltage (V_{out}) at the output of the integrating amplifier. The output voltage of the amplifier is given by

$$V_{out} = V_{REF} \frac{C_1 - C_2}{C_3} \tag{7.5}$$

where C_1 and C_2 are the sensor capacitances
C_3 is the integrator capacitance

IPR2023-01234
Petitioner - Ex. 1017 - Page 143

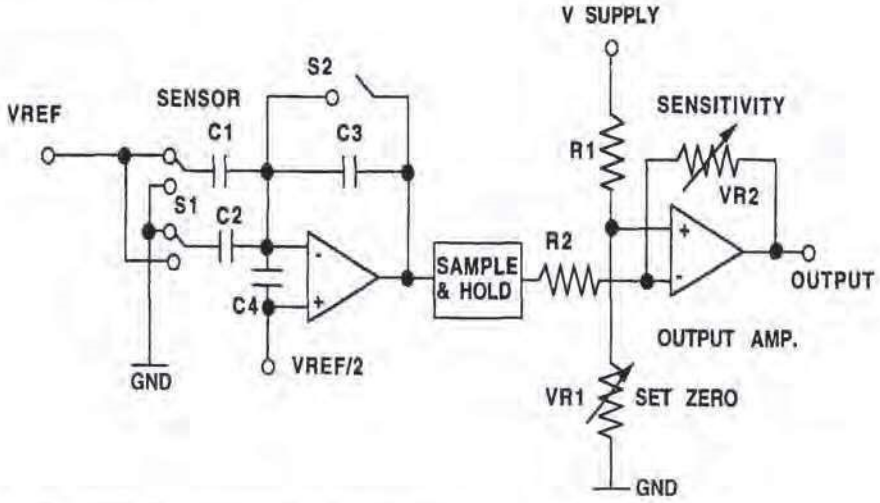


FIGURE 7.13 Capacitive sensing integrator circuit.

If the reference voltage is made proportional to the supply voltage, a ratiometric output is obtained. That is, the system gain is proportional to the supply voltage. This is a requirement in some systems to facilitate the design of the A/D converter.

A block diagram of the system is shown in Fig. 7.14. The system contains an internal oscillator, voltage reference, amplifier, sample and hold, switched capacitor filter, trim network, and output buffer. The output voltage in such a circuit is proportional to the capacitance change. This change is proportional to 1/displacement, or 1/acceleration, giving rise to some nonlinearities. However, the displacement is small compared to the spacing between the plates, so that the output voltage approximates to acceleration, giving less than 3 percent nonlinearity. The filter is used for noise reduction and to set the bandwidth for specific applications. Trimming is used to set the zero operating point and sensitivity of the system.

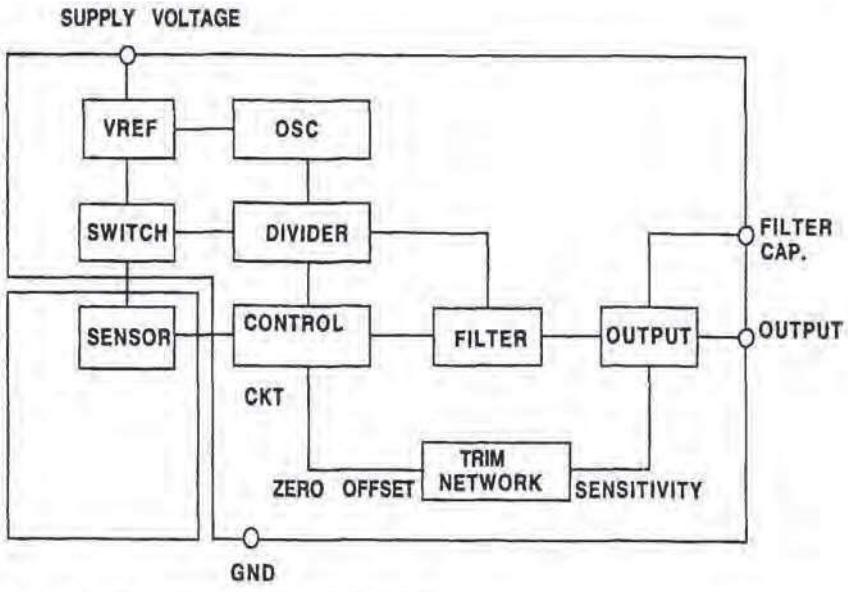


FIGURE 7.14 Signal-conditioning block diagram.

IPR2023-01234
Petitioner - Ex. 1017 - Page 144

An alternate circuit with improved linearity is shown in Fig. 7.15. In this case, the output voltage is fed back to the input of the integrator, forming a bridge circuit. The feedback also sets the amplitude of the driving voltage across the sensing capacitors, so that it is proportional to their displacement. This also balances the electrostatic forces on the middle plate.

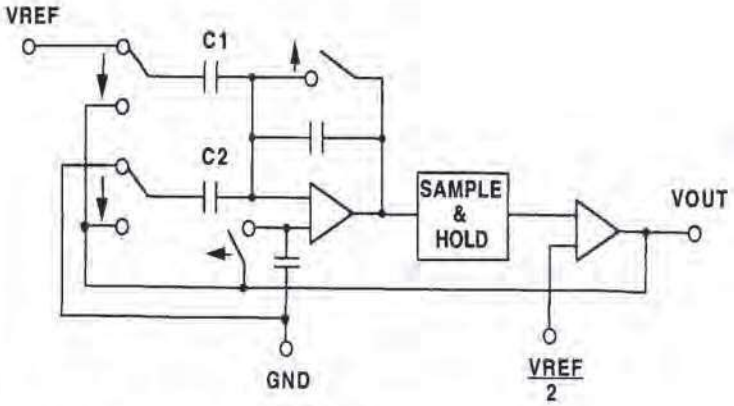


FIGURE 7.15 Linearized circuit schematic.

In this case

$$V_{out} = \frac{(C_1 - C_2)}{(C_1 + C_2)} \frac{V_{REF}}{2} \tag{7.6}$$

where $C_1 \propto 1/d_1$
$C_2 \propto 1/d_2$
$d_1 + d_2 = K$ (constant)

so that

$$V_{out} = V_{in} \frac{(d_1 - d_2)}{K} \tag{7.7}$$

showing that, in this case, V_{out} is proportional to displacement and acceleration giving improved linearity (<1 percent nonlinearity).

Closed-Loop Sensing. An alternative to the open-loop sensing circuit is the closed-loop sensing circuit, which can be configured to give an analog or digital output. Figure 7.16*a* shows the balanced electrostatic forces exerted on a seismic mass by upper and lower capacitor plates, which are at voltages of $+V$ and $-V$. If the seismic mass experiences a force due to acceleration, and a voltage δV is applied to the middle plate to generate enough electrostatic force to counterbalance the acceleration force, then the forces are as shown in Fig. 7.16*b*.

That is

$$m \times a = \frac{C(V + \delta V)^2}{2d} - \frac{C(V - \delta V)^2}{2d} \tag{7.8}$$

from which

$$m \times a = 2\,C \times V \times \frac{\delta V}{d} \tag{7.9}$$

IPR2023-01234
Petitioner - Ex. 1017 - Page 145

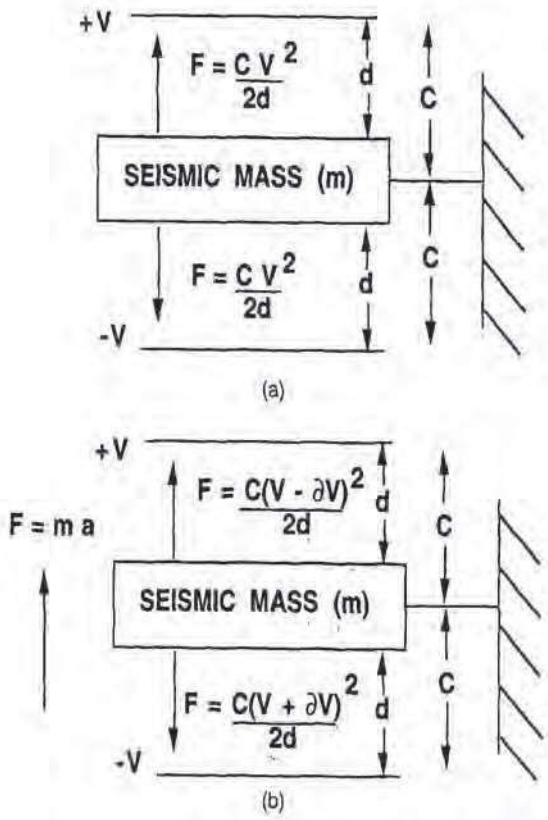


FIGURE 7.16 Electrostatic force diagram.

This shows that an acceleration force can be balanced by a linear voltage applied to the center plate. This voltage can be amplified to give a linear output voltage proportional to acceleration.[6]

In a micromachined structure, the electrostatic force produced by a δV of about 1 V can counterbalance the force produced by an acceleration of 50 g on the seismic mass. Figure 7.17 shows a block diagram of the analog closed-loop system. The top and bottom plates are dc-biased by the resistor divider network consisting of R1, R2, and R3. The ac antiphase signals used for sensing the position of the center plate are fed to the top and bottom sensor plates via the capacitors (C1, C2) from the control logic. The analog output voltage from the filter is feedback to the positive input of the integrator. When the integrator is clocked into the unity gain phase, the feedback voltage is applied to the center plate of the sensor. The electrostatic forces produced on the center plate by the differential voltage between the top and bottom plates, and the feedback voltage on the center plate, will force the center plate back to its normalized position as given in Eq. (7.9). Other methods that have been used for closed-loop operation are pulse width modulation (PWM), and delta sigma modulation (DSM).

The block diagram and waveforms of a PWM system are shown in Fig. 7.18. In this case, the center plate is held at a fixed voltage (0). The output of the integrator is amplified and converted into a PWM signal (VP), this signal and the inverted signal (VPN) are fed to the top and bottom plates of the sensor. The leading edges of the VP and VPN signals are used to sense the position of the middle plate. The electrostatic force generated by the voltage × time differential between the middle plate and the top and bottom plates, will act on the middle plate to counterbalance the forces on the plate due to acceleration. With zero acceleration, the PWM signal has a 50 percent duty cycle, so that the resulting electrostatic forces on the seismic mass are zero. The transfer function of the PWM system is given by

$$\text{Duty cycle} = \frac{\text{Acc} \times g \times d}{C \times V_{\text{REF}}^2} \tag{7.10}$$

IPR2023-01234
Petitioner - Ex. 1017 - Page 146

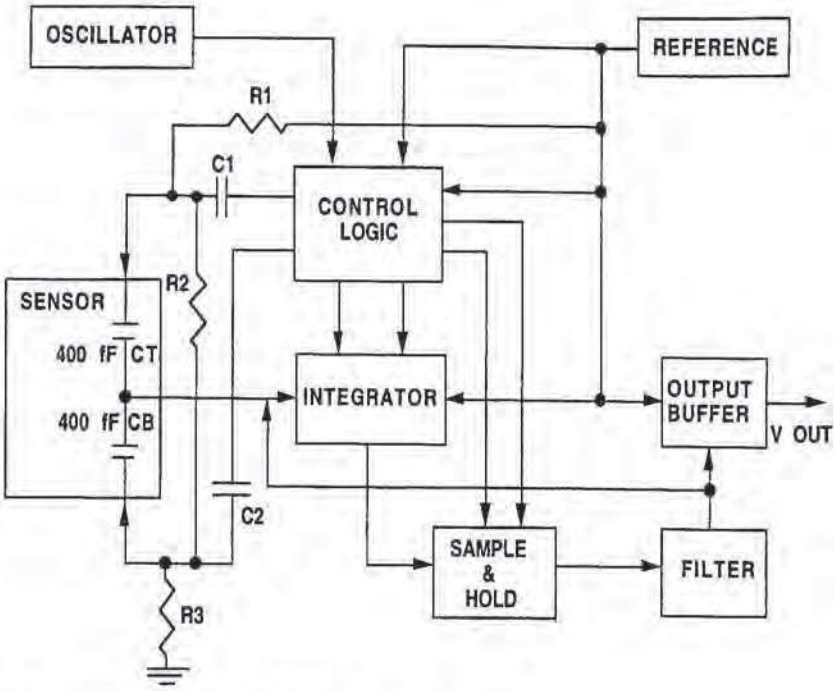


FIGURE 7.17 Block diagram of analog closed-loop system.

where g = gravitational constant
d = plate spacing
C = plate capacitance

The output can either be the PWM digital signal, or an analog output (obtained by feeding the PWM signal through a low pass filter).

Figure 7.19 shows the block diagram and waveforms of a DSM system. In this case, the middle plate is held at VF (volts). As can be seen, transient edges of the plate-drive waveforms are used for sensing the position of the center plate. The output from the integrator is fed to a comparator, whose output is then clocked into a latch where it sets up a "1" or a "0" (high or low) depending on the output from the integrator. The output from the latch is used to apply a voltage V_{REF} to the appropriate top or bottom capacitor plate, so that the electrostatic forces generated by the voltage V_{REF} – VF will maintain the center plate in its no-load position. The one-bit serial data stream from the latch can be fed directly to the MCU, or fed via a decimator circuit (which will convert the data into an 8-bit word) to the MCU. Alternatively, an LPF can be used to convert the data into an analog output. Bipolar or CMOS circuits can be used for signal conditioning. However, CMOS signal conditioning has the following advantages: a very high input impedance, good switching characteristics, low power requirements, small size, compatibility with MCU processes with the prospect of future integration, switched capacitor filters are available for noise reduction and bandwidth control, and EPROM technology is available for trimming (see Fig. 7.14). BiMOS circuits have also been used for signal conditioning.[6] In the BiMOS circuits, thin-film resistors are used to enable laser trimming of the zero offset and voltage reference; external capacitors and resistors are used for filtering and gain control.

Single vs. Multichip Control Circuits. The processing of sensors is not completely compatible with IC fabrication. Consequently, for the integration of sensors and ICs, a number of additional steps are required, which can have a detrimental effect on yields. The question then arises as to which is the most cost effective: a sensor die plus a control die with the additional cost of assembly, or a monolithic approach.

IPR2023-01234
Petitioner - Ex. 1017 - Page 147

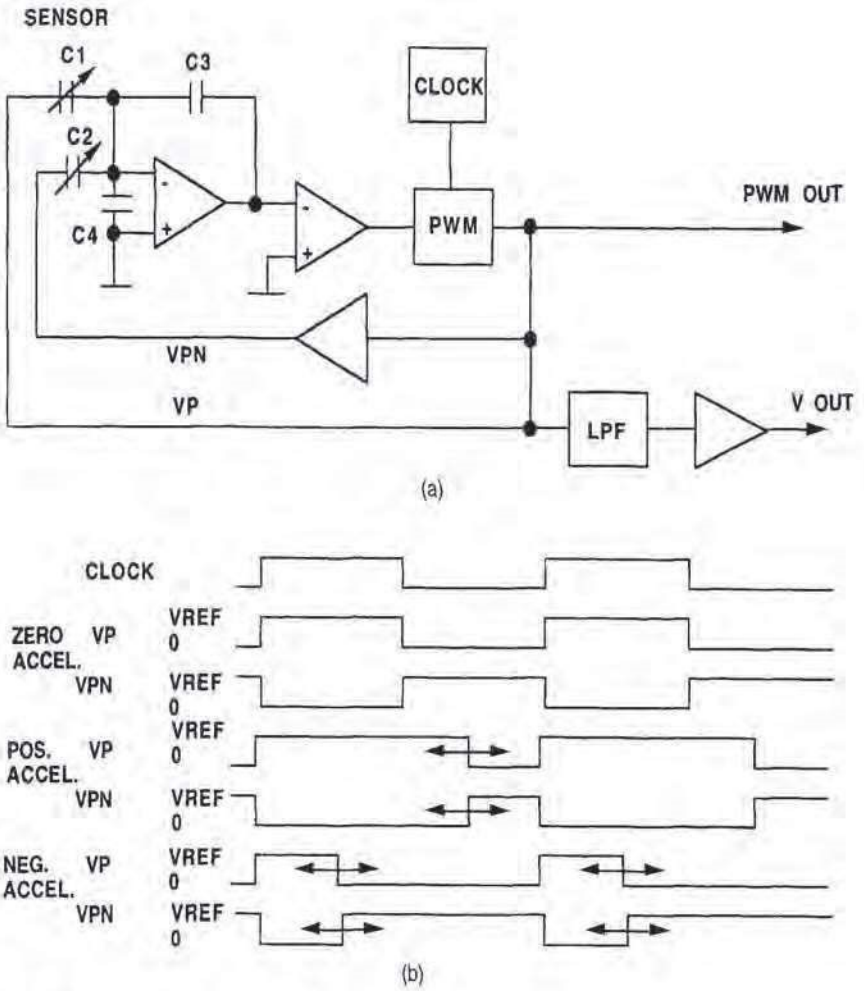


FIGURE 7.18 PWM block diagram.

In the case of micromachined devices, there are a number of advantages to using the dual-chip approach, such as flexibility, in that one type of sensor can be interfaced with a number of different types of control die, or several types of sensors can be interfaced with one type of control die. This provides a variety of input and output options. The control die and sensor can be developed simultaneously, minimizing development time. Problem solving is made easier, and the processing for both die can be optimized for performance. With the two-die approach, the sensor can also be capped and sealed during processing in a clean room atmosphere, thus eliminating contaminants and particles for good longevity. In the monolithic approach, this is not the case. In the monolithic approach, changes required to improve one section can affect the other section, which may then require additional changes in that section. The main disadvantage of the dual-chip approach is the introduction of parasitic capacitances. However, these can be addressed by existing control circuit design techniques.

7.5 AUTOMOTIVE APPLICATIONS FOR ACCELEROMETERS

Accelerometers have a wide variety of uses in the automobile. The initial application is as a crash sensor for air bag deployment. This application is normally associated with head-on collisions, but can also be applied to rear-end impact collisions to prevent rebound impact between the passengers and the windshield. An extension of this application is the use of

IPR2023-01234
Petitioner - Ex. 1017 - Page 148

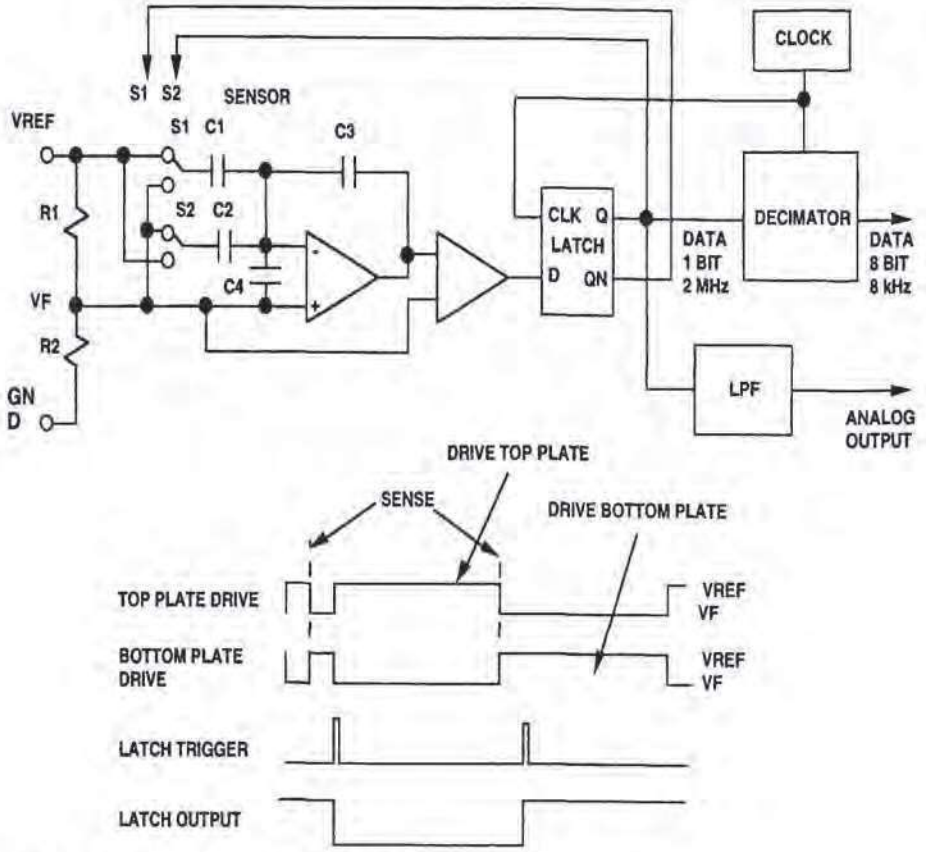


FIGURE 7.19 *Block diagram of Delta Sigma Modulator.*

accelerometers for the detection of side impact. This application will require additional air bags to the side of the occupants. Other low *g* linear accelerometers are being developed for ride control, ABS, traction, and inertial navigation applications.

Solid state acceleration sensors have special mounting requirements that are different from normal integrated circuits. These are to ensure that acceleration forces are transmitted to the sensor package. An advantage of the solid state device is self-test features for diagnostics. In acceleration applications, the devices are required to operate over the temperature range –40 to 85 °C (125 °C under the hood), and to withstand >2000 *g* shock. Other similar devices that have application in the automotive arena are vibration devices.

7.5.1 Air Bag Deployment Application

Crash sensors that use mechanical switches (sensors) are typically located some 40 cm from the point of impact, which necessitates the use of multiple sensors (normally 3 to 5 sensors are used in multipoint sensing) for crash sensing and air bag deployment. These devices are velocity change detectors, and are calibrated to make contact when the change of velocity in the passenger compartment is at least 20 km/h, this being the velocity change at which the front seat occupants will strike the windshield.

A centrally located analog sensor can be used as a crash sensor (single point). In the case of a centrally located accelerometer, the g level to be sensed is lower than that of a point-of-impact device. However, only one device is required to monitor the crash signature. This signature will vary with different types of chassis and different types of impacts. Consequently, an MCU is used to monitor the output of the accelerometer to determine if a crash has occurred. The typical output of a centrally located accelerometer during a 48 km/h crash is shown in Fig. 7.20. Deceleration of the vehicle and occupant displacement are also shown. At 48 km/h, the sensor has 20 ms to detect the crash and trigger the air bag. This results in infla-

IPR2023-01234
Petitioner - Ex. 1017 - Page 149

tion of the air bag 50 ms after impact, at which time the occupant has moved about 18 cm or approximately halfway to the windshield and at the contact point with the inflated air bag. During the initial 20 ms, deceleration can reach 20 *g*, but the average is about 5 *g* when the air bag is triggered. The centrally located accelerometer can take one of several forms: a piezoelectric sensor, a piezoresistive device, or a capacitive sensor.

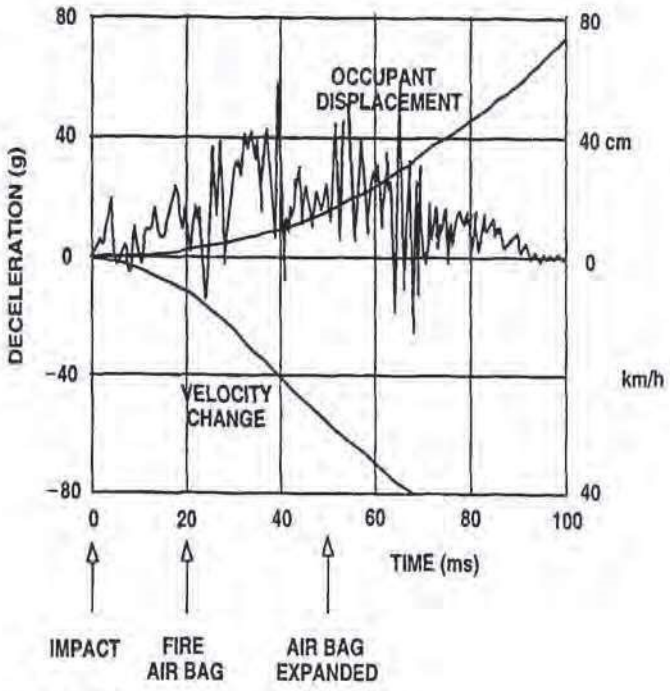


FIGURE 7.20 Typical 48 km/h crash waveform.

The centrally located accelerometer has a number of performance advantages over its mechanical counterpart. These are the reduction in the number of sensors and required bussing, which makes the centrally located system much more cost effective. There is an improvement in sensing and signal-processing accuracy with the single-point sensing accelerometer over the mechanical sensor. This gives a better-defined trigger point and overall improved performance across different chassis types. Capacitive sensors appear to have the edge in this application, because they have the potential of being cost effective, meet the requirements of the application, and have self-test features plus diagnostics available. In this application, a typical accelerometer specification is ±50 *g* full-scale output, accuracy ±5 percent over temperature, bandwidth dc to 750 Hz, and cross-axis sensitivity <3 percent. During impact, the crash sensor can also be used for seat belt locking.

7.5.2 Ride Control Application

In ride control systems, the leaf or coil springs located on the axles are replaced by four *wheel stations,* which form an active suspension. Each wheel station contains an oil-filled cylinder with a piston to set the distance of the frame above the axles and to isolate the frame from axle vibration. This is achieved using a servo feedback system. When a vehicle with conventional suspension encounters a foreign object on the highway, the load on the wheel increases as it moves up to negotiate the obstacle. This load increase makes the vehicle rise up. With a fully active suspension, the increase in load is detected and a servo valve is opened to transfer the necessary amount of oil from the appropriate cylinder to a storage container. Consequently, the load exerted on the chassis by each wheel is maintained at its specific level and

IPR2023-01234
Petitioner - Ex. 1017 - Page 150

the chassis remains at its static level. After the object has been traversed, oil is pumped back into the cylinder to reestablish the static load conditions.

An alternative to the active suspension is the adaptive suspension system. In this case, information from the front wheels is gathered and used to predict road conditions for the control of the rear wheels. The advantage over the fully active suspension is one of cost, as the number of acceleration sensors is halved. During cornering, oil is also pumped into the outside wheel cylinders to minimize roll angle.[7]

A combination of sensors is used for active suspension. These are accelerometers, wheel speed sensors, chassis-to-ground sensing, and piston-level sensing in the suspension system. The low g accelerometers used on the axles of the four wheels to detect the load changes on the wheels have the following specifications: ±2 *g* full-scale, accuracy ±5 percent over temperature, bandwidth dc to 10 Hz, and cross-axis sensitivity <3 percent. The acceleration information and data from the wheel speed sensors is used to provide the information necessary for the MCU to operate the servo control valves. Hall effect, MRE, and opto sensors have been used for monitoring the level of the pistons in the wheel stations cylinders.

7.5.3 Vibration Applications

Lean-burn engines are being developed for improved emission levels and for better fuel economy (10 to 15 percent improvement). NO_x emissions are greatly reduced to meet federal standards. Lean-burn engines use high stoichiometric ratios; 20:1 and higher are necessary. At these ratios, combustion becomes unstable and torque fluctuations large. Consequently, antiknock and vibration sensors are required to supply the information necessary to the MCU, so that it can adjust the injected fuel amount and ignition timing for stability over widely varying conditions.

There are two types of solid state sensors that can be used in this application: piezoelectric devices and capacitively coupled vibration sensors. A typical vibration sensor contains a number of fingers of varying length which vibrate at their resonant frequencies when those frequencies are encountered. The resonance is capacitively coupled to the sensing circuit, and the outputs as shown are obtained. Optical sensors have also been used as antiknock sensors. In this case, the ignition spectrum is monitored for the detection of misfiring or knocking. Vibration sensors can also be used for vibration monitoring in maintenance applications.

7.5.4 Antilock Brake System Applications

In antilock brake systems, speed sensors are attached to all wheels to determine wheel rotation speed and slip differential between wheels. VR devices, as well as Hall effect and MRE devices, can be used in this application, as zero speed sensing is not required. VR devices have been used and shown to be cost effective in this application, but Hall effect and MRE devices are now being designed into these systems. Pressure sensors are used to monitor brake fluid pressure, and an accelerometer or ground-speed sensor can be used to provide information on changes in the vehicular speed. Brake pedal position and brake fluid pressure information are also required for control. All of this information is fed to an MCU, which processes the data and adjusts the brake fluid pressure to each wheel for optimum braking. Many of the elements of the ABS system can be used for the detection of lateral slippage on high-speed cornering, and can be used for traction and the direction of power to the wheels. Traction control applies in particular to slippery surfaces and with four-wheel-drive vehicles. Additional information over that used in ABS systems is required by the MCU for ASR applications, such as engine speed and throttle angle. In this application, servo feedback to the throttle may also be necessary.

A more cost-effective, but less accurate, system for ABS and ASR is the adaptive control system in which accelerometers are normally used to measure deceleration when braking, and

IPR2023-01234
Petitioner - Ex. 1017 - Page 151

acceleration when the throttle is opened. If skidding occurs during braking, the brake pressure is reduced and adjusted for maximum deceleration, or the throttle adjusted for maximum traction. Typical specifications for the accelerometer required in this application are: ±1 g full-scale output, accuracy ±5 percent over temperature, bandwidth 0.5 to 50 Hz, and cross-axis sensitivity <3 percent.

7.6 NEW SENSING DEVICES

New cost-effective sensors are continually being developed. The technology and cost are often pushed by the application and volume requirements of the automotive industry and federal mandates. Today's silicon sensors and control electronics are limited in operating temperature to 150 °C to ensure long life of the devices. This operational temperature is adequate for most applications, but higher temperature operation may be required for sensors mounted in the engine compartment. The limit on the operating temperature of silicon devices can be extended to between 200 and 250 °C by the use of special isolation techniques such as dielectric isolation (this operating temperature applies to surface micromachined devices). For higher-temperature operation, alternative materials such as GaAs or SiC are being developed, but the cost of these devices limits their use at present.

A list of semiconductor conductor materials and maximum practical operating temperatures is given in Table 7.3. Higher operating temperatures have been reported but with poor longevity.

TABLE 7.3 Device Operating Temperatures

Material	Maximum practical operating temperature, °C
Si	150
Si (dielectric iso.)	250
GaAs	300
AlGaAs	350
GaP	400
SiC	500

7.6.1 New Rotational Speed-Sensing Devices

A number of new devices are being investigated to detect magnetic fields. These are flux gate, Weigand effect, magnetic transistor, and magnetic diode. The magnetic transistor at present is showing the most promise. The device operates on a similar principle to the Hall effect device. That is, the current division between split collectors (bipolar) or split drains (MOS) can be changed by a magnetic field. This current differential can then be detected and amplified to give an output voltage proportional to magnetic field strength. These devices can use either majority or minority carriers, and can be either vertical or lateral bipolar or MOS devices. The magnetic transistor has the potential of higher sensitivity than the Hall effect device.

Figure 7.21 shows the cross section of a lateral PNP magnetic transistor. The current from each collector is equal until a magnetic field is applied perpendicular to the surface of the device. The magnetic field causes an imbalance of current between the two collectors. Sensitivities with this type of structure have been reported as being an order of magnitude greater than in the Hall effect device.[8] Magnetic transistors and diodes can be directly integrated with the signal-conditioning circuits, which could make them very cost effective in future applications. A comparison of the magnetic transistor to other practical devices is given in Table 7.2.

IPR2023-01234
Petitioner - Ex. 1017 - Page 152

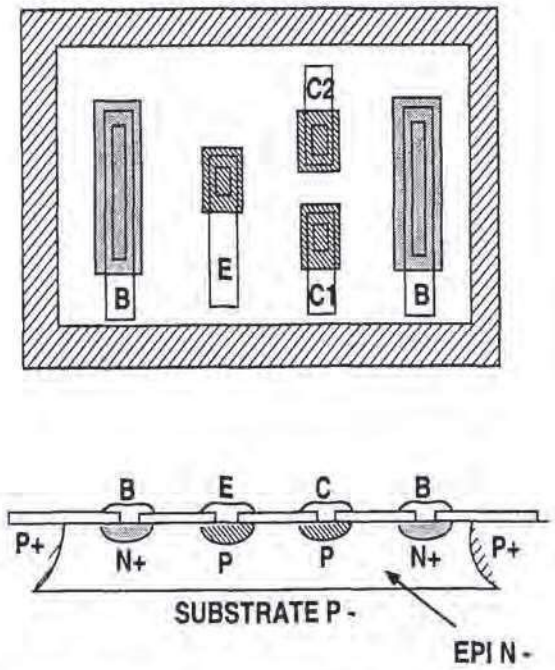


FIGURE 7.21 Cross section of a field-assisted *PNP* magnetic transistor.

7.6.2 New Linear Speed-Sensing Devices

A number of different sensing technologies can be used for distance, object detection, and approach speed measurements. Shown in Fig. 7.22 are the areas covered by blind-spot, rear, and forward-looking sensors. Ultrasonics, infrared, laser, and microwaves (radar) can be used in the detection of objects behind vehicles and in the blind areas. From a practical standpoint, no technology has come to the forefront. However, with new innovations in technology the situation may change very rapidly. Ultrasonics and infrared sensors are cost effective but degrade with inclement weather conditions such as ice, rain, snow, and the accumulation of road grime. Infrared devices are also color-sensitive, in that the sensitivity to shiny black objects is very low compared to other colors. Microwave devices appear to have the edge

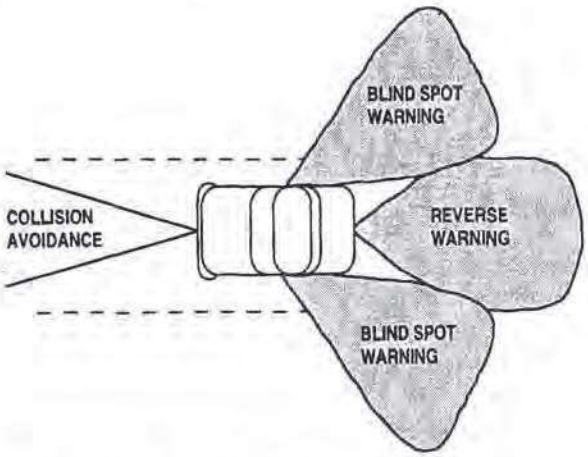


FIGURE 7.22 Collision-avoidance patterns.

IPR2023-01234
Petitioner - Ex. 1017 - Page 153

when considering environmental conditions,[9] but are expensive, and radar can be affected by false return signals and clutter.

For the detection of obstacles and vehicles in front of a vehicle, the choice is between laser and microwaves due to the distances involved (up to 90 m). Microwaves have the disadvantage of high cost and large antenna size when considering available devices in the 60 GHz range. Frequencies greater than 100 GHz are preferred for acceptable antenna size. However, collision avoidance radar in the 76/77-GHz band has been developed in Europe. Collision avoidance radar in the 77, 94, and 144 GHz is being considered in the United States. A typical system uses a 38.5-GHz VCO (voltage controlled oscillator) with frequency-doubling to obtain about 40 mW of power at 77 GHz. A frequency-modulated continuous wave or pulse-modulated system can be used. The system uses GaAs devices to meet the frequency and power requirements. Lasers can be cost effective in this application, but also have their drawbacks: degradation of performance by fog, reflections from other light sources (sun, etc.), build-up of road grime on sensor surfaces, and poor reflecting surfaces at laser frequencies, such as grimy and shiny black surfaces.

7.6.3 New Inertial and Acceleration-Sensing Devices

Recent developments in solid state technology have made possible very small cost-effective devices to sense angular rotation. The implementation of one such gyroscopic device is shown in Fig. 7.23. This device is fabricated on a silicon substrate using surface micromachining techniques. In this case, three layers of polysilicon are used, with the first and third layers being fixed and the second layer free to vibrate about its center. The center is held in position by four spring arms attached to four mounting posts as shown. This device can sense rotation about the X and Y axes and sense acceleration in the direction of the Z axis. The center layer of polysilicon, driven by electrostatic forces, vibrates about the Z axis. These forces are produced by voltages applied between the fixed comb fingers and the comb fingers of the second polysilicon. Capacitor plates as shown are formed between the first and third polysilicon on the X and Y axes, and the second layer of polysilicon. Differential capacitive sensing techniques can then be used to sense any displacement of the vibrating disc caused by angular rotation. For example, if angular rotation takes place about the X axis, Coriolis forces produce a deflection of the disc about the Y axis. This deflection can be detected by the capacitor plates on the X axis. The sensing of the three functions is achieved by using a common sensing circuit that alternatively senses the X rotation, Y rotation, and acceleration. The gyroscope is designed to have a resolution of <10 degrees per hour for angular rate measurements, and an acceleration resolution of 0.5 mg.

7.7 FUTURE APPLICATIONS

New applications to increase creature comfort and safety are constantly being developed, but their rate of introduction will depend on the cost effectiveness of the technology, demand, and government mandates. Other concerns of automotive manufacturers are size, weight, power requirements, and adverse effects on styling and appearance. Many of the new sensor technologies are in their infancy, and thus are not yet cost effective on medium- and low-priced automobiles, but are being made available as options on luxury cars.

7.7.1 Future Rotational Speed-Sensing Applications

A future application for speed-sensing devices will be in continuously variable transmissions. In this application, engine and wheel speed, as well as torque, will be measured, and the infor-

IPR2023-01234
Petitioner - Ex. 1017 - Page 154

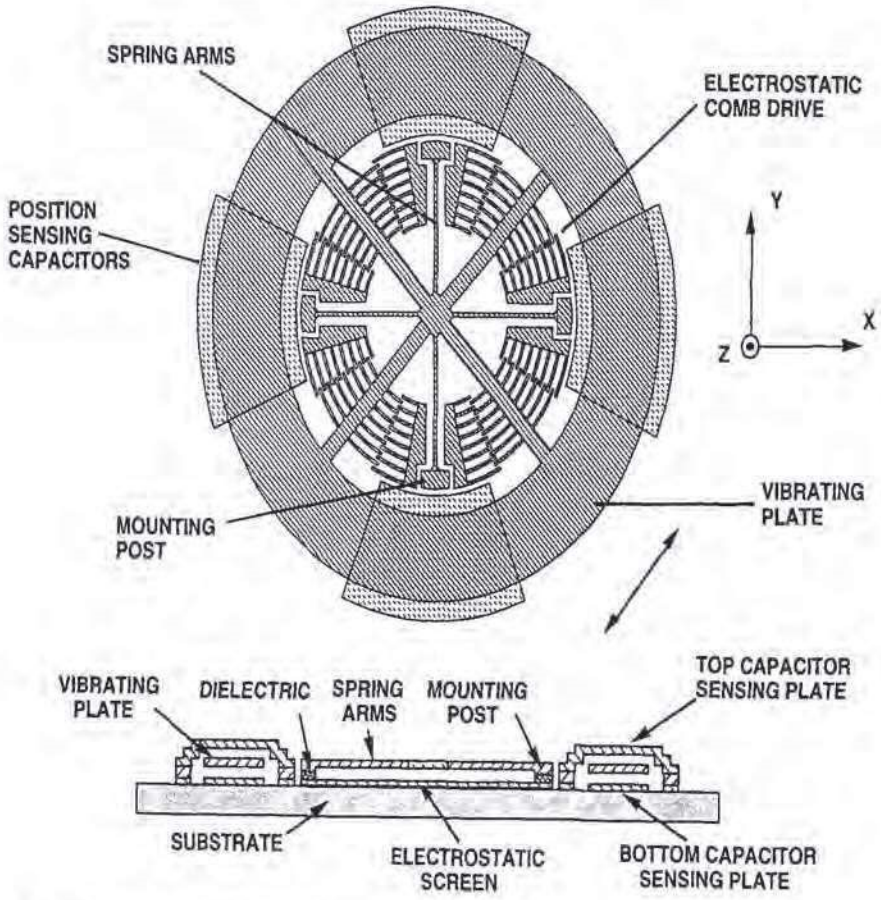


FIGURE 7.23 Solid state gyroscope.

mation processed by an MCU to optimize transmission ratios for engine performance and efficiency. All-wheel steering is also under development, and requires speed-sensing information, in addition to steering, front-, and rear-wheel angle position data for processing and control.

7.7.2 Future Linear Speed-Sensing Applications

Another application that has been developed is the use of speed- and distance-measuring devices for collision avoidance. These devices fall into three categories: near-obstacle detection (rear), blind-spot detection, and semiautomatic frontal object detection and control[9] (see Fig. 7.22).

Near-obstacle detection is used to prevent accidents during reversing. Blind-spot detection is used to prevent accidents due to careless lane changing, and when backing out of a driveway, garage, or alley into traffic. The semiautomatic frontal detection is a long-range system. The distance and closing speed between vehicles, or between a vehicle and a fixed object, can be measured and the speed adjusted as necessary to avoid a collision,[10] or the driver can be warned of impending danger. An addition to this is to monitor road surface conditions for friction—for example, dry roads compared to wet or icy roads—and also to use this information to adjust approach speeds and distance. Without collision avoidance, road condition monitoring can be used to caution vehicle operators. Collision avoidance systems can be used to minimize collisions, or can be used to operate protection systems before an unavoidable collision happens to protect the automobile passengers. In this case, vehicles closing at or approaching an obstacle at 80 km/h will be less than 7 m apart before a collision-is-imminent

IPR2023-01234
Petitioner - Ex. 1017 - Page 155

determination can be made. This gives 200 ms decision-making time for the system MCU. This is, however, long compared to today's air bag deployment systems, which have 20 ms decision-making time after the event. In the future, an idealistic system may be a combination of the two systems.

7.7.3 Future Acceleration Applications

One of the future applications being considered is the expansion of the air bag system to include side impact protection. The sensor used for crash sensing is unidirectional, so that it can only detect forward impact. A similar sensor, mounted perpendicular to the air bag sensor, can be added to the system to detect side impact and to deploy protection for the passengers. This device will typically require a 250-*g* accelerometer. Another application for accelerometers is to detect slippage during cornering in advanced steering systems. These systems will employ a low-*g* accelerometer (1–2 *g*).

7.7.4 Inertial Navigation Applications

A number of inertial navigation systems are being developed for short- and long-range travel. Long-range inertial navigation systems normally obtain their location by using a triangulation method. This method references three navigation satellites with known locations in fixed orbits. However, there are certain conditions under which contact with all three satellites is lost. This occurs when the vehicle is in the shadow of tall buildings or high hills, and triangulation is not possible. Under these conditions, the guidance system has to rely on such devices as gyroscopes, which sense angular rotation or change in direction, and/or monitor vehicular motion relative to the road.

Short-range inertial navigation systems or inertial measurement units (IMU) rely to a large extent on high-accuracy accelerometers and gyroscopes. A typical accelerometer specification for this application is: ±2-*g* full-scale output, accuracy 0.5 percent over temperature, bandwidth dc to 20 Hz, and a cross-axis sensitivity <0.5 percent. A centrally located IMU can be expanded to cover other applications such as suspension, ABS, ASR, and working with crash avoidance sensors. This may be the way to handle cost-effective system design in the future. The IMU can also be designed to provide location data for intelligent vehicle highway systems. These systems (Prometheus,[11] Amtics[12]) improve travel efficiency and reduce fuel consumption and pollution by selecting the optimum route to a given destination. The route is chosen to avoid traffic congestion, road construction, and accidents (see Chap. 29).

7.8 SUMMARY

In this chapter, a number of speed-sensing devices, both rotary and linear, have been described, together with potential applications. VR, MRE, Hall effect, and opto devices (possibly magnetic transistor in future applications) can be used in rotational applications for engine control, transmission, and wheel speed sensing. Of these devices, Hall effect, VR, and opto have been widely used. With the tendency for direct pickoff, optical devices may become impractical. MRE devices are being designed in and will become a serious contender to the Hall effect device. In linear applications for crash avoidance, microwave devices have the edge over performance and optical devices in terms of cost. However, as the cost of microwave devices declines, they could become cost effective. For blind-area alert and reversing obstacle detection, ultrasonics and infrared devices are cost effective, but performance degrades during inclement weather.

IPR2023-01234
Petitioner - Ex. 1017 - Page 156

The accelerometer has possibly the greatest potential for applications in the automobile. These applications range from crash sensing, ride control, ABS, and ASR to IMU systems. Accelerometers needed will range in sensitivities from 50 *g* in crash sensing to 1 *g* in the IMU. Advances in technology are providing a number of new sensors that are showing potential, such as the magneto transistor and the micromachined gyroscope. To summarize, Figs. 7.24 and 7.25 show the types of sensors used in specific applications, and the technologies used for specific sensors. As can be seen, one type of sensor can be used in a number of applications. In applications where a sensor output is shared, care must be taken to ensure that a failure in one system does not disable the sensor or other systems. Because of the similarities in several of the systems and the use of shared sensors, the greatest potential for cost-effective system design is a single control system. The IMU shows great potential to be the controller for ride control, ABS, ASR, four-wheel-drive, and steering applications. The rate of introduction of new sensors and systems will depend on federal mandates, customer demand, and the need to improve engine fuel efficiency and to reduce emissions.

GLOSSARY

Adaptive suspension A suspension system that monitors motion of the front wheels and adjusts the suspension of the rear axle accordingly.

Arntics Acronym for Advanced Mobile Traffic Information and Communication System.

ASR (traction) A system to prevent wheel spin on slippery surfaces, to give maximum traction and acceleration.

Sensor / Application	Air Bag Deployment	Ride Control	ABS	Engine Control	Transmission	4 Wheel Drive	All Wheel Stearing	Engine Vibrarion	Cruise Control	Seat Belts	Power Steering Assist	Traction (ASR)	Collision Avoidance	Obstacle Detection	Inertial Navigation
Speed Rotation	▨	▨	▨	▨	▨	▨	▨		▨		▨	▨			
Speed Linear			□		□				□		□	□	□	□	□
Acceleration	▨	▨	▨	▨						▨		▨			▨
Vibration								▨							
Angular Rotation															▨

▨ USED □ MAY BE USED

FIGURE 7.24 Sensor applications.

IPR2023-01234
Petitioner - Ex. 1017 - Page 157

Measurand / Sensing Technique	Mechanical	Piezoelectric	Piezoresistive	Capacitive	Optical	Infrared	Radar	Laser	Ultrasonic	Hall Effect	Variable Reluctance	Magnetoresistive
Speed Rotation					☒					☒	☒	☒
Speed Linear						☒	☒	☒	☒			
Acceleration	☒	☒	☒	☒								
Vibration		☒		☒								
Angular Rotation				☒								

FIGURE 7.25 Sensor technologies.

Coriolis forces Forces exerted by a spinning body to oppose any motion at right angles to the axle.

Crash signature Shock waveform projected through a chassis during a collision.

Inertial navigation Guidance system giving accurate location.

IMU (inertial measurement unit) System used for guidance between two locations indicates road hazards and delays.

Lean burn Engine with high compression ratios and high air-to-fuel ratios for increased efficiency and low emissions.

Micromachining Manufacturing technology for micromechanical structures using chemical etching techniques.

NO_x Chemical symbol for oxides of nitrogen.

Prometheus Acronym for PROgraM for a European Traffic with Highest Efficiency and Unprecedented Safety.

Switched capacitor filter Technique for switching capacitors to simulate high-value resistors for low-frequency filters to minimize size.

REFERENCES

1. Osamu Ina, Yoshimi Yoshino, and Makio Lida, "Recent Intelligent Sensor Technology in Japan," S.A.E. paper 891709, 1989.
2. D. E. Bergfried, Mattes, B., and Rutz, R., "Electronic Crash Sensors for Restraint Systems," *Proceedings of the International Congress on Transportation Electronics,* Detroit, Oct. 1990, pp. 169–177.

IPR2023-01234
Petitioner - Ex. 1017 - Page 158

3. E. Peeters, Vergote, S., Puers, B., and Sansen, W., "A Highly Symmetrical Capacitive Microaccelerometer with Single Degree of Freedom Response," *Tranducers 91,* 1991, pp. 97–103.
4. J. T. Suminto, "A Simple High Performance Piezoresistive Accelerometer," *Transducers 91,* 1991, pp. 104–107.
5. J. C. Cole, "A New Capacitive Technology for Low-Cost Accelerometer Applications," *Sensors Expo. International,* 1989.
6. T. A. Core, Tsang, W. K., and Sherman, S. J., "Fabrication Technology for an Integrated Surface-Micromachined Sensor," *Solid State Technology,* Oct. 1993, pp. 39–47.
7. H. Wallentowitz, "Scope for the Integration of Powertrain and Chassis Control Systems: Traction Control—All Wheel Drive—Active Suspension," *Proceedings of the International Conference on Transportation Electronics,* S.A.E. paper 901168, 1990.
8. H. Kaneko, Muro, H., and French, P. J., "Optimization of Bipolar Magneto-Transistors," *Micro Systems Technologies 90,* 1990, pp. 599–604.
9. L. Raffaelli, Stewart, E., Borelli, J., and Quimby, R., "Monolithic Components for 77 GHz Automotive Collision Avoidance Radars," *Proceedings Sensors Expo,* 1993, pp. 261–268.
10. S. Aono, "Electronic Applications for Enhancing Automotive Safety," *Proceedings of the International Conference on Transportation Electronics,* SAE 901137, 1990, pp. 179–186.
11. J. Hellaker, "Prometheus-Strategy," *Proceedings of the International Congress Transportation Electronics,* SAE 901139, 1990, pp. 195–200.
12. H. Okamoto, and Hase, M., "The Progress of Amtics-Advanced Mobile Traffic Information and Communication System," *Proceedings of the International Congress Transportation Electronics,* SAE 901142, 1990, pp. 217–224.

ABOUT THE AUTHOR

William C. Dunn is a member of the technical staff in the Advanced Custom Technologies group at Motorola's Semiconductor Product Sector in Phoenix, Arizona. He has over 30 years' experience in circuit design and systems engineering. For the past 15 years he has been involved in the development of semiconductor sensors, smart power devices, and control systems for the automotive market. Prior to joining Motorola, he worked for several large corporations in the United Kingdom and United States, has written over 30 papers, and has over 30 patents issued and pending on mechanical sensor structures, semiconductor technology, and circuit design.

IPR2023-01234
Petitioner - Ex. 1017 - Page 159

CHAPTER 8
ENGINE KNOCK SENSORS

William G. Wolber
Executive Engineer
Cummins Electronics Co., Inc.

8.1 INTRODUCTION

Knock is a phenomenon characterized by undesirable structural vibration and noise generation and is peculiar to spark-ignited engines. Knock is undesirable both from a customer acceptance standpoint and also because severe knock can cause engine damage. The terms *ping* (light, barely observable knock) and *predetonation* (knock caused by ignition of the charge slightly before the full ignition of the flame front by the spark plug) are also commonly used in the industry, and not always with precision.

Historically, knock became an important engine phenomenon in the 1930s. In their search for performance improvements, designers of spark-ignited engines increased compression ratios beyond the capabilities of the gasoline formulations available to provide smooth, knock-free combustion. The discovery of gasoline additives such as tetraethyl lead, which improve the stability of the combustion process primarily by decreasing burn rate, permitted the fuel suppliers to provide a range of fuel knock properties at the pump to match with the range of engine requirements. As a result, by 1950, knock was not regarded as a significant engine performance limiting parameter since the car company could specify what fuel should be selected, ranging from "regular" to "super premium" grades. A blending fuel pump was even provided by one fuel company which allowed the operator of the vehicle to select exactly what grade of fuel he or she wished to use from a selection of six grades.

In the late 1960s, the situation began to change drastically. In response to public concern about air quality and health, legislation on automotive emissions became a new constraint on automotive engine design, first in the United States and more recently worldwide. The use of fuel additives to improve gasoline knock characteristics fell into disfavor for two reasons:

- Many of the better additives resulted in combustion products not desirable in the air. For example, most lead compounds are toxic at low levels to human and animal life.
- As engine designers strove to provide lower engine emissions, the use of the three-way catalytic converter cleanup device in the exhaust system became nearly universal. Unfortunately, most good fuel additives that improve knock characteristics poison the catalyst of the converter, rendering it ineffective. Also, many engine controls began to make use of the oxygen sensor feedback control loop. The catalyst on the oxygen sensor also is poisoned by the better additives.

This situation led to gradually more stringent federal regulation of the fuel industry, a trend which, in the end, legislated fuels with knock-improving additives completely off the

IPR2023-01234
Petitioner - Ex. 1017 - Page 161

market, so that by the mid 1980s, all spark-ignited automobile engines in the United States were being operated using lead-free gasoline. Of course, as leaded gasoline disappeared, the knock phenomenon returned. The auto industry knew what to do—lower compression ratios—but this step alone has accompanying negative consequences, such as lower fuel economy. Thus, the situation was one driven by the need to optimize between several principal goals: emission regulations, fuel supply characteristics, fuel economy goals, customer acceptability, and vehicle performance.

8.2 THE KNOCK PHENOMENON

8.2.1 Definition

Spark-ignited engine knock has been defined as "an undesirable mode of combustion that originates spontaneously and sporadically in the engine, producing sharp pressure pulses associated with a vibratory movement of the charge and the characteristic sound from which the phenomenon derives its name."[1] This definition at once conveys some of the difficulties of measuring the phenomenon and devising engine controls to minimize it. First, the ultimate standard is the reaction of the human to the vibration felt or the sound heard as a result of the knock. An attempt to measure the cause of the phenomenon leads one to the difficult problem of observing pressure waves in the cylinder. In fact, over the years these difficulties led the industry to devise an experimental comparison measurement technique which measured the octane rating of the *fuel*, not of the engine.

8.2.2 Laboratory Measurements

The CFR Engine. The basic comparison method which evolved for rating fuel knock quality involved the use of a simple, single-cylinder, spark-ignited engine called the CFR engine, and a pure hydrocarbon fuel—100 percent isooctane. Researchers discovered that they could reproduce knock phenomenon, laboratory to laboratory, by running this engine under specified conditions with this fuel.

Gasoline Octane Rating. A system of rating the knock characteristics of fuels, called the octane rating, was developed based on a comparison of the CFR engine performance with the test fuel compared to pure isooctane. On this scale, osooctane has an octane rating of 100; passenger car engine fuels ranged from the high 70s for "regular" to the high 90s for "super premium." (Fuel formulations with an octane rating over 100 were possible but were used mainly for aircraft engines.)

As the industry strove to put knock on a solid engineering basis, methods of measuring the resulting phenomena on the CFR engine, and commercial engines as well, were developed. The parameter on which the industry standardized was "jerk," the third-time derivative of engine block displacement. Scales evolved for comparing the relative knock performance of fuels and of engines based on the output of this kind of sensor. Much work was also done to correlate jerk sensor measurements with cylinder pressure phenomena.

The fundamental resonant frequency of the knock-generated pressure signal is dependent on engine cylinder geometry and the speed of sound in the charge gas. The structural vibration characteristics of the engine block that are excited by the fundamental knock event are determined by the engine block transfer function. Testing conducted on one cylinder of a six-cylinder spark-ignited engine demonstrates that high-frequency structural vibration components are good indicators of knock, despite the relatively low frequency high-pressure excitation event.[2] Structural vibration induced by mechanical events, such as valves opening

IPR2023-01234
Petitioner - Ex. 1017 - Page 162

and closing, introduces noise that can be confused with knock-induced vibrations. Careful signal analysis is required to overcome a sometimes poor signal-to-noise ratio.

The reverberation resonance of the cylinder typically lies in the range between 2 and 12 kHz. A useful rough estimate of the knock frequency for a given engine cylinder geometry is given by Draper's equation[3]:

$$\text{fr} = \frac{\text{Pmn} \times C}{\pi B} \tag{8.1}$$

where fr is the knock resonant frequency
Pmn is a vibration mode constant
C is the velocity of sound in the gas in the cylinder
and B is the radius of the cylinder

Using this equation, assuming that the average gas temperature is 2000 K so that C is 900 m/s, the first circumferential mode resonant frequency is estimated at 5.75 kHz for a cylinder of 10-cm bore.

As better cylinder pressure sensors have become available, cylinder pressure wave measurements, along with signal analysis techniques for deriving a knock rating number, have supplemented jerk measurements in the laboratory. The most popular signal analysis approach is to declare the maximum amplitude or peak-to-peak value of the bandpass filtered pressure data as a knock number, usually referred to as *knock intensity.*

Other ways of describing knock level are the root-mean square, mean square, or integral of the absolute value of the bandpass pressure oscillations during the knocking portions of the cycle. The spectral power of the pressure transformed into the frequency domain has been used for measurement. Derivative-based methods have also been established, based on rapid changes of cylinder pressure during the knock phenomenon, using the first, second, and third derivatives of the cylinder pressure history.

8.2.3 On-Board Knock Control

Improved Fuel Economy by Lowering Engine Compression Ratio. As engine control using microcomputers became established in the late 1970s and early 1980s for gasoline passenger car engines, and the octane rating of the fuels available for them dropped below 90, the automotive industry responded by lowering engine compression ratios. However, some of these smaller engines were equipped with turbochargers to recover some of the lost performance at wide open throttle. It was found that these engines could experience destructive high-speed knock at maximum speed and power. Not only were the knock reverberations in the cylinder large, but they were modulating a high base pressure wave. This could occur because the extra boost pressure from the turbocharger permits additional fuel to be metered to the engine without violating emissions restrictions on the control, since the amount of oxygen available to react with the fuel is greater. This could result in knock wave peaks exceeding the cylinder head pressure limit, as well as excessive vibration of the entire engine.

The knock occurring at wide open throttle had to be decreased, but retaining the additional power from the turbocharger at part throttle was very desirable. The electronic control was available to modulate the amount of fuel injected during the dangerous engine state; however, a means of sensing engine knock on-board in real time was needed. The sensors used are described in Sec. 8.3. The control operates by sensing that knock is over the permissible limit, and then reduces it either by retarding ignition timing or by opening a wastegate valve on the boosted manifold pressure.

Improved Fuel Economy by Raising Compression Ratio. Following the successful implementation of knock limit control on turbocharged engines, considerable experimentation was carried out to assess whether or not there is value in applying knock limit control to naturally aspirated spark-ignited engines. It was determined that if the engine knock was always kept

IPR2023-01234
Petitioner - Ex. 1017 - Page 163

less than an empirically determined limit for that type of engine and stored in the microcomputer control memory, then the knock level would not be objectionable even to the more critical car operators. Moreover, this could be accomplished while raising the compression ratio one full number—for example, from 8:1 to 9:1. If used to improve fuel economy, this change results in a 3 percent improvement in the corporate average fleet economy (CAFE) rating for that model/engine combination. At today's CAFE values, this is close to a one-mile-per-gallon improvement.

CAFE values are extremely important to a passenger car original equipment manufacturer (OEM). The larger, heavier luxury cars cannot achieve as low a CAFE value as the smaller, lighter cars. However, the larger cars are more profitable to produce. Thus, the mix of cars produced by an OEM can depend on just how close his CAFE results are coming to the mandated value. A way of improving fuel economy without downsizing, adding significant cost, or losing performance is very valuable.

Starting in the early 1980s, more and more passenger cars had a knock limit control and increased compression ratio. Such a change is usually scheduled at a time when the engine design and the tooling to make the engine are changing for other reasons. By 1990, 25 to 30 percent of the naturally aspirated passenger car engines produced in the United States (and all of the turbocharged engines) featured knock limit control.

8.2.4 Measurement and Control System Considerations

In addition to the problem of developing a suitable on-board sensor for knock, once the parameter to use had been selected, a number of other considerations had to be settled in effecting a satisfactory control. It was already pointed out that engine knock can be reduced either by retarding spark timing or by opening a manifold boost wastegate valve. In the United States, the candidate engines already had electronic control of spark timing, so that all that was needed to implement the knock control was an easily added change in the timing command in the control microcomputer. However, many control strategies exist for processing the knock signal. Perhaps the most elaborate of these was implemented on the first turbocharged engine knock limit control:

- The vibration frequency of the knock is specific to the engine model but lies between 2 and 12 kHz for passenger car engines. The sensor used was mechanically bandpass-tuned to match this characteristic with a Q of about 2.
- The major knock reverberations for a given cylinder occur during a time window that starts shortly after the cylinder reaches top dead center and ends 60 to 90 crank-angle degrees later. The control opened a signal gate to allow the knock signal to pass through and be averaged only when the engine was in these time windows.
- To prevent engine damage, whenever the knock signature exceeded the limit value, the control very rapidly retarded ignition by as much as 10 crank-angle degrees so that the engine would not be in severe knock even for the next few cylinder events. Then the control would very slowly advance the timing until the process repeated. This resulted in somewhat less than best engine performance but assured a comfortable margin of safety for the engine.
- The knock threshold limit in the control was modulated to increase with engine speed so as to compensate for greater noise background at high engine speed.

8.3 TECHNOLOGIES FOR SENSING KNOCK

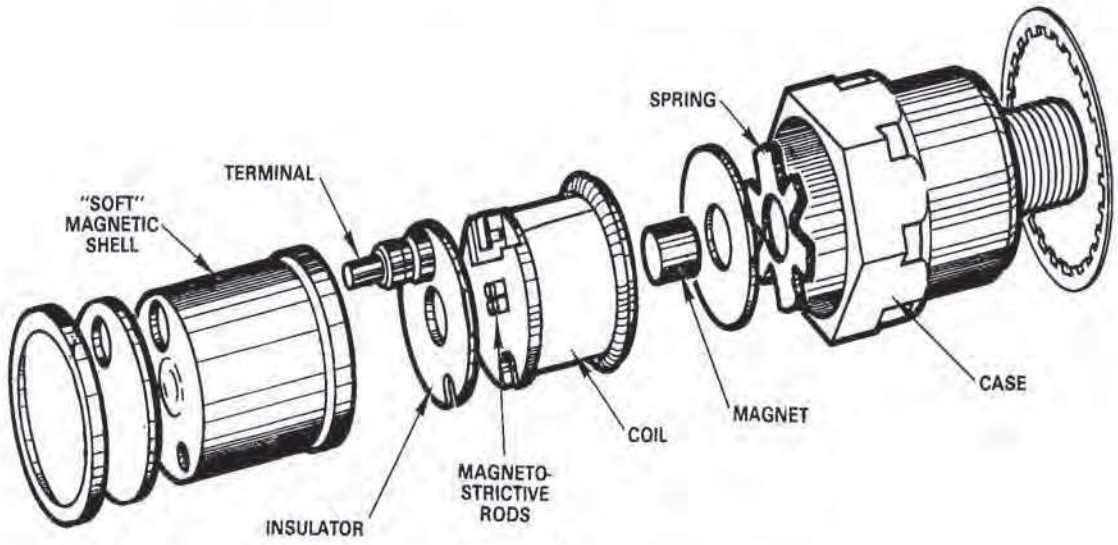
A number of different parameters have been selected for measuring knock in real time on board, and sensors have been developed for this purpose. It must be recognized that these

IPR2023-01234
Petitioner - Ex. 1017 - Page 164

sensors measure the magnitude of a consequential parameter driven by the knock, rather than the knock phenomenon itself. The overall effectiveness of the control is therefore determined not only by the intrinsic performance and stability of the sensor and control, but also by how robust the chain of causality is between the knock phenomenon and the parameter measured.

8.3.1 Jerk Sensors

Naturally enough, the first turbocharged engine knock limit control used a jerk sensor, a productionized version of the kind of sensor used for laboratory CFR engine testing. An exploded view of this sensor is shown in Fig. 8.1.



(a)



(b)

FIGURE 8.1 (*a*) An exploded view of a jerk sensor, and (*b*) a photograph of the sensor.

IPR2023-01234
Petitioner - Ex. 1017 - Page 165

Referring to the exploded view, it must be understood that when the sensor is fully assembled, the spider spring is preloaded, and all parts of the sensor except the coil cover are in compression. The nickel alloy magnetostrictive rods are biased mechanically in lengthwise compression and magnetically by the field impressed through the rods from the permanent magnet, returning through the ferromagnetic soft iron coil cover. The nickel alloy rods are the highest reluctance element in this magnetic circuit, and are in magnetic saturation.

The vibrations which are picked up and transmitted from the engine block through the mounting stud appear in the nickel alloy rods. These rods are of such a length that they comprise a broad passband mechanically resonant element. The compressive mechanical bias is sufficiently strong that the compression and rarefraction waves picked up are never large enough to take the rods out of net compression. The waves present in the rods therefore linearly modulate the magnetic reluctance of the magnetic circuit.

The many-turn coil wound around the magnetostrictive rods generates a voltage proportional to the rate of change of the magnetic flux; the flux, in turn, is inversely proportional to the magnetic reluctance of the rods. Since the vibrations picked up are already due to accelerations from the knock reverberations transmitted through the engine block, the voltage from the coil represents the third-time derivative of displacement, or jerk.

The vibration signal from a knocking engine is present virtually everywhere on the engine block, with signals from all cylinders superimposed. For passenger car engines, which rarely have more than eight cylinders, the major part of the knock signatures from the successive cylinder events are not superimposed in time, but rather consecutive without overlap. The time delay due to the distance from the cylinder to the sensor is always much less than 1 ms, whereas the cylinder-to-cylinder time is 2.5 ms even for an eight-cylinder engine at 6000 rpm.

However, the *absolute amplitude* of the knock signal does vary from location to location on the block. There is no best place to mount the sensor; rather, a site with a strong amplitude should be selected for a given engine model, and the sensor should always be mounted at that point on that engine model. The knock threshold is experimentally determined on that engine model with the sensor mounted at that location.

The method used for processing the knock signal and effecting control was described in Sec. 8.2.4. As time has gone on, the knock signal processing has tended to become simpler, although in the 1990s this may be changing. Time windows and mechanically resonant sensors have largely disappeared, and much of the filtering is now done digitally.

8.3.2 Accelerometer Sensors

The magnetostrictive jerk sensor, while satisfactory in performance, has too many parts to be a low-cost solution to measuring knock on board. Moreover, its mechanical assembly is not simple. In an effort to achieve lower-cost solutions, the industry found that the second-time derivative of displacement—acceleration—could be measured and used to implement a satisfactory knock control. The drawback to using an accelerometer compared to a jerk sensor is that it does not yield as good a signal-to-noise ratio; however, by using appropriate filtering, a good control signal can be achieved.

The first accelerometers used were mechanically bandpass-tuned, and some still are. However, in the 1990s, the trend has been to broadband sensors, again used with much electronic filtering. This has the advantage that one sensor model can be used for all engines, with the engine-specific frequency filtering characteristics built into the electronics module, which has to be engine-specific anyway. If the crucial filtering features are provided digitally, they can be installed as part of the engine-specific software.

Piezoelectric Accelerometer. Certain crystals of a specific cut or orientation possess the property that, when stressed, they produce a corresponding voltage. If such a crystal is loaded with a mass and spring, vibrations entering the assembly squeeze and pull the crystal with respect to the mass, and result in a signal which is a measure of the acceleration of the body to

IPR2023-01234
Petitioner - Ex. 1017 - Page 166

which the assembly is attached. These signals can be substantial in size but appear electrically to be sourced at a high (capacitive) driving point impedance. Thus, care has to be taken to ensure that capacitively coupled noise does not contaminate the signal.

There are a variety of single crystals which exhibit the piezoelectric effect, but silicon is not one of them. Efforts to devise a silicon micromachined accelerometer were stymied for a long time by this fact, but a solution will be described below. Single crystal quartz is the material which was used in the single-crystal piezoelectric accelerometers.

In some cases, it is possible to use the mass of the piezoelectric element itself as the mass, and to combine the spring with one of the crystal electrodes. In such a design, the only parts are a spring, a contact, the crystal, and the housing.

Piezoceramic Accelerometer. Another type of piezoelectric element is the piezoceramic device. Piezoceramics are not single crystals. They can be fired into just about any shape, just like a ceramic insulator or a vase. By impressing a high voltage across electrodes on the ceramic while the material is at a high temperature—above its Curie temperature—and then gradually lowering the temperature, the piezoceramic becomes *poled,* or piezoelectric across the electrodes.

The best piezoceramics tend to belong to the lead-zirconate-titanate (PZT) family. These materials have a Curie temperature from 250 to 500 °C. If the sensor ever gets above its Curie temperature, its poling becomes degraded, and its calibration is no longer valid. However, these engine block-mounted sensors will not experience temperatures higher than about 125 to 150 °C, even during hot soak, so they can be used for the knock sensor.

Single-crystal piezoelectric accelerometers also have a Curie temperature, but it is typically much higher than for the piezoceramics. Quartz, for example, has a Curie temperature over 600 °C.

Because the piezoceramic materials can be molded into any shape, handled roughly, sawn and machined, coated with thick-film metallic electrodes, and so on, they lend themselves to easy, low-cost mass production. As a result, they have become pretty much the knock sensor of choice for the automobile industry. A drawing of a piezoceramic accelerometer knock sensor is shown in Fig. 8.2. In this particular design, the spring and top electrode have been combined into one part, but the mass is a separate metallic part between the piezoceramic disc and the spring. The whole assembly is stacked on a mandrel which extends up from the base-stud which forms most of the package.

8.3.3 Silicon Accelerometer

As previously noted, silicon itself cannot be made piezoelectric. However, it is possible to make a silicon micromachined accelerometer by anisotropically machining a cantilevered T-shaped structure into each cell of a silicon wafer, using a chemical etch. Strain gauges are diffused or implanted into the cantilever—the vertical bar of the T. The mass of the horizontal crossbar of the T and the spring constant of the cantilever provide the mechanical-to-strain transduction. Such accelerometers are in mass production for use in antiskid braking systems and as triggers for air bag safety devices. Whether or not they will replace piezoceramic knock sensors is primarily a matter of economics. Technically, the silicon accelerometer is satisfactory; its temperature limit is about 150 °C, which is adequate for on-block mounting.

8.3.4 Other Sensors

Instantaneous Cylinder Pressure Sensor. The direct measurement of instantaneous cylinder pressure permits the extraction of the pressure reverberation signal, which is the direct cause of knock. While this would be a very desirable signal to use for knock detection, it has not been implemented in on-board knock control systems for several reasons:

IPR2023-01234
Petitioner - Ex. 1017 - Page 167

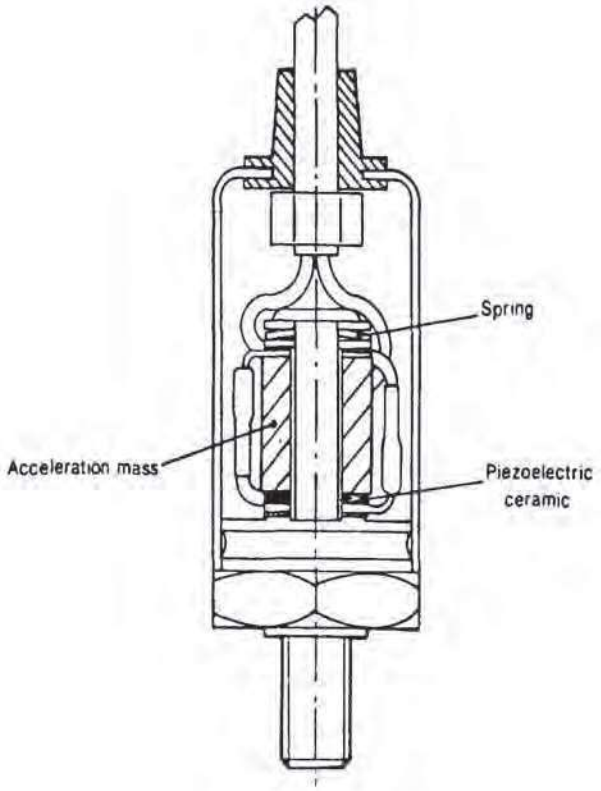


FIGURE 8.2 A piezoceramic accelerometer knock sensor.

- Either the same cylinder must always be the one to experience knock first and most severely, or one must have a sensor on every cylinder.
- The cylinder pressure wave is complex, and knock is only one of many signature elements present. Deriving a unique knock signal requires considerable signal processing in real time.
- While cylinder pressure sensors exist which are suitable for test purposes, a durable, low-cost, mass-producable on-board pressure sensor is not yet available.

In spite of these difficulties, work continues on cylinder pressure sensors for on-board control use, not so much to be used as knock-sensing devices as for use in deriving an instantaneous torque measurement (see Chap. 9). If this approach succeeds, then it is reasonable to suppose that the cylinder pressure sensor will be used to provide the inputs for obtaining both torque and knock measurements.

Since a spark-ignited engine already has a spark plug mounted in each cylinder head, it is possible to convert the spark plug into a kind of "poor man's pressure sensor" by mounting a piezoceramic washer held in compression between the spark plug and the cylinder head when the plug is torqued down. This arrangement has in fact appeared on a commercial passenger car engine. While the signal is not presently being used to extract a knock signal, suitable signal processing would make this possible.

Hydrophone in Coolant. In Sec. 8.3.1, it was mentioned that the knock signal appears virtually everywhere on the block. In fact, it even appears in the coolant fluid faithfully reproduced. This fact led to experiments in which hydrophones were mounted in the coolant and used as knock sensors. This approach has never reached production because it has no advantage over a block-mounted sensor and is in fact more difficult to package and to mount on the engine.

IPR2023-01234
Petitioner - Ex. 1017 - Page 168

8.4 SUMMARY

In a remarkably short span of time, the on-board sensing of knock and its control have become a rather standard feature of passenger car engine control electronics. At the same time, the on-board sensors have been developed and are now largely mature. Acceleration has become the parameter of choice for most of these control systems, and the required accelerometers are typically based upon piezoceramic technology; it seems likely that this will remain the case at least through the 1990s. The rapid proliferation of these systems was facilitated by three factors:

- A solid background of experimental knowledge about knock and how to control it was established in the laboratory during the several decades before lead-free gas was mandated.
- The three legislated pressures of emissions limits, CAFE fuel economy goals, and no-lead fuel, combined with a customer base used to engines without knock, made solving the knock problem a high priority.
- The already widespread use of digital microcomputer engine control made the addition of knock limit control a straightforward design change.

GLOSSARY

Curie temperature The temperature above which a piezoelectric crystal or piezoceramic element no longer reliably retains its original piezoelectric characteristics.

Jerk sensor A sensor which measures the third-time derivative of displacement.

Knock Acoustic engine noise and vibration of characteristic frequency caused by uneven combustion in the engine cylinder(s).

Octane rating A measure of the resistance of a gasoline fuel to knock, as compared to pure isooctane hydrocarbon.

Retarding Causing engine combustion to occur at a larger angle past top dead center, by delaying the time at which the signal to start the spark event occurs.

Turbocharger A device which compresses engine intake manifold air by using the engine exhaust to drive a turbine and compressor.

Wastegate valve A valve in the exhaust system of a turbocharged diesel engine which causes part of the exhaust to bypass the turbine. The same name is also applied to a valve on a turbocharged gasoline engine which causes part of the boosted intake manifold air to dump to the atmosphere, dropping the manifold pressure.

REFERENCES

1. Paulius V. Puzinauskas, "Examination of methods used to characterize knock," SAE Paper 920808, Superflor Corp.
2. Karp P. Schmillen (FEV Motorentechnik, Aachen, Germany) and Manfred Rechs (Institute for Applied Thermodynamics, Technical University of Aachen, Germany), "Different methods of knock detection and knock control," SAE Paper 910858.
3. Masayoshi Kaneyasu (Hitachi America, Ltd.), Nobuo Kurihara, Kozo Katogi, and Hiroatsu Tokuda (Hitachi Ltd.), "Engine knock detection using multi-spectrum method," SAE Paper 920702.

IPR2023-01234
Petitioner - Ex. 1017 - Page 169

ABOUT THE AUTHOR

William G. Wolber, executive engineer, Cummins Electronics Co., Inc., has 38 years' experience in the development of sensors, actuators, and instruments for application in automobiles and other products. Since 1981, he has been involved principally in the development of sensors and controls for heavy duty diesel engines for Cummins Electronics Co. He holds 15 U.S. patents and is the author of over 50 technical papers. He has lectured and conducted seminars internationally for the Society of Automotive Engineers and other organizations.

IPR2023-01234
Petitioner - Ex. 1017 - Page 170

CHAPTER 9
ENGINE TORQUE SENSORS

William G. Wolber
Executive Engineer
Cummins Electronics Co. Inc.

9.1 INTRODUCTION

Torque is one of the primary state parameters of an engine; along with speed it is a fundamental measure related to the output power. Torque can be defined as the moment produced by the engine crankshaft tending to cause the output driveline to turn and thereby deliver power to the load. For rotary motion, the torque multiplied by the rotational speed equals the power delivered by the shaft. In derivative form, Newton's law states that torque T equals the rotational moment of inertia I times the angular acceleration α. Hence, at constant rotational speed, instantaneous power is proportional to instantaneous torque. This is an important relationship because torque and, thus, delivered power can change rapidly compared to rotational speed.

Portraying the engine as a torque-delivering device is a useful concept. When an engine is used in road service as prime mover power, the operator of the vehicle tends to ask the vehicle for positive or negative incremental acceleration, as the operator perceives it to be falling behind or closing upon the vehicle ahead. Hence, the operator asks the engine for more or less torque. If the engine is spark ignited, this happens naturally through the modulation of the engine air intake flow path. In a diesel engine, it happens indirectly. The operator controls fuel rate, which to first approximation is linearly related to power. For slowly varying engine speed and load, an incremental change in power results in a change in torque and therefore a change in acceleration.

9.1.1 Time-Scale Definitions

At this point, it is useful to define two time scales which will be used with regard to the engine. A reciprocating engine is never truly operating steady state. It is a cyclic succession of batch processes, a kind of system which chemical engineers have termed "continuous-by-jerks." Each cylinder absorbs shaft energy during the compression stroke and releases a larger amount of shaft energy through combustion during the power stroke. These actions are so interleaved that the drive shaft is continually accelerating and decelerating in step with cylinder events. Nevertheless, a quasi-steady-state model for the engine can be defined in which these rapid fluctuations are ignored and attention is focused on the more slowly varying state parameters which are nearly stationary during one engine revolution. This is the situation the operator senses and controls and it is also the primary focus of the control algorithms in a microcomputer-based engine control today. (As of 1994, all electronic engine controls operate on the "engine time scale.")

IPR2023-01234
Petitioner - Ex. 1017 - Page 171

Quasi-Steady-State Torque. Quasi-steady-state torque is defined as that running average value of torque that varies slowly with respect to the cylinder-to-cylinder period, but rapidly with respect to vehicle changes in motion and load. To quantize this state, it is noted that an unloaded engine coupled to flywheel inertia may accelerate from idle to maximum speed in one to five seconds when subjected to wide open throttle and that this performance is essentially reproduced whether the change in throttle position occurs in 20 ms or 1 ms. Quasi-steady-state torque is what the operator is interested in commanding, and so, if we visualize a torque command-feedback engine control, it is the parameter of interest.

Instantaneous Torque. Today's electronic engine control can usefully respond much more rapidly than this for those state parameters having to do with each cylinder batch process itself. The preparation of the fuel and air charges and the timing of ignition take place on a time scale measured in fractions of a cylinder period, and thus the time scale of interest ranges from 30 μs to 20 ms. This time scale corresponds to the instantaneous engine state. It is the time scale of the torque impulses that are termed instantaneous torque.

In order to use instantaneous torque measurements, it must be recognized that the reciprocating engine is a cyclic machine in which major functions and the parameters that characterize them are tied together in sequence mechanically by the crankshaft and camshaft. Proper adjustment of those other parameters that are free to be changed independently of the train of instantaneous cylinder events allows optimization of the overall torque impulse generation in real time. For example, a theoretical examination of the internal combustion engine cycle has shown that the centroid of the cylinder pressure wave should occur about 15 crank-angle degrees after top dead center ("Powell's Magic Angle") to maximize the instantaneous incremental torque from that cylinder.[1,2] No spark or injection timing algorithm can do any better than to effect such timing of the torque impulse. Note, however, that we are stating where the centroid of the pressure wave should be for the best torque impulse, not where the fuel injection or ignition should be commanded.

State-of-the-art scheduled spark timing controls are based upon test data from one or more prototype engines run extensively in the laboratory on a dynamometer under quasi-steady-state conditions. From the data obtained, families of spark plug or injection timing (crank angle) surfaces versus engine speed, load, etc., are derived that correspond to optimum economy and performance while meeting emission requirements. These data then form the schedule embedded in the control microcomputer memory for all engines of that model produced. This type of scheduled computer control is standard throughout the industry today for all electronically controlled engines, both spark-ignited and compression ignition, with just two exceptions. These are the oxygen sensor feedback control loop, which keeps an engine equipped with a three-way catalyst in the stoichiometric "window" of the catalyst efficiency performance, and the speed governing feedback control algorithm used for power takeoff (PTO) operations, diesel all-speed governors, and generator-set frequency control.

By contrast, the addition of an on-board instantaneous torque measurement would permit the direct feedback control of several key engine control parameters. To take maximum advantage of such feedback control, an advanced instantaneous crankshaft position sensor is also required.

The controls which could be implemented through use of an instantaneous torque feedback control system are:

- Quasi-steady-state torque feedback control in response to torque command.
- Spark-ignition or compression-ignition timing control by feedback of instantaneous torque impulse timing compared to the norm of the "Magic Angle." Torque impulse amplitude can also be optimized against timing. These controls can be implemented on a cylinder-by-cylinder basis, for spark-ignited pulse sequential fuel injected engines, and for unit-injected diesel engines.
- Cylinder-by-cylinder torque-leveling feedback control can be implemented by adjusting the amount of fuel injected into each cylinder to obtain equal torque impulses from each one.

IPR2023-01234
Petitioner - Ex. 1017 - Page 172

This results in a quiet, smoothly running engine with a somewhat improved maximum power, because the torque limit can be set for a more nearly constant cylinder event instead of for the worst case cylinder.

- The instantaneous torque signal is also rich in a variety of diagnostic information—for example, to measure engine power or for use as a miss detector.

9.2 AUTOMOTIVE APPLICATIONS OF TORQUE MEASUREMENT

9.2.1 Off-Board Measurement

The principal automotive use of torque measurement today is in the testing and evaluation of engines using the engine dynamometer. The torque sensor is inserted as a drive shaft between the engine and the dynamometer; the shaft of the sensor is a torsional Hooke's law member and its twist is measured. Typically the torque is actually measured using a strain gage bridge on the drive shaft. Full-scale twist is limited to no more than about a degree per foot of shaft for engines in the 50 to 500 hp range.

In a dc torque sensor, the strain gage bridge is powered from an external source through slip rings, and the offset voltage is taken off the bridge the same way (Fig. 9.1). The sensor is necessarily bulky, large, fragile, and costly. A more rugged ac strain gage sensor can be made using rotational transformers, as shown schematically in Fig. 9.2.

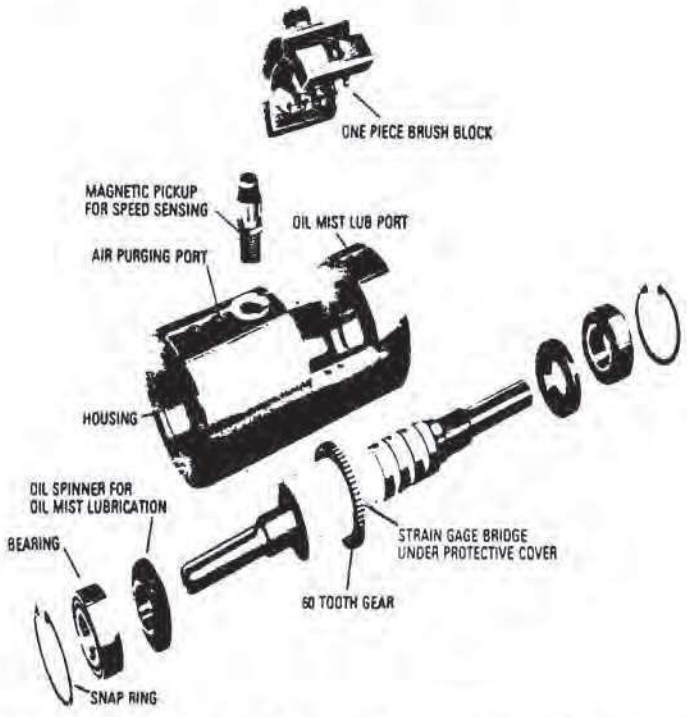


FIGURE 9.1 Exploded view of rotating shaft torque sensor with slip rings. *(Courtesy of the Lebow Div., the Eaton Corp.)*

Developmental Tests. In engine development, a good bit of the work involves fine-tuning the engine to get the maximum power and minimum fuel consumption at various engine conditions. Since power equals torque multiplied by engine speed, if tests are carried out at constant speed, maximum power occurs at maximum torque. Thus, the torque sensor can be used as a direct indicator of whether changes in the engine design or control will improve power.

IPR2023-01234
Petitioner - Ex. 1017 - Page 173

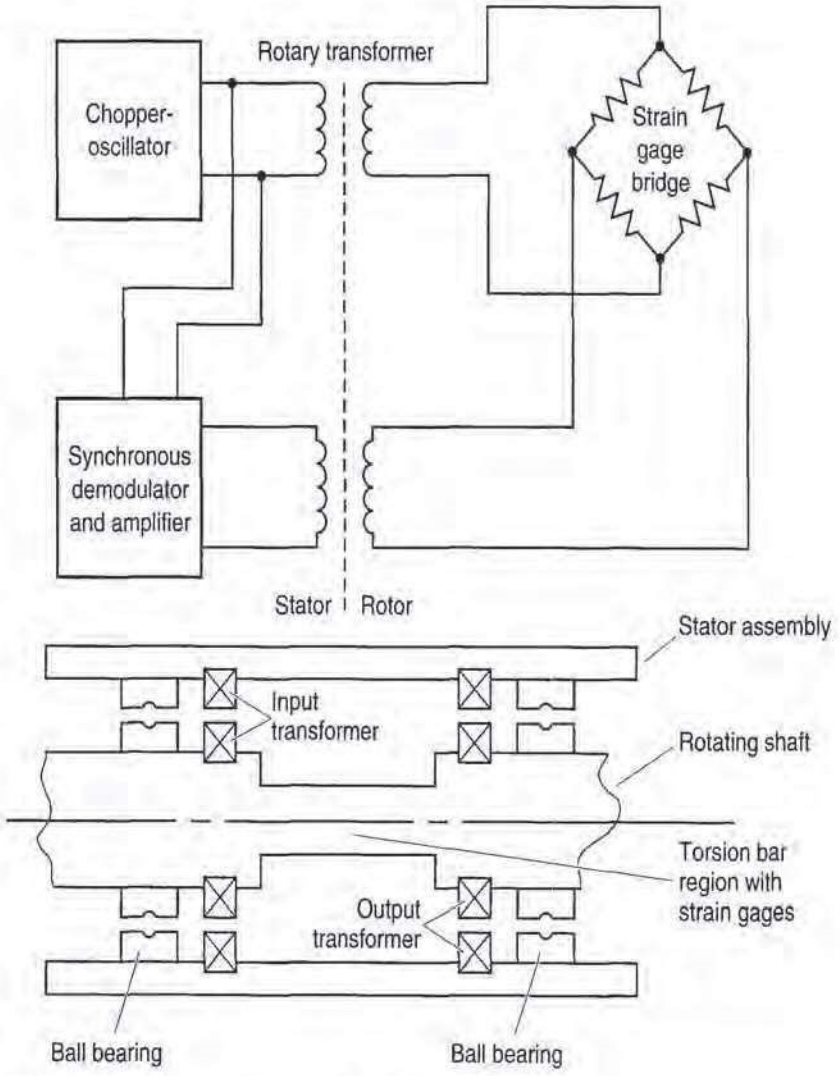


FIGURE 9.2 Rotary transformer rotating shaft torque sensor.

End-of-Line Manufacturing Tests. Particularly in the case of heavy duty diesel engines, the price of the engine is directly related to engine rated horsepower. Such engines are in a real sense sold by the horsepower. The manufacturer certifies that a certain model will deliver no less than a certain horsepower when run at rated conditions. The engine is tested at the end of the assembly line for a number of attributes, chief among which is assurance that it exceeds stated horsepower at rated speed. The assurance is provided by accurate torque and speed measurements.

In-Service Tests. Occasionally, torque sensors may be used with an engine that is being tested under field conditions. This is relatively straightforward when the engine is being used in a stationary application, but not if it is installed in a vehicle.

9.2.2 On-Board Measurements

To be most useful on board, a torque sensor should not only be accurate but also fast in response. Most of the sensors available today do not have this attribute, because they were developed for use in dynamometer tests.

To be a useful on-board engine control sensor, the torque sensor of the future also needs several other attributes:

IPR2023-01234
Petitioner - Ex. 1017 - Page 174

- It must be extremely rugged, which for practical purposes means noncontacting with respect to the driveline.
- It must be able to withstand torque impulses of 10 to 20 times its full-scale measuring capability without degrading its accuracy. For strain gage type sensors, this means that the sensor would always have to measure in the lowest 5 to 10 percent of its range, where it is not very accurate.
- Installation of the sensor must not cause any significant change in the compliance of the driveline. This is a requirement imposed by engine application engineers to avoid spoiling the tradeoffs that have been made to avoid severe torsional vibrations.
- Ideally, the shaft of the sensor should be very short in length (in part to achieve the preceding characteristics). Unfortunately, for a torsional Hooke's law device, that means the full-scale shaft twist angle will be very small.

In spite of these formidable barriers to a satisfactory design, a wide variety of desirable applications could be made using an on-board instantaneous torque sensor. As a result, many researchers and developers both in academia and industry are working to achieve such a measurement directly or indirectly.

Power Measurement of Large Engines. Means exist for field service personnel to measure engine power in the field for engines installed in a vehicle and rated at up to 400 to 500 hp. For larger vehicle-mounted engines, this measurement is a difficult problem for a number of reasons:

- A rugged on-board sensor is not available.
- These engines are often installed in very large machines such as mine-haul trucks and front-end loaders located off the road in remote areas.
- Dynamometers large enough to load down the engine to full power are not available except in a very few locations.

One of the most frequent customer complaints about heavy duty engines is perceived loss of power. Often such complaints must be resolved at the field location and on a subjective basis. The engine and vehicle can be fully loaded in actual work operation, and engine speed is known accurately. If an on-board torque sensor were available, such complaints could be quickly resolved, and it would be well worth installing on large engines.

Miss Detection. The California Air Resources Board has mandated that all passenger vehicles shall be equipped with an engine diagnostic capability that includes a miss detector. While the regulation is not yet in force as of the time of this writing, the automotive industry knows that every segment will be affected by the requirement by the end of the decade. Many vehicle OEMs, first-tier automotive suppliers, entrepreneurial sensor firms, and academic researchers are working hard to meet the miss detector requirements, mainly basing their efforts on the same technologies useful for measuring or inferring torque.[3]

Torque Feedback Control. The reciprocating engine could be configured in a feedback control mode if equipped with an on-board quasi-steady-state torque sensor capable of responding at least as fast as the engine/driveline. In a torque command drive-by-wire system, the operator input would be a command for a new torque, greater or less than the present torque. The engine control would do its best to provide the new torque as rapidly as possible. The feedback error signal would be the difference between the torque command and the sensor output. Of course, the new torque and the resulting acceleration or deceleration would have to be limited within bounds set by maxima for cylinder pressure, emissions production, exhaust gas temperature, fuel economy, and so on.

Feedback Control of Timing. As was described in the introduction to this chapter, the measurement of instantaneous torque, on board, along with instantaneous crank angle position,

IPR2023-01234
Petitioner - Ex. 1017 - Page 175

would allow the engine control computer to use signature recognition to measure the crank angle at which the centroid of the torque impulse is located, for each cylinder. From this information, probably with some compensation for seriously off-normal engine conditions as stored in computer memory, the engine control can determine if that impulse was centered at Powell's Magic Angle, and, if not, how much earlier or later the chain of combustion events needs to be started. Most likely, the computer also needs to decide between updating that cylinder based upon that information alone and waiting a whole engine revolution to update, or also basing the correction upon abrupt changes in operator input, load, knock level, etc. In any case, under quasi-steady-state conditions, the best efficiency of that engine for converting chemical energy into shaft power by proper engine timing could be achieved this way whether the engine is spark-ignited or compression-ignition.

Cylinder Torque Leveling. Individual trimming of the amount of fuel for each cylinder can be realized on pulse sequential fuel injected spark-ignited engines and on unit injector diesel engines by matching the torque impulse for each cylinder to the average of all cylinders. Then the average impulse can be raised to very nearly the maximum value the engine is designed for. In today's engines, the control must provide a guard band between the maximum torque for the worst case cylinder and the design limit for the engine (commonly called the maximum cylinder pressure limit or the peak torque limit). If the torque impulses delivered by each cylinder were known to be controlled to be equal, the guard band could be reduced and more power obtained from a given engine.

While cylinder-to-cylinder torque leveling is not the same as compression leveling, an engine controlled cylinder by cylinder for timing and torque leveling intuitively would appear to be as smoothly running and low in acoustic noise emission as can be visualized.

Engine Diagnostics. The instantaneous torque signature is very rich in diagnostic information. A figure of merit for engine roughness can easily be obtained in real time, from which a lean-limit control signal can be derived. The miss detector responds to an extreme case of roughness. Ragged ignition and flame front formation, imperfect injection, poor distribution, and many other engine and control problems can be measured or inferred from such a signal, on board and in real time.

9.3 DIRECT TORQUE SENSORS

9.3.1 Reaction Force

The use of a strain-gaged torsional Hooke's law shaft to measure torque at the dynamometer has been described in Sec. 9.2.1. Torque can also be measured in the test cell by instrumenting the engine or dynamometer mounting with strain gage load cells to measure reaction torque. This is a useful way to measure quasi-steady-state torque, but is not a good measuring system for instantaneous torque, as both the engine and its load have considerable inertia and damping which attenuate the torque impulse and may introduce phase delay. It is also not a good on-board measurement because the engine mounts on a vehicle are designed to attenuate and damp out bouncing from road and load irregularities. Also, as a function of time, temperature, ozone concentration, and other variables, they tend to stiffen substantially and change the deflection of the engine at its mounts as a function of torque.

9.3.2 Torsional Strain (Twist) Sensors

Magnetic Vector Sensors. The strain-gaged torsional Hooke's law sensor was described in Sec. 9.2.1. A more practical approach to an on-board torque sensor is a noncontacting design

called a magnetic vector sensor.[4,5] This sensor operates on the principle that the magnetic domains in a ferromagnetic shaft delivering torque are randomly distributed when no torque is being delivered, but that each domain, on average, is slightly rotated in the tangential direction when torque is delivered by the shaft and twists it. If an ac-driven coil is placed near the shaft and surrounded by four sensing coils arranged mechanically and electrically as a bridge, the amplitude of the bridge offset is proportional to the magnetic vector tangential component, and therefore to twist and torque.

If the magnetic domains were truly statistically distributed over a small range of shaft angle, such a sensor would be able to measure instantaneous torque. Unfortunately, they are not. Over a small shaft angle increment, the average torque vector does not net to zero when torque is zero, and the output is characterized by a fixed pattern noise which repeats every 360°. The magnetic vector sensor is reasonably accurate measuring quasi-steady-state torque, but the signal-to-noise ratio becomes poor when an attempt is made to measure instantaneous torque.

Further work on this sensor simplified and miniaturized it.[6] The bridge was replaced by a single tangential coil, and the sensor was made small enough so that it could be mounted in the rear crankshaft bearing. However, it still was not able to measure instantaneous torque.

Investigation continues on techniques to reduce the fixed pattern noise, and some claims of progress have been made. However, at this writing, a production on-board torque sensor is not available.

Optical Twist Measurement. Research work has been reported on a sensor that changes the duty factor of light pulses sensed after passing through sets of slits at both ends of a shaft.[7] The principle of its operation is shown in Fig. 9.3. Such a sensor is noncontacting and can be made robust, but it requires appreciable shaft length and therefore adds compliance to the driveline. The work has not been engineered to produce an economical on-board device.

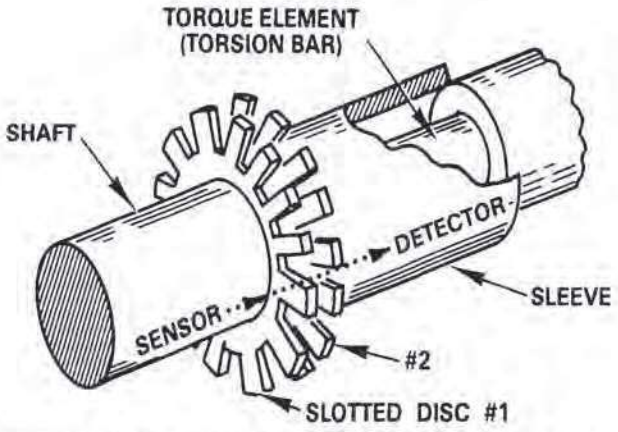


FIGURE 9.3 Optical torque meter. *(Courtesy of The Bendix Corp.)*

Capacitive Twist Sensor. An electrode pattern can be made using interdigitated electrodes spaced one or two degrees apart on two facing flat discs.[8] One of the discs is stationary; the other rotates with the crankshaft. Two such pairs of electrodes can be operated with phase detection measurement to provide a virtually instantaneous signal proportional to the twist of the shaft; the rotating halves of the electrode pairs are attached to the ends of the Hooke's law torsional spring. Obviously, this arrangement has the same drawback as the optical sensor in that it has to have some shaft length to twist and, therefore, some compliance. However, it is robust, has good accuracy, and is a more practical on-board device than the optical twist sen-

IPR2023-01234
Petitioner - Ex. 1017 - Page 177

sor. This sensor can also yield an accurate crankshaft position measurement. Nevertheless, an on-board version is not available today.

9.4 INFERRED TORQUE MEASUREMENT

Indirect measurements of torque-related parameters can be made with a view to inferring torque from the measurements. Typically, such measurements require considerable real-time computation in the control microcomputer, along with precision measurement of the instantaneous crank angle position. Much work is in progress in a variety of locations to make these methods into practical instantaneous torque control signals.

9.4.1 Instantaneous Cylinder Pressure Sensors

Engine development engineers have long used piezoelectric crystal cylinder pressure sensors in the laboratory to make engine power and heat release measurements and as an aid to development. The best of these sensors use doped quartz single crystals. They are accurate and reasonably robust, but expensive and unforgiving if overranged or subjected to excessive temperatures. Much work continues on development of a mass-producable on-board cylinder pressure sensor.[9] One of the Japanese car manufacturers is reported to have a top-of-the-line passenger car model, available only in Japan, with engine control using piezoceramic cylinder pressure sensors.

The signals from cylinder pressure sensors need considerable real-time data processing to produce inferred "torque" signals. In one method, the noise always present is filtered, the pressure signal is multiplied by an instantaneous shaft angle term, and integrated over the angle range representative of the power stroke of the cylinder. From this a measure of torque contribution from that cylinder is obtained. The best digital signal processing (DSP) chips available in the early 1990s are barely able to keep up with cylinder events in such a process. Nevertheless, we can be confident that if the proper sensors are available in the late 90s, the microcomputer chip performance required will be available and cost effective too.

9.4.2 Digital Period Analysis (DPA)

When an engine is run at low speed and heavy load, the instantaneous angular velocity of its output shaft on the engine side of the flywheel varies at the fundamental frequency of the cylinders, since the compression stroke of each cylinder abstracts torque and the power stroke adds a larger amount. The signal-to-noise ratio of the measurement of instantaneous angular velocity (or rather of its reciprocal, instantaneous period) degrades with increasing engine speed and lighter load, but is a useful way to infer torque-like measures of engine performance.

Figure 9.4 shows an idealized plot of instantaneous crankshaft period against crank angle under constant speed, lean conditions. The instantaneous period wave is seen to be a variation about the mean period value. This waveform can actually be measured using a precision, multitoothed crankshaft position sensor. For reasons which will be explained later, the instantaneous angular velocity lags the torque inputs producing it. As a result, the period wave appears to lead the torque or cylinder pressure variations.

Timing Control by DPA. The general case of the variation in crankshaft velocity in a four-cylinder engine can be described by:

$$T_N = AL\,P_N(\theta)\sin\theta = AL\,P_{(N+3)}(\theta)\sin\theta + T_F(\theta) + T_L + I\ddot{\theta} \qquad (9.1)$$

IPR2023-01234
Petitioner - Ex. 1017 - Page 178

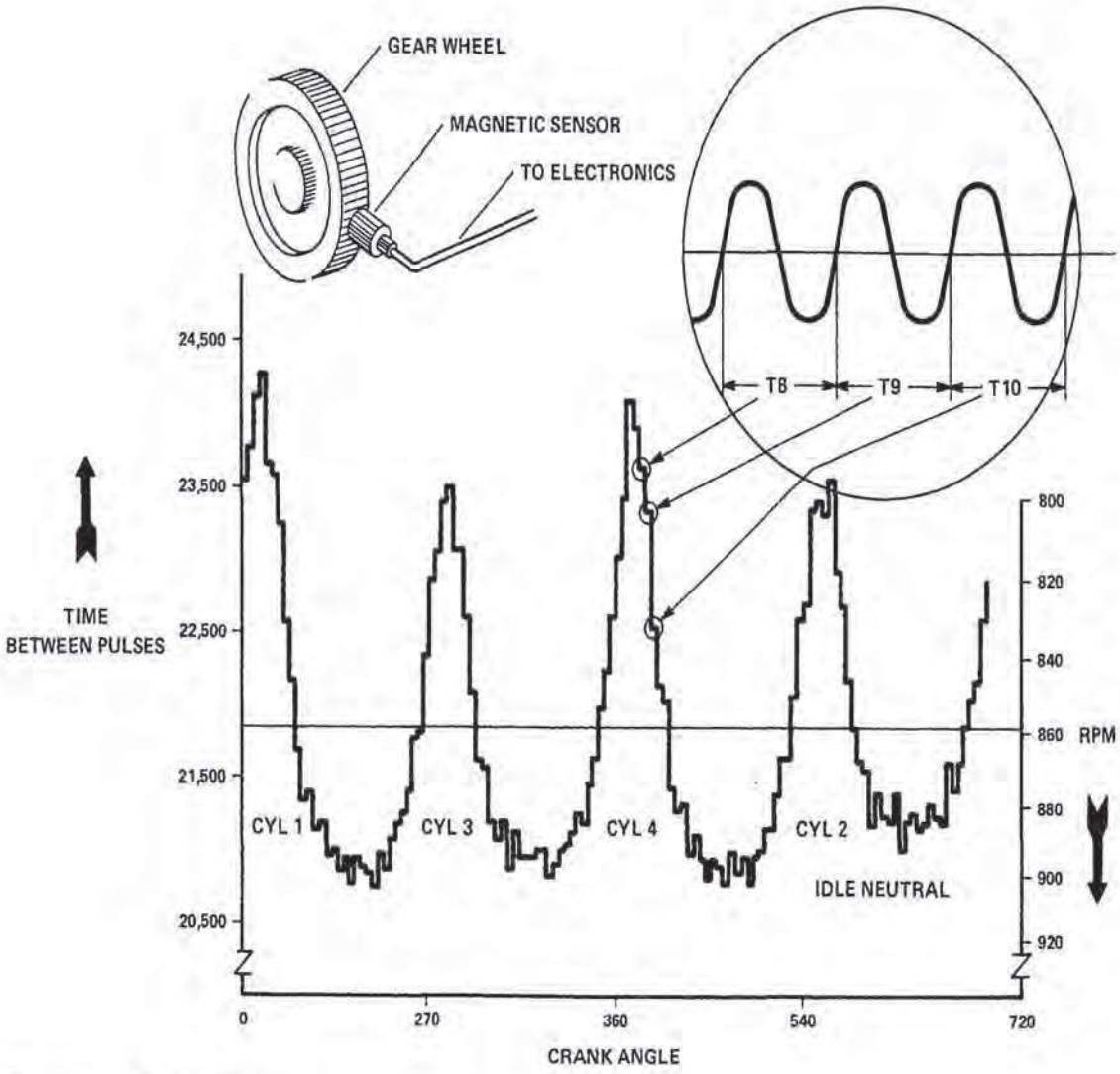


FIGURE 9.4 Digital period input.

where T_N = instantaneous torque due to burning gases in cylinder N at angle θ
A = area of piston
L = maximum effective crank lever arm
$P_N(\theta)$ = pressure in cylinder N (a function of crank angle and many other variables)
$P_{(N+3)}(\theta)$ = pressure in third cylinder to fire after N which is in its compression stroke when cylinder N is in its power stroke
$T_F(\theta)$ = so-called "fixed load" torque due to friction, accessories, etc., and is generally a function of $d\theta/dt$
T_L = torque delivered to the load
I = inertia of the engine, drivetrain, and vehicle reaction through the wheels
$\ddot{\theta}$ = instantaneous angular acceleration of the crankshaft

In order for Eq. (9.1) to remain valid, as T_N varies with angle θ due to the variations of $P_N(\theta)$ and the sin θ term, some term in the right-hand side of the equation must vary correspondingly. In fact, the major effect is upon $\ddot{\theta}$, the angular acceleration, which varies both in magnitude and sign; being positive when P_N is large and θ is near $\pi/2$, and negative when P_N is small and θ is near 0 and π. If Eq. (9.1) is integrated as a function of θ from $\theta = 0$ to $\theta = \pi$ and

IPR2023-01234
Petitioner - Ex. 1017 - Page 179

then the summation is extended to angles larger than π by adding in the contributions of cylinders $N + 1$ and $N + 3$, the term in $I\ddot{\theta}$ becomes an average angular velocity over a complete engine cycle.

One important consequence of the preceding analysis is that, upon integration of the equation, the sin θ term becomes cos θ—that is, the angular velocity wave lags the torque impulses causing it by π/2. Another consequence is that the amplitude of the period wave reflects the net contribution of the cylinders—if the load increases, and $P_N(\theta)$ increases to keep average angular velocity constant, the amplitude of the period wave must increase. The $I\ddot{\theta}$ term has become an Iω, it is the reciprocal of this term which was plotted in Fig. 9.4.

When a spark plug fires or fuel is injected into a diesel cylinder, the pressure in the cylinder takes a finite length of time to build—first, because of a delay to get the fire started and then because of the finite and relatively constant flame propagation time, and second, because the temperature rise which causes pressure to rise, peaks only shortly before combustion is completed. Thereafter, pressure falls as the piston displaces under the pressure of the gases. Mean best torque (MBT) will be achieved from that cylinder when the pressure pulse, convolved with sin θ yields a maximum upon integration. As described previously, researchers at Stanford University have found analytically and confirmed experimentally that this condition prevails for a fairly wide range of engine conditions when the centroid of the pressure pulse occurs at 15 degrees past top dead center (TDC). Because of the delays described previously, ignition must occur early enough to position the pressure peak near this value. It is this "anticipation" in spark plug firing that is termed *ignition advance*. The reason why advance angle has to be larger at higher speeds is now obvious: the flame propagation delay time covers more degrees of crank angle when the engine is running faster.

Further experiments by the Stanford researchers and others confirmed the suspicion that the period wave is a strong function of the crank angle, and that the angle associated with the centroid of the pressure wave is a unique function of the phase of the fundamental component of the period wave measured with respect to a crankshaft angle index point, say top dead center of cylinder no. 1. The period wave is measured with a sensor which is a precision version of a crankshaft position sensor.[10] It produces a fast, sharp pulse for every small and equal angle increment—say one degree—through which the shaft turns. Pulses from a high-frequency quartz crystal clock are counted to measure each period. The crankshaft angle index is available from the crankshaft position sensor. In principle, the period wave could be Fourier analyzed into the Fourier integral coefficients A_n and B_n by computing the Fourier integrals, and the phase of the fundamental (first harmonic) is then arctan B_1/A_1. To perform this computation in real time is a bit much to ask of today's microcomputer (but not tomorrow's!) and various shortcuts are utilized to achieve an approximate result. Remembering that the period wave appears to lead the torque impulses that cause it by π/2, the spark timing can now be varied so as to place the centroid of the pressure wave, on the average, at or very near the 15-degree-after-TDC point.

It is instructive to consider what performance is required of the DPA and crankshaft position sensors to achieve a given signal-to-noise ratio. The repeatability of the crankshaft angle marked by the sensor is a function of the diameter of the sensing disc. For the various magnetic sensors, a repeatability better than ±0.5 degree can be achieved with a 10-cm-diameter disc. In the DPA sensor, the concern is for the period-to-period jitter. It is obviously worse for smaller angle increments both because the angle jitter is a larger part of the period, and also because the period-counting roundoff error is larger for any given clock frequency. At the same time, the more periods measured per revolution, the more fidelity the period wave will have for its high-frequency components. The period-to-period jitter of the magnetic sensor in this example is about ±0.5 degree. This is satisfactory for 24 periods per revolution but marginal for 60 periods; a typical period wave amplitude is only ±3 percent of the average period. On the other hand, even 60 periods per revolution is marginal for ignition or injection timing control.

The granularity due to counting roundoff also needs to be considered. Today's low-cost LSI circuits can count reliably at 20 MHz, so that is a practical clock frequency. If a four-cylin-

IPR2023-01234
Petitioner - Ex. 1017 - Page 180

der engine is running at 1800 rev/min (30 Hz), the associated period wave will have a fundamental of 60 Hz. If the DPA sensor has one degree angle indices, referred to the crankshaft, each period will have about 2000 counts from the clock. Therefore, the period counting round-off noise will be ±1 part per 2000. Referred to a nominal ±3 percent amplitude period wave, this jitter amounts to ±2 percent of the peak value of the period wave (not of the period itself), not counting any smoothing.

For the fundamental of the period wave, the phase of which is used for DPA timing control, a good deal of smoothing can be realized, so that for a "clean" engine, estimation of the correct angle to ± one crankshaft degree is feasible.

Figure 9.5 shows an actual period wave measured using an electromagnetic DPA sensor with one-degree increments and a 10-MHz clock. Both the jitter described previously and a fixed pattern noise can be discerned in the signal. The latter effect is due to slight imperfections in the tooth spacing of the precision gear used as the sensing disc. Such systematic errors can be eliminated in the microcomputer, but they are troublesome and consume integration time. The better solution is to design a precision DPA sensor which minimizes fixed pattern noise.

DPA Used for Diagnostics. During the 1980s, one of the heavy duty diesel engine manufacturers introduced an off-board diagnostic instrument capable of doing DPA on the engine with the clutch disengaged and using snap acceleration and deceleration to load the engine

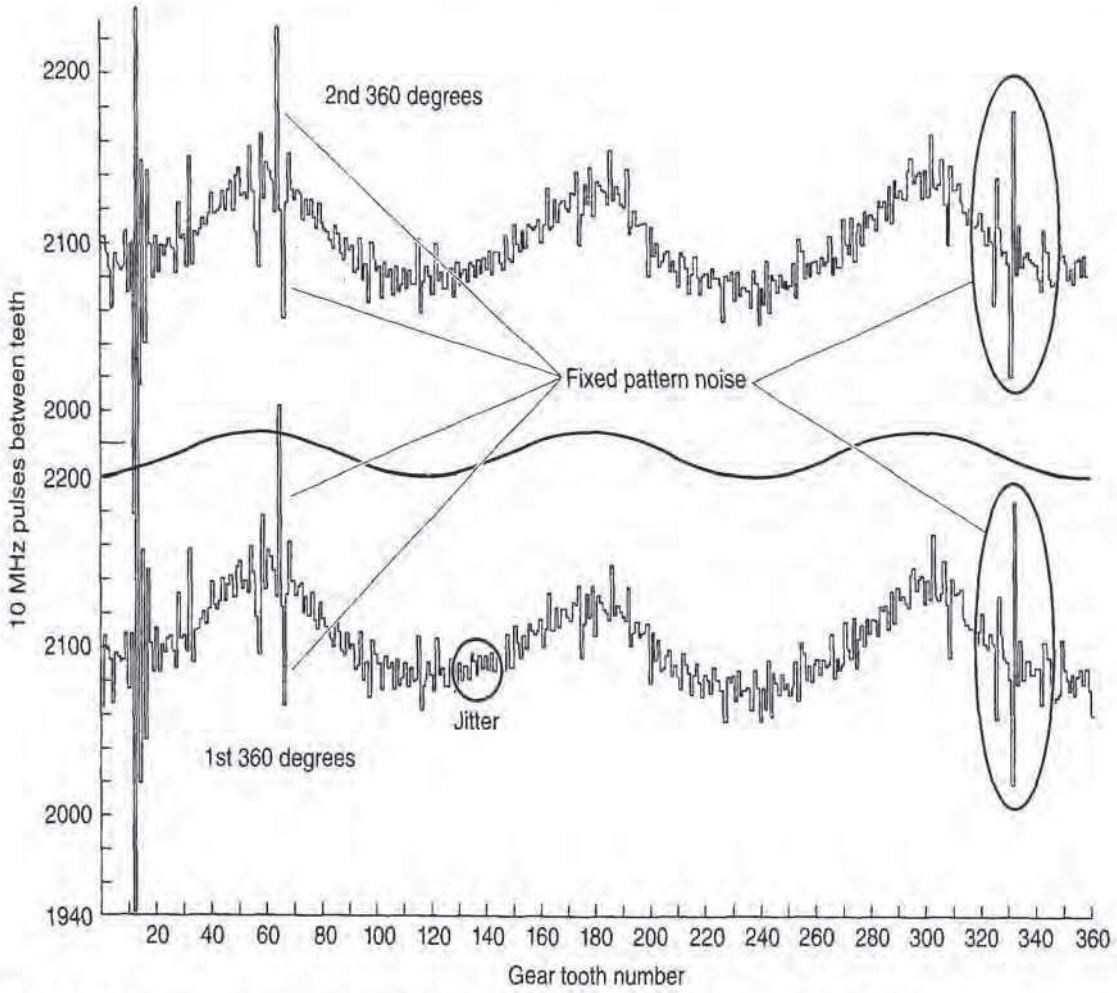


FIGURE 9.5 Actual period wave data from engine crankshaft; unsmoothed data. *(Courtesy of The Bendix Corp., Diesel Operation)*

IPR2023-01234
Petitioner - Ex. 1017 - Page 181

inertially. This instrument used the very imperfect engine ring gear as the DPA target but solved the fixed pattern noise problem in a very elegant way.[11] The position sensor is actually a dual sensor, with the two magnetic circuits disposed tangential to the ring gear and closer together than one tooth pitch. A particular tooth is sensed by the first magnetic circuit and then by the second before the next tooth is sensed by the first circuit. Virtually all of the fixed pattern noise is eliminated.

What would be achieved in an on-board DPA system would be real-time, nearly ideal closed-loop control of spark timing. As with most controls for spark-ignited engines, there are some trims required to make the system work. Flame front propagation is in fact a complex process which has a substantial jitter in the time of propagation, so it is necessary to average the computation of the phase angle over a number of cylinder pulses in order to obtain a good phase estimator. Under transient conditions, the shape of the pressure pulse may change enough so that the angle for mean best torque (MBT) shifts slightly. These factors can also be incorporated in the control. A similar method could be used for compression-ignition engines; in fact, the period wave has a more reproducible signature than for a spark-ignited engine.

It is useful at this point to emphasize again that these principles hold under any conditions, but that the control works well only in the lean regime. As the air/fuel ratio nears stoichiometry, the amplitude of the period wave becomes quite small. Because the method of measuring the instantaneous period—counting clock pulses over a finite angle increment—is a differencing method, the signal-to-noise ratio (S/N) is always a problem, since a differencing process always yields a poorer S/N than that of the original function. Hence, the DPA technique yields poorer results the nearer the engine is to stoichiometry and the higher the engine speed.

Referring to Fig. 9.6, if a figure of merit is formed

$$R = \left| \frac{T_2 - T_1}{t_1 + t_2} \right| \tag{9.2}$$

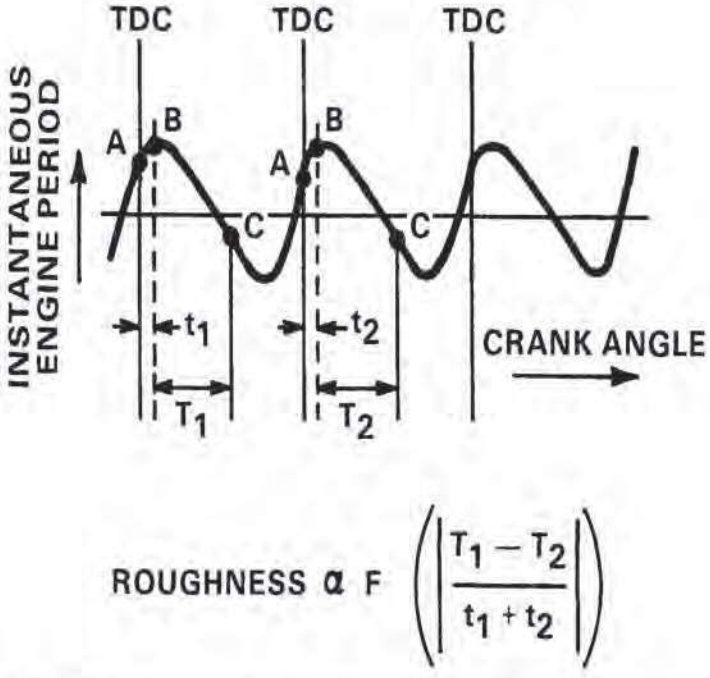


FIGURE 9.6 Digital roughness control.

IPR2023-01234
Petitioner - Ex. 1017 - Page 182

we have a measure of the "roughness" of the engine useful for lean limit control or misfire detection. This is one example of many such optimizing algorithms which may be derived from DPA

9.5 SUMMARY

One can conclude from this chapter that torque measurement, whether direct or inferred, is a useful parameter for engine evaluation off-board, but that the proper sensors and computer analysis equipment for on-board control are not yet available. Yet the number of facilities working to advance this art, the resources being added, and the sporadic reports of progress are such that one can predict with some confidence that a breakthrough is imminent. Just what kind of control will first appear, and what kind or kinds will ultimately be successful, is not yet clear.

GLOSSARY

Algorithm A set of software instructions causing a digital computer to go through a prescribed routine. Because embedded computer engine controls have become so common, algorithm has become essentially synonymous with control law for automotive engineers.
Compression leveling A (theoretical) type of engine control which would cause each piston in each cylinder to compress its air charge to the same maximum pressure.
Dynamometer A machine to absorb power in a controlled manner, especially from an engine under test.
Hooke's law A relationship for an ideal elastic member which says that the displacement is proportional to the force.
Interdigitated An arrangement of two multiple-finger structures such that each pair of fingers from one structure has a finger from the other interposed.
Pulse sequential A type of fuel control for gasoline spark-ignited engines in which the fuel for each cylinder is injected into the air manifold near the intake valve for that cylinder just as it opens.
Robust Able to survive and operate properly in a severe environment.
Stoichiometric Pertaining to a combustion process in which the oxidizing agent (oxygen) and the reducing agent (fuel) are in balance such that, were the reaction to go to completion, there would be neither oxygen nor fuel left over, and all the reaction products such as carbon monoxide would be oxidized to their highest state—carbon dioxide.
Torsional Hooke's law A relationship for an ideal elastic shaft which says that the angle through which the shaft twists is proportional to the torque.
Torque The moment tending to make the output shaft of an engine turn. Torque can be expressed as a force acting perpendicular to a lever arm at a distance from the center of rotation. Its units are Newton-meters (pound force-feet).
Unit injector A type of fuel control for diesel engines which has fuel metered into a piston-barrel injector for injection into a specific cylinder at a specific time. Each engine cylinder has its own cam-driven injector, which operates something like a hypodermic syringe.

IPR2023-01234
Petitioner - Ex. 1017 - Page 183

REFERENCES

1. J. A. Tennant, Rao, H. S., and Powell, J. David, "Engine characterization and optimal control," *Proceedings of the IEEE Conference on Decisions and Control* (including the 18th Symposium on Adaptive Processes), Ft. Lauderdale, Fla., Dec. 12–14, 1979. IEEE 79CH 7486-OCS, vol. 1, pp. 114–119.
2. Itshak Glaser and Powell, J. David, "Optimal closed-loop spark control of an automotive engine," SAE Paper No. 810058, Society of Automotive Engineers Inc., Warrendale, Pa.
3. Anders Unger and Smith, Kent, "Second-generation on-board diagnostics," *Automotive Engineering* vol. 102, no. 1, Jan. 1994, pp. 107–111.
4. William J. Fleming, "Automotive torque measurement: a summary of seven different methods," *IEEE Transactions on Vehicular Technology,* VT-31, No. 3, Aug. 1982, pp. 117–124.
5. William J. Fleming and Wood, P. W., "Non-contact miniature torque sensor for automotive applications," SAE Paper No. 820206.
6. Yutaka Nonomura; Sugiyama, Jun; Tsukado, Koja; Masahoru, Takeuchi; Itoh, Koji; and Konami, Toshiaki; "Measurements of engine torque with the intra-bearing torque sensor," SAE Paper No. 87042.
7. G. W. Pratt Jr., "An opto-electronic torquemeter for engine control," SAE Paper No. 760007.
8. Charles D. Hoyt, "DC excited capacitive shaft position transducer," U.S. Patent No. 4 862 752 Sept. 5, 1989.
9. Hiroki Kusakabe; Okauchi, Tohru; and Takigawa, Masuo; "A cylinder pressure sensor for internal combustion engine," SAE Paper No. 92071.
10. Stephen J. Citron and Orter, Kevin C., "On-line engine torque measurement utilizing crankshaft speed fluctuations," SAE Paper No. 850496.
11. Clarence E. Kincaid, "Computerized diagnostics for Cummins engines," *Proceedings of Convergence '84,* IEEE '84 CH 1988–5.

ABOUT THE AUTHOR

For biographical information on William G. Wolber, see Chap. 8.

IPR2023-01234
Petitioner - Ex. 1017 - Page 184

CHAPTER 10
ACTUATORS

Klaus Müller
Manager, Development of Magnet Valves, Pressure Supply
Automotive Equipment Division 1
Robert Bosch GmbH, Stuttgart

10.1 PREFACE

10.1.1 Introductory Remarks

Numerous open- and closed-loop control systems find application in modern production vehicles, where they provide improved operating characteristics together with enhanced safety, comfort, and environmental compatibility.

The actuators respond to position commands from the electronic control unit to regulate energy, mass, and volume flows.

10.1.2 Actuators: Basic Design and Operating Principles

Conventional final-control elements (standard and spool valves, etc.) have been familiar for some time. A provision for electronic control is required for actuator applications in modern vehicles. The actuator consists of a transformer to convert the input signal from the control unit into (usually) mechanical output quantities, and the conventional final-control element which it governs. (See Fig. 10.1.)

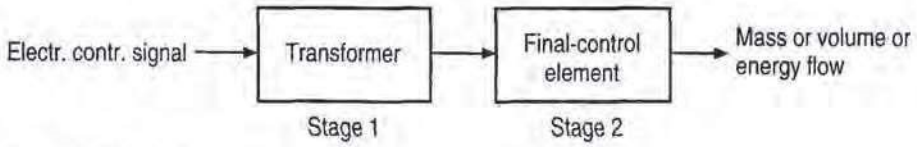


FIGURE 10.1 Basic actuator elements.

Either the control unit or the actuator itself will feature an integral electronic output amplifier. The energy conversion principles (stage 1) determine the classification of the actuators. Electromechanical actuators will also be discussed in the following pages.

IPR2023-01284
Petitioner - Ex. 1017 - Page 185

10.2 TYPES OF ELECTROMECHANICAL ACTUATORS

10.2.1 Magnetic Actuators

dc Solenoids

Actuator Principles. In order to operate, actuators depend on the forces found at the interfaces in a coil-generated magnetic field when current passes through it. The solenoid actuation force F_m is calculated as

$$F_m = \frac{A B^2}{2 \mu_o} \tag{10.1}$$

where A = pole face area
B = magnetic induction
μ_o = permeability constant ($\mu_o = 4 \pi 10^{-7}$ Vs/Am)

On the flat-armature solenoid illustrated in Fig. 10.2*a*, the total solenoid force is $2 F_m$. Equation (10.1) can also be applied to versions equipped with a permanent magnet (Fig. 10.2*b*). A particular solenoid force is specified for each technical application. The pole face area, the magnetic circuit, and the coil are then determined for this force.

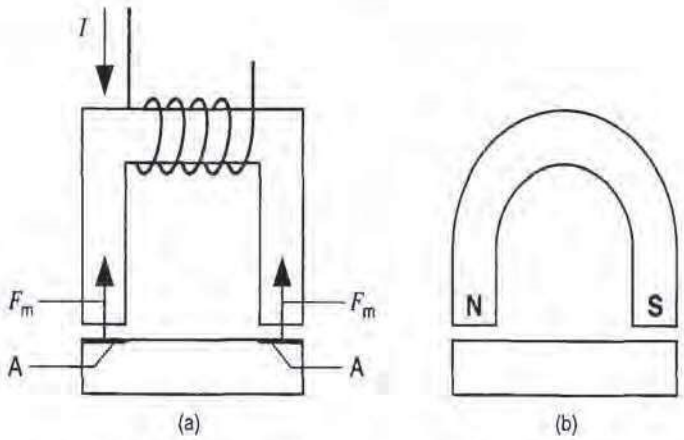


FIGURE 10.2 Flat-armature solenoid featuring field excitation (*a*) via coil; (*b*) via permanent magnet.

Determining Magnetic Circuit and Coil Specifications. The magnetic circuit consists of the working gap (between the armature and the base) and the ferrous regions. Permeability in iron is approximately three orders of magnitude greater than in air. For this reason, the iron regions conduct the field. If the effects of leakage flux are discounted, the absence of magnetic charge, $\oint\!\!\oint B \, dA = 0$, means that the magnetic flux Φ_m remains constant for all cross sections A in the magnetic circuit:

$$\Phi_m = \iint_{A_1} B \, dA_1 = \iint_{A_2} B \, dA_2 = \iint_{A_i} B \, dA_i = \text{const.} \tag{10.2}$$

If the magnetic induction is assumed to be homogeneous for all cross sections A_i, then Eq. (10.2) can be simplified to:

$$\Phi_m = B_1 A_1 = B_2 A_2 = B_i A_i = \text{const.} \tag{10.3}$$

IPR2023-01234
Petitioner - Ex. 1017 - Page 186

The induction lines run at a 90° angle to the surfaces A_i. Equation (10.3) defines the magnetic induction in each section of the magnetic circuit (Fig. 10.3). If, as an example, Index 1 is assigned to the gap section, then B_1 and A_1 are derived with the assistance of Eq. (10.1), and one can proceed to calculate B_i for the other sections.

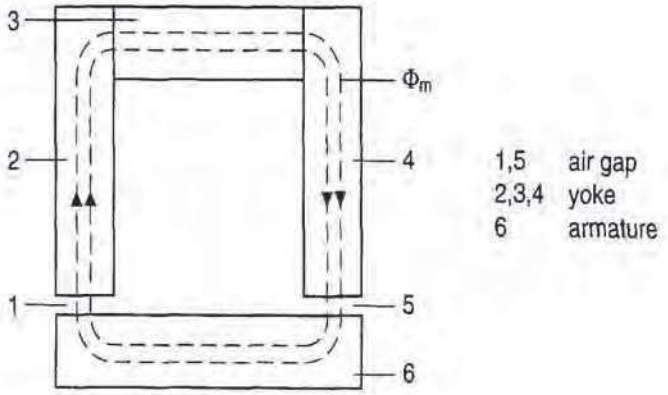


FIGURE 10.3 Magnetic circuit divided into individual sections.

The magnitude of the magnetic field strength $\mathbf{H}_i$ is determined by the material properties (permeability μ_n) of the section in question. Field strength $\mathbf{H}_i$:

$$\mathbf{B}_i = \mu_0 \mu_{ri} \mathbf{H}_i \tag{10.4}$$

In air, $\mu_r = 1$. In ferromagnetic materials, μ_r does not remain constant. Rather, it varies as a function of the magnetic field strength **H** (see Fig. 10.4). The relationship between **B** and **H** is defined by the **B-H**-curve.

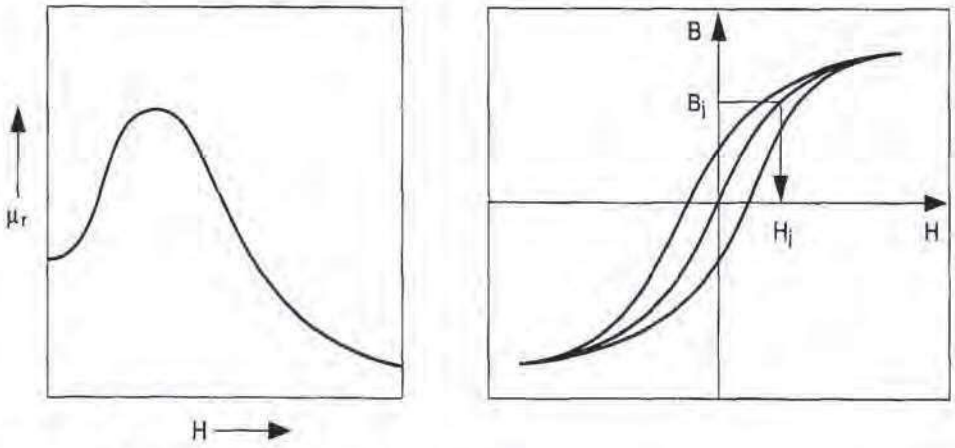


FIGURE 10.4 Progression of permeability and **B-H** curve.

Using the magnetic voltage $V_{mi} = \int \mathbf{H}_i \, d\mathbf{s}$ for the individual section, it is possible to calculate the peripheral magnetic voltage as the sum of the individual magnetic voltages V_{mi}. According to Ampere's law,

$$\Theta = \int \mathbf{H} \, d\mathbf{s} \tag{10.5}$$

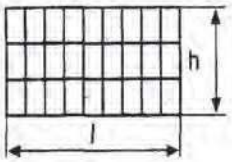
this magnetic peripheral voltage is equal to the magnetomotive force Θ. It defines the *total current* of the coil, $\Theta = I\,w$. (I = current, w = number of windings.)

IPR2023-01234
Petitioner - Ex. 1017 - Page 187

Because the preceding calculation fails to consider leakage flux, the results must frequently be treated as approximations only. It is possible to increase the precision of the calculations by portraying the magnetic circuit as a general network (with gaps and iron regions as reluctance elements) instead of as a series circuit. The results will then reflect the effects of a large proportion of the leakage flux. Maximum precision is achieved with numeric field calculations, which provide numerical solution of Maxwell's equations.

After magnetomotive force Θ has been determined, the field coil must be dimensioned to produce the required magnetic field. The formulas contained in Fig. 10.5 can be employed to determine the field coil's specifications. For a graphic interpretation, see Fig. 10.6.

$A_w = h \cdot l$



Winding cross section area:

$$A_w = \frac{R\,\pi\,\rho\,(d_a+d_i)(1+\alpha\,\Delta\vartheta)^2\,\Theta^2}{2\,k_w\,U^2}$$

Winding number:

$$w = \left(\frac{2\,A_w\,k_w\,R}{\Pi\,\rho\,(d_a+d_i)}\right)^{1/2}$$

Wire diameter:

$$d = \left(\frac{8\,\rho\,(d_a+d_i)\,A_w\,k_w}{\pi\,R}\right)^{1/4}$$

A_w	Winding cross section area	$\Delta\vartheta$	Temperature differential between coil and room temperature
R	Coil resistance	Θ	Magnetomotive force
ρ	Specific resistance of coil wire	k_w	Coil space factor (ratio of total wire area (w/o insulation) to winding cross section area)
d_a	Outer diameter of windings	U	Voltage at coil
d_i	Inside diameter of windings		
α	Thermal resistivity coefficient of coil wire		

FIGURE 10.5 Determining coil data for specified coil resistance and voltage levels.

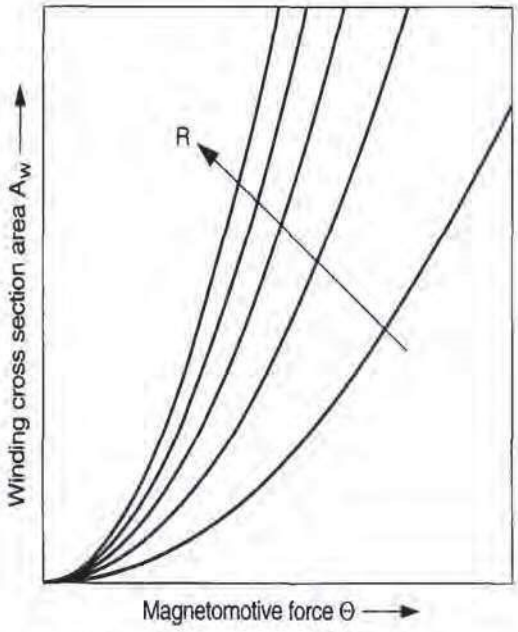


FIGURE 10.6 Area of winding A_w as function of magnetomotive force Θ (parameter coil resistance).

IPR2023-01234
Petitioner - Ex. 1017 - Page 188

To minimize the size of the solenoid assembly, the magnetic circuit and the coil must be dimensioned to produce the smallest overall size. The formulas for coil dimensions (Fig. 10.7) can be used to minimize the volume of pot-shaped solenoids.

$$\frac{l}{d} \approx 1.5 \qquad \frac{h}{d} \approx 0.4 \ldots 0.5$$

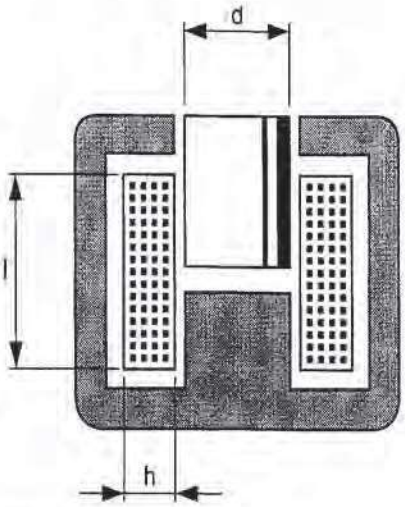


FIGURE 10.7 Selecting coil dimensions for pot-shaped solenoids.

In general, the solenoid is iteratively optimized by changing geometry in those critical areas within the magnetic circuit requiring a high magnetic voltage V_{mi}. The magnetomotive force Θ is then recalculated for the modified magnetic circuit. Figure 10.8 shows the optimization of solenoid diameter D for a particular armature diameter d.

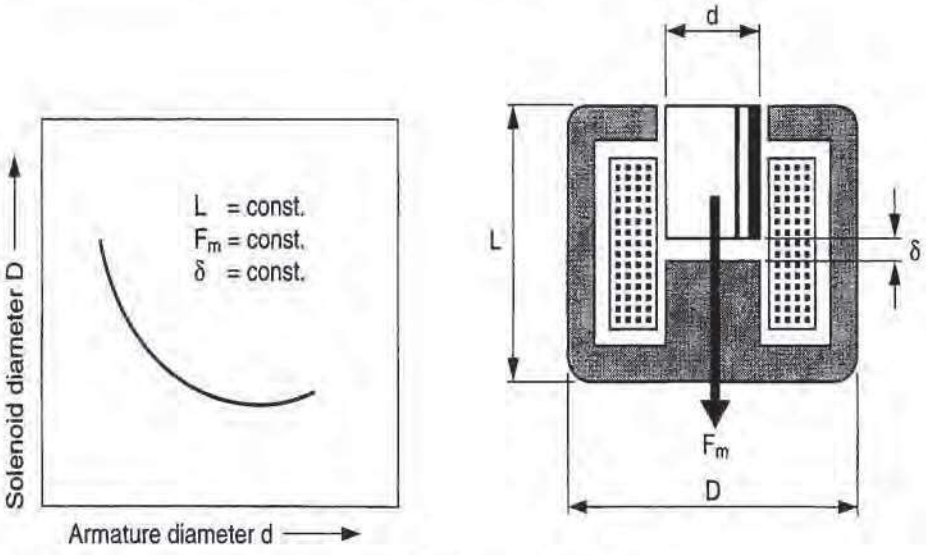


FIGURE 10.8 Relationship between solenoid and armature diameters.

Magnetic Force Curve. When the unit is intended for use in an actuator, the relationship between magnetic force and stroke will be required. With a flat armature and base, and without including the iron regions, Ampere's law [Eq. (10.5)] and Eq. (10.4) provide the following:

$$\Theta = H_\delta \delta = \frac{B_\delta \delta}{\mu_o} \tag{10.6}$$

where δ = working gap

IPR2023-01234
Petitioner - Ex. 1017 - Page 189

Together with the force relationship, Eq. (10.1), the following result is obtained:

$$F_m = \frac{\Theta^2 \mu_0 A_1}{2\,\delta^2}, \text{ i.e., } F_m \sim \frac{1}{\delta^2} \tag{10.7}$$

The substantial drop in magnetic force will be undesirable in many applications. Modifications to the curve for magnetic force versus stroke represent an alternative to increases in solenoid dimensions. This expedient can be effected through control of the current in the coil or by means of design modifications to the armature and base (see Fig. 10.9).

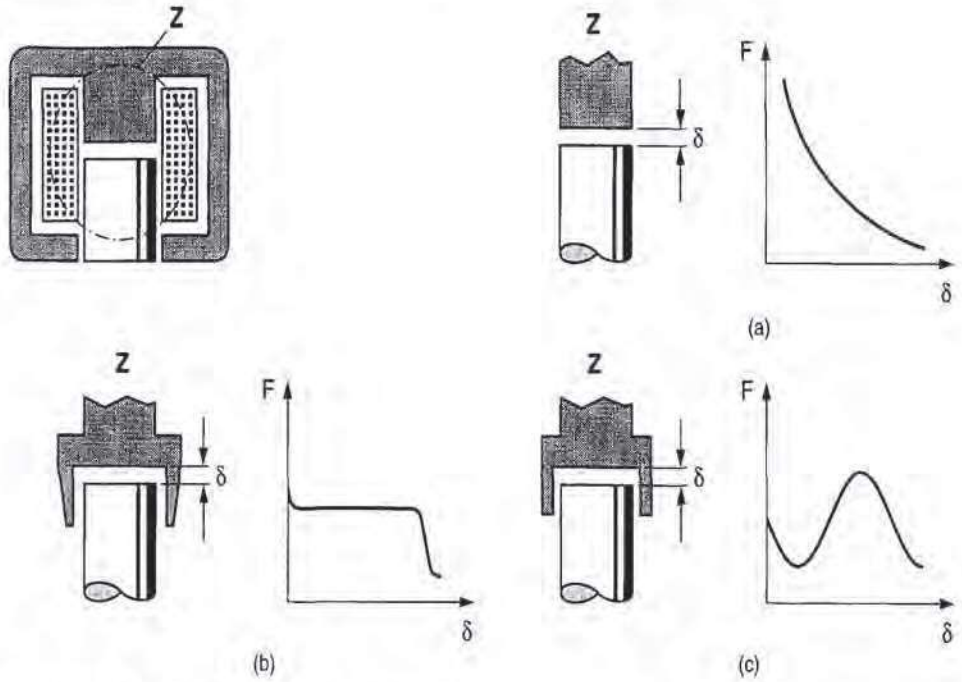


FIGURE 10.9 Design modifications and force curve.

The areas below the force-travel curves, a measure of the work performed, are always the same.

$$\int_0^\infty F_m(\delta)\, d\delta = \text{const.} \tag{10.8}$$

$$\text{with} \quad I = \text{const.}$$

Configuration c can be employed together with a spring to produce a proportional solenoid in which armature travel can be regulated as a function of current. This type of system is sensitive to interference from extraneous factors such as mechanical friction, and hydraulic and pneumatic forces. Thus, final-control systems for high-precision applications must also incorporate a position sensor and a controller (Fig. 10.10).

Dynamic Response. To show the dynamic response pattern more clearly, Fig. 10.11 provides a schematic illustration of the progression over time of three parameters: voltage u at the excitation coil, excitation current i, and armature position s.

The dynamic response pattern can be calculated using computer programs that apply Maxwell's equations (field propagation with eddy currents, self-induction) in conjunction with the motion equation.

Approximation formulas can be employed to derive rapid estimates (eddy currents and magnetic resistance in the iron regions are not taken into account):

IPR2023-01234
Petitioner - Ex. 1017 - Page 190